SCINTILLATION MECHANISMS
OF
CERIUM-DOPED RARE EARTH OXYORTHOSILICATES

Thesis by
Hideyuki Suzuki

In Partial Fulfillment of the Requirements
for the Degree of
Doctor of Philosophy

California Institute of Technology
Pasadena, California
1994
(Defended February 1, 1994)

Acknowledgments

The hardest thing I ever did in my life was to leave my home country and go to the opposite side of the earth — for it was a terribly lonely path. Accepting that challenge, however, changed my life.

I am most grateful to my adviser, Professor Thomas A. Tombrello, for constantly giving me exciting opportunities. The research environment, people and life he introduced me to, both at Caltech and at Schlumberger-Doll Research (SDR), were invaluable, and my school life has been, because of those experiences, twice as substantial as usual.

I thank Alan Rice and Steve Stryker for their help in designing and setting up the equipment I initially used. Their technical knowledge always saved me a lot of time. I also thank Michelle Vine for her thoughtful care at Sloan Annex and assistance in communicating with the administration at Caltech when I was off campus. I appreciate Dr. Steve Spicklemire for his thrilling guidance and Dr. Shouleh Nikzad for her encouragement and helpful advice on graduate study.

I spent the second half of my graduate study at SDR and I partly owe my Ph.D. research to the people there. I learned from Dr. Jeffrey Schweitzer how to utilize academic knowledge to analyze and interpret real physical data. I received from Dr. Charles Melcher useful advise on most experiments at SDR. I thank both of them for their help in getting over failure at the first Candidacy exam and their encouragement. The technical support as well as daily cheerful greetings I received from Carl Peterson were a key to my success in finishing my degree. I thank Ralph Manente for his assistance in growing crystals, Dr. Joel Groves for giving me an opportunity to work at the Nuclear Science Department of SDR, and Peggy Dow for her assistance in doing miscellaneous business.

Others to whom I am indebted include Dr. John Sutherland at Biology Department of Brookhaven National Laboratory for providing me with precious beam time; Dr. John Trunk and Dr. Krzysztof Polewski, for their hospitable assistance with experimental work

on the U9B beamline; Ann Emrick, for logistic assistance.

All of the members of the Basic Applied Physics Group at Caltech and of Schlumberger-Doll Research have in some way contributed to my work and I acknowledge their support in training me as both a scientist and an international person.

Abstract

Rare earth oxyorthosilicates $(RE)_2(SiO_4)O$ (RE = rare earth) have high densities and effective atomic numbers for efficient gamma-ray detection. Among these, $Gd_2(SiO_4)O$, $Y_2(SiO_4)O$ and $Lu_2(SiO_4)O$ have no absorption lines at visible wavelengths and thus were examined as potential single crystal scintillators by doping with cerium (Ce).

The light emission mechanism of the activator Ce^{3+} ion in $(RE)_2(SiO_4)O$ was investigated with UV light, by selectively exciting absorption bands of Ce^{3+} at low temperature (~11 K). It was found that all three compounds have two types of excitation and emission spectra and decay constants, and they were attributed to two Ce^{3+} centers (Ce1 and Ce2) occupying two different host rare earth sites.

The origins of two decay constants in the gamma-ray excited decay of $Gd_2(SiO_4)O$:Ce (GSO) were investigated. We focused on GSO since the gamma-ray excited decay times of GSO are much slower than the intrinsic Ce^{3+} decay, in contrast with $Y_2(SiO_4)O$:Ce and $Lu_2(SiO_4)O$:Ce. Since Gd^{3+} emission bands overlap Ce^{3+} absorption bands, the energy transfer from Gd^{3+} to Ce^{3+} was analyzed for a possible explanation for the slow Ce^{3+} decays. The Gd^{3+} absorption bands in the UV region were excited by a synchrotron light source and the Ce^{3+} decay was monitored. With excitation into the ^6P_J and ^6I_J states of Gd^{3+}, a slow decay component and a build-up were observed in the Ce^{3+} decay, consistent with energy transfer from ^6P_J and ^6I_J states of Gd^{3+} to Ce^{3+}.

The energy migration through the Gd sublattice in GSO was investigated. The Gd was diluted by optically inactive rare earths, Y and Lu, and the macroscopic energy transfer rate from Gd^{3+} to Ce^{3+} was measured as a function of Gd concentration. The results show that the macroscopic transfer rate from Gd^{3+} to Ce^{3+} increases as Gd concentration increases, indicating that the energy of the excited Gd^{3+} can migrate through the Gd sublattice before one of the Gd^{3+} near a Ce^{3+} can transfer its energy to the Ce^{3+}.

Table of Contents

Lists of Figures

Lists of Tables

Acronyms

BGO	bismuth germanate $Bi_4Ge_3O_{12}$
GSO	cerium-doped gadolinium oxyorthosilicate $Gd_2(SiO_4)O:Ce$
LO	longitudinal optical phonon
LSO	cerium-doped lutetium oxyorthosilicate $Lu_2(SiO_4)O:Ce$
PMT	photomultiplier tube
RE	rare earth
YSO	cerium-doped yttrium oxyorthosilicate $Y_2(SiO_4)O:Ce$

List of Publications

H. Suzuki, T.A. Tombrello, C.L. Melcher and J.S. Schweitzer, "UV and Gamma-ray Excited Luminescence of Cerium-doped Rare Earth Oxyorthosilicates," Nucl. Instr. and Meth. A320 (1992) 263-272 (chapter 2 in this dissertation).

H. Suzuki, T.A. Tombrello, C.L. Melcher and J.S. Schweitzer, "Light Emission Mechanism of $Lu_2(SiO_4)O$:Ce," IEEE Trans. Nuc. Sci. NS-40 (4) (1993) 380-383.

H. Suzuki, T.A. Tombrello, C.L. Melcher and J.S. Schweitzer, "Energy Transfer from Gd to Ce in $Gd_2(SiO_4)O$:Ce," J. Lumin. in press.

H. Suzuki, T.A. Tombrello, C.L. Melcher and J.S. Schweitzer, "Energy Transfer Mechanism in $Gd_2(SiO_4)O$:Ce Scintillators," submitted to IEEE Trans. Nuc. Sci. (chapter 4 in this dissertation).

R. Visser, C. L. Melcher, J. S. Schweitzer, H. Suzuki and T. A. Tombrello, "Photostimulated Luminescence and Thermoluminescence of LSO scintillators," submitted to IEEE Trans. Nuc. Sci.

H. Suzuki, T.A. Tombrello, C.L. Melcher, C.A. Peterson and J.S. Schweitzer, "The Role of Gadolinium in the Scintillation Processes of Cerium-doped Gadolinium Oxyorthosilicate," submitted to Nucl. Instr. and Meth. A. (chapter 3 in this dissertation).

Chapter 1

Introduction

This work examines the scintillation mechanisms of cerium-doped rare earth oxyorthosilicates $(RE)_2(SiO_4)O$:Ce (RE = rare earths Gd, Y and Lu), which have been successfully grown in single crystal form by the Czochralski technique. $Gd_2(SiO_4)O$, $Y_2(SiO_4)O$ and $Lu_2(SiO_4)O$ have no absorption lines at visible wavelengths and thus have been examined as potential single crystal scintillators by doping with cerium (Ce). Because of their high density and average atomic number, reasonably high scintillation emission intensities, and fast scintillation decay times, they all show good potential for applications in such fields as medical imaging, geophysics, nuclear physics, high energy physics, etc. The purpose of this research is to understand better the light emission mechanisms of $(RE)_2(SiO_4)O$:Ce, in order to help realize their high potential as scintillators. For a systematic and consistent discussion of the mechanisms, we give in the first chapter a clear understanding of the terminology, a description of the structure of the crystals, the method of crystal growth, the basic properties of the light emitting centers, and the requirements that the scintillator must satisfy. Thus, the first chapter is mainly devoted to a general review of the single crystal scintillators, $(RE)_2(SiO_4)O$:Ce.

1.1 Luminescence

Luminescence refers to any emission of light which is not purely thermal in origin [1]. According to the means by which a luminescent material is excited, luminescence is generally categorized into four types: (1) *photoluminescence* if the excitation is by light (or usually ultra-violet radiation), (2) *cathodeluminescence* if the excitation is by fast electrons, (3) *electroluminescence* if the excitation is by electric field or current, (4) *radioluminescence* if the excitation is by high energy radiation such as x-rays, gamma rays, α and β particles,

protons, etc. *Scintillations* refer to the individual emissions due to single particles and their use in the detection of the specific particles [1].

In general, luminescent materials can be divided into two groups [2]: one for which the host lattice is an insulator and the other for which the host lattice is a semiconductor. In the former case, the photon energy involved in the luminescent transition is determined primarily by the impurity atom, known as the *activator*. In the latter case, the energy bands of the host crystal as well as the energy levels of the activators are involved in determining the photon energy of the luminescent transition.

The luminescent materials discussed in this dissertation, cerium-doped rare earth oxyorthosilicates $(RE)_2(SiO_4)O$:Ce, were studied primarily for scintillation applications. The rare earth oxyorthosilicates, $(RE)_2(SiO_4)O$, are good insulators ($E_g \sim 6$ eV), and the dopant Ce acts as an activator.

1.2 Scintillators for gamma-ray detection

A scintillator is a luminescent material which converts the energy of ionizing radiation into the luminescent emission of photons [3]. There exist various scintillators, whose required forms and properties depend on their particular applications: medical imaging, nuclear physics, high energy physics, and geophysics. The radiation detected by the scintillator depends on the applications: heavy charged particles (protons, heavy ions, mesons), electrons (e^- and e^+), electromagnetic radiations (x-rays and gamma rays), and neutrons. Many advances have been made in recent years in the development of new scintillating materials, primarily for use as gamma-ray detectors.

As an example, $(RE)_2(SiO_4)O$:Ce have been introduced for use in well logging measurements, where the scintillation crystals are coupled to photomultiplier tubes to measure the natural gamma radioactivity of the formation, the gamma rays of ^{137}Cs scattered back from the geological formation, and gamma rays produced in neutron-induced nuclear reactions[4]. The requirements for a detector in this application are generally useful

also for most other applications.

In characterizing scintillator performance, three properties are of primary importance [5]: detection efficiency (stopping power), scintillation efficiency (light output) and speed (decay time). The detection efficiency of a scintillator is the fraction of ionizing radiation incident on the scintillator which is detected, i.e., that part that produces individual scintillations of sufficient magnitude to be recorded [3]. The detection efficiency for gamma rays is characterized reasonably well by the density and atomic number of the materials as discussed in section 1.2.1, and thus scintillators used in well logging should have high density and atomic number. The scintillation efficiency is defined as the fraction of all incident particle energy which is converted into visible light (see section 1.2.2) [6]. One would always prefer both detection and scintillation efficiencies to be as large as possible. It is also important to maximize the speed with which the light is produced by the scintillator to improve the count-rate capability of the detector.

1.2.1 Detection efficiency

The absorption of gamma rays by scintillators differs fundamentally from the absorption of other radiations [3]. For example, charged particles dissipate their energy continuously in a sequence of many ionization and excitation events, and penetrate a certain distance into the absorber in doing so [3]. Gamma rays, on the other hand, are absorbed or scattered in single events. The detection of gamma rays is therefore critically dependent on having the gamma ray photon undergo an interaction that transfers all or part of the photon energy to an electron in the absorbing material [6]. The most important of the interactions which can occur are:

(i) the Compton effect;

(ii) the photo-electric effect; and

(iii) pair production.

The number of transmitted photons (gamma rays) I is then given in terms of the number of

incident photons I_0 as

$$I = I_0 \exp(-\mu d) \tag{1.1}$$

where μ is the linear attenuation coefficient, in cm^{-1}, and d is the thickness of the scintillator. The linear attenuation coefficient μ is made up of the linear attenuation coefficients corresponding to each of the three types of interactions, σ is the Compton linear attenuation coefficient, τ is the photoelectric linear attenuation coefficient and χ is the pair production linear attenuation coefficient, so that

$$\mu = \sigma + \tau + \chi. \tag{1.2}$$

Each of these quantities depends on the energy of the gamma ray (E), and on the nature of the scintillator. τ is the largest component when E is low, but it decreases rapidly with increasing E. σ decreases steadily with increasing E. χ is zero at energies below 1.02 MeV, and at higher energies it increases steadily with increasing E.

The dependence of the components of μ on the density ρ and atomic number Z is the following: σ, τ and χ depend linearly on the electron density of the scintillator ρ. σ depends on the number of electrons available as scattering targets, and therefore increases linearly with Z. τ is roughly proportional to Z^n, where the exponent n varies between 4 and 5 over the gamma ray energy region of interest. χ varies approximately as the square of the atomic number. Therefore, $\sigma \propto \rho Z$, $\tau \propto \rho Z^n$ and $\chi \propto \rho Z^2$.

Since the above quantity μ determines the potential detection efficiency, it is essential that the scintillator used in well logging has high density and atomic number to enhance detection efficiency (i.e., the linear attenuation coefficient μ).

1.2.2 Scintillation efficiency and speed

High scintillation efficiency (high light output) is desirable to give good energy resolution and ensure that the scintillation signal is well above thermal and electronic noise [4]. A short decay constant (fast speed) is also desirable to increase count-rate capability. Another desirable scintillation property is an emission peak near 400 nm to match the

relatively narrow quantum efficiency response of high-temperature logging photomultipliers [4].

Scintillation efficiency (η) is determined by the product of the efficiencies for three processes [5]: energy conversion (β), energy transfer (S) and luminescence (Q):

$$\eta = \beta S Q; \qquad 0 \le \eta, \beta, S, Q \le 1. \tag{1.3}$$

where β describes the efficiency of the conversion process, in which the energy E_γ of a gamma-ray is used to produce a large number of electron-hole pairs, S describes the efficiency of the transfer process, and Q describes the quantum efficiency of the luminescent center itself.

According to Robbins [7], β can be expressed by:

$$\beta = 2.3E_g / (E_i + KE_i + 2L_fE_i) \tag{1.4}$$

where E_g is the band gap energy of the material, E_i is the ionization energy ($E_i = 1.5\ E_g$) and K is an energy loss ratio (energy lost by an average secondary electron to optical phonons vs. energy lost by this electron to ionization of the atoms in the material). L_f is the fraction of the energy of an electron (or hole) that is wasted when, because of loss to phonons and ionization events, it becomes unable to ionize atoms in the material ($L_f < 1$). Since once K is determined, one can apply the statistical model of van Roosbroeck [8] to evaluate the wasted energy L_f, β is a function of K only. Robbins [7] showed that for a given material:

$$K = \frac{\text{optical phonon generation rate}}{\text{ionization rate}} \frac{(\hbar\omega_{LO})}{1.5E_g} .$$

Using the relation

$$\text{(optical phonon generation rate)} \propto \frac{\alpha\omega_{LO}}{2} \quad \text{and}$$

$$\alpha \text{ (polaron coupling constant)} = \frac{e^2}{h}\left(\frac{1}{\varepsilon_\infty} - \frac{1}{\varepsilon_s}\right)\left(\frac{m}{2\hbar\omega_{LO}}\right)^{1/2} ,$$

he derived

$$K = 0.244 \times 10^4 \left(\frac{1}{\varepsilon_\infty} - \frac{1}{\varepsilon_s}\right)\frac{(\hbar\omega_{LO})^{3/2}}{1.5E_g}, \tag{1.5}$$

where e is the electron charge and m is the electron rest mass. ε_∞ (= n^2, n = refractive

index) and ε_s are the high frequency and static dielectric constants, respectively, and $\hbar\omega_{LO}$ is the longitudinal optical (LO) phonon energy. The relative phonon loss parameter K can be calculated from accessible physical constants of a particular material: $\hbar\omega_{LO}$, E_g, ε_∞, and ε_s. Since β can be calculated using the proper material constants and measurements of E_g, and η and Q are standard in optical spectroscopy of solids, we can estimate the transfer efficiency S from eq. (1.3). This model, developed by van Roosbroeck [8], is independent of details of band structure, and thus we can apply it to the various $(RE)_2(SiO_4)O$:Ce materials, which have two different crystal structures (see section 1.3).

One of the goals of this study is to examine the three steps (conversion, transfer and luminescence) which affect the overall scintillation efficiency η.

1.2.3 Additional requirements on scintillators in well logging

The usefulness of a scintillator used in well logging depends on both the scintillation properties (the light output, the decay time, the emission spectrum) and the physical properties (the density, atomic number, ruggedness, hygroscopicity) of the material [4].

The scintillation properties are affected by the variable borehole temperature, which varies from -50 °C to 200 °C, and thus a reasonably stable temperature response of the scintillation properties is important. The physical properties are important because of the shock and vibration experience in the borehole and the limited space. Ruggedness and hygroscopicity are also important factors in evaluating a scintillator for use in the borehole.

1.2.4 Scintillators in well logging application

Table 1.1 lists the scintillation and physical properties of five scintillators (as of 1989). Clearly no one scintillator material provides optimum properties for all applications. NaI(Tl) has high light output but its decay constant is relatively long resulting in poor count-rate capability [4]. Its detection efficiency is poor due to its low density. In

Table 1.1 Scintillation and physical properties

	NaI(Tl)	BGO[a]	GSO[b]	LSO[c]	YSO[d]
Density (g/cm^3)	3.67	7.13	6.7	7.4	4.54
Eff. atomic no.	51	75	59	66	39
Light output	100	12	25	75	25
Decay time (ns)	230	300	56, 600	12, 40	37, 82
Peak wavelength(nm)	410	480	430	420	420
Hygroscopic ?	yes	no	no	no	no
Rugged ?	no	yes	no	yes	yes
Temperature response	good	poor	good	poor	—
Index of refraction	1.85	2.15	1.85	1.82	1.8[e]

[a] BGO = bismuth germanate $Bi_4Ge_3O_{12}$, [b] GSO = $Gd_2(SiO_4)O:Ce$,
[c] LSO = $Lu_2(SiO_4)O:Ce$, [d] YSO = $Y_2(SiO_4)O:Ce$, [e] ref. [9]

addition, it is hygroscopic and thus requires careful packaging. BGO, on the other hand, has a high detection efficiency and is rugged and nonhygroscopic but has low light output. BGO must be maintained at about 50 °C or less due to its poor temperature response. So far, NaI(Tl) has been used for the vast majority of borehole applications. BGO is used in gamma-ray spectroscopy in oil well logging because of its higher detection efficiency [10]. However, an increasing desire for higher count-rate capability and greater detection efficiency is leading to the use of high density and atomic number scintillators with shorter decay constants.

Cerium-doped gadolinium oxyorthosilicate ($Gd_2(SiO_4)O:Ce$ or "GSO") was developed as a single crystal scintillator by Takagi and Fukazawa [11] in 1983, and this material was studied as a possible detector for positron emission tomography. Its high

density, high effective atomic number, fast decay time and good performance at high temperature made GSO the scintillation detector of choice for a new generation of neutron-induced, inelastic gamma-ray spectroscopy tools for borehole measurements [12,13]. Although there have been some investigations into the scintillation mechanism of GSO, some questions remain, whose answers could potentially improve GSO's scintillation properties. The existence of two decay time components (56 and 600 ns for 0.5 mol% GSO) [14] and the broadening of the emission spectrum at 77 K compared with that at room temperature [15] had not been explained. In addition, the strong dependence of the decay times and the emission intensity on Ce concentration remained to be explained [14].

Cerium-doped lutetium oxyorthosilicate ($Lu_2(SiO_4)O$:Ce or "LSO") has been recently discovered [16,17] and has a number of advantages over existing scintillators. It has a light output which is ~75% of NaI(Tl) with a decay time of ~40 ns. The peak emission wavelength is 420 nm. It has a very high gamma-ray detection efficiency due to its density of 7.4 g/cm^3 and its effective atomic number of 66. These properties result in excellent signal-to-noise ratios, fast coincidence timing, high count-rate capability, and high detection efficiency making LSO superior to any other known scintillator for many applications.

The light emission properties of cerium-doped yttrium oxyorthosilicate ($Y_2(SiO_4)O$:Ce or "YSO") have been analyzed for cathode ray tube applications [18] but due to its low effective atomic number, YSO has attracted less interest as a scintillator. However, because its crystal structure is the same as LSO, YSO also can be used to understand the scintillation mechanism of $(RE)_2(SiO_4)O$:Ce.

1.3 Crystal structure and crystal growth of cerium-doped rare earth oxyorthosilicates $(RE)_2(SiO_4)O$:Ce

There are two different types of crystal structure for $(RE)_2(SiO_4)O$, depending on the ionic radius of the rare earth atom [19]. One type is the monoclinic structure of space

group $P2_1/c$ (fig. 1.1 [19]), for larger ions from La^{3+} to Gd^{3+}; and the other is the monoclinic structure of space group C2/c (fig. 1.2 [20]), for smaller ions from Tb^{3+} to Lu^{3+}, including Y^{3+}. GSO belongs to the former group, while YSO and LSO belong to the latter group. The $P2_1/c$ structure type contains two crystallographically independent RE sites: one site is surrounded by seven oxygen ligands, and the other site is surrounded by nine oxygen ligands. The C2/c structure type also has two different rare earth sites, whose oxygen coordination numbers are six and seven. In both structure types, the ratio of the rare earths at each of the two sites is 1:1. When $(RE)_2(SiO_4)O$ is doped with Ce, the activator Ce is assumed to occupy two different host rare earth sites. This assumption that there exist two activator sites in $(RE)_2(SiO_4)O$ is a basis for our two-activation-center model, which is proposed in chapter 2.

The rare earth oxyorthosilicates $(RE)_2(SiO_4)O$ are congruent melting materials and all the $(RE)_2(SiO_4)O$ crystals used in this study (RE = Gd, Y and Lu) were grown by the Czochralski technique. The melting points of these compounds are ~1900 to ~2100 °C. The dopant Ce^{3+} ion has a larger ion radius (1.034 Å) than the host rare earths, Gd^{3+} (0.938 Å), Y^{3+} (0.910 Å) and Lu^{3+} (0.848 Å), and thus the Ce content in the boule is less than in the melt, with the relative concentration depending on the distribution coefficient of Ce in each host material.

The distribution coefficients of various dopant rare earths in $(RE)_2(SiO_4)O$ were investigated by Brandle et al. [21], who found them to depend linearly on the rare earth ionic radius difference. That is, the distribution coefficients of rare earth dopants in $(RE)_2(SiO_4)O$ vary linearly with the difference between the ionic radii of the dopant and the ionic radii of the host rare earth cations.

The GSO crystals studied here were purchased from Hitachi Chemical Co., Ltd. The GSO crystals were grown in a N_2 atmosphere, using GSO seeds [22]. RF induction heating of an iridium crucible was used to melt the raw materials. The chemical composition of GSO crystals was analyzed by X-RAY ASSAY LABORATORY using

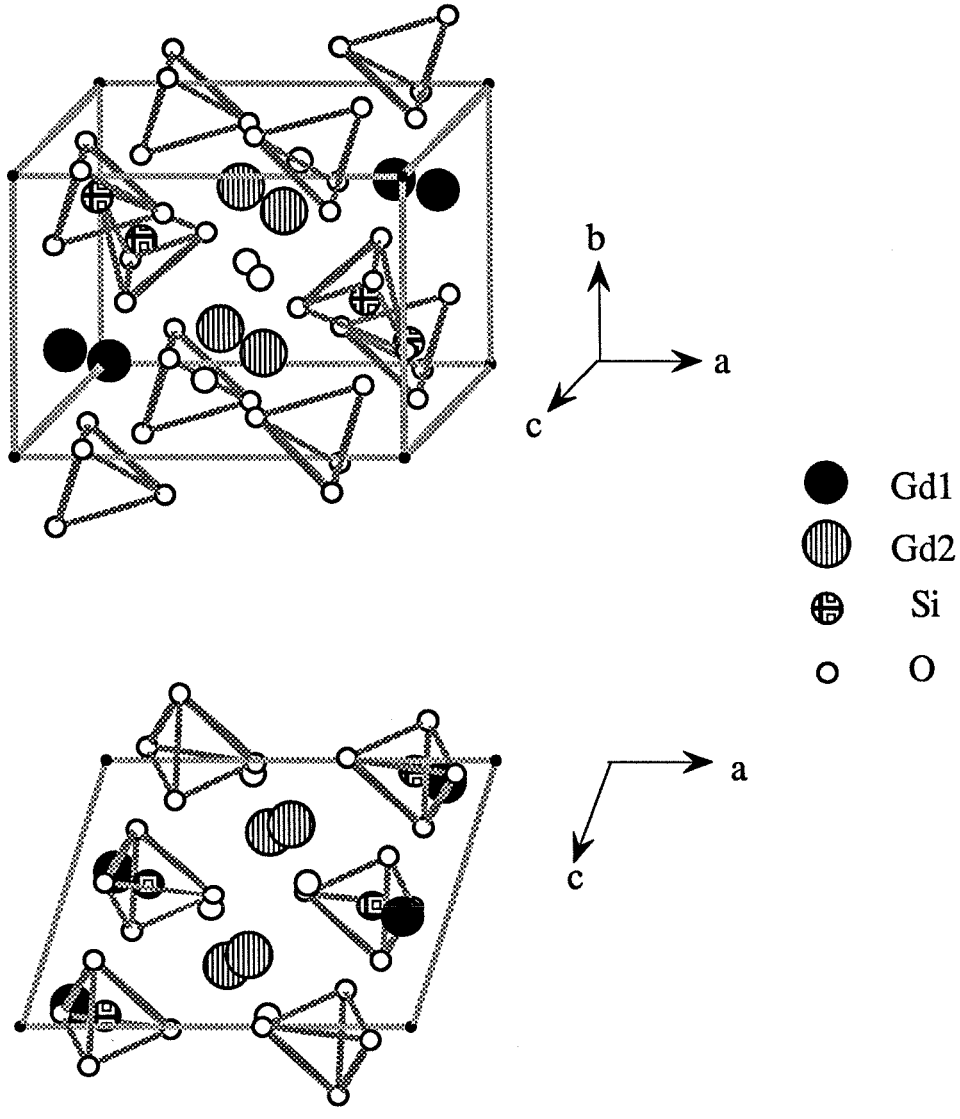

Fig. 1.1 Crystal structure of GSO (space group $P2_1/c$) [19]: a = 9.131 Å, b = 7.045 Å, c = 6.749 Å, β = 107.52°.

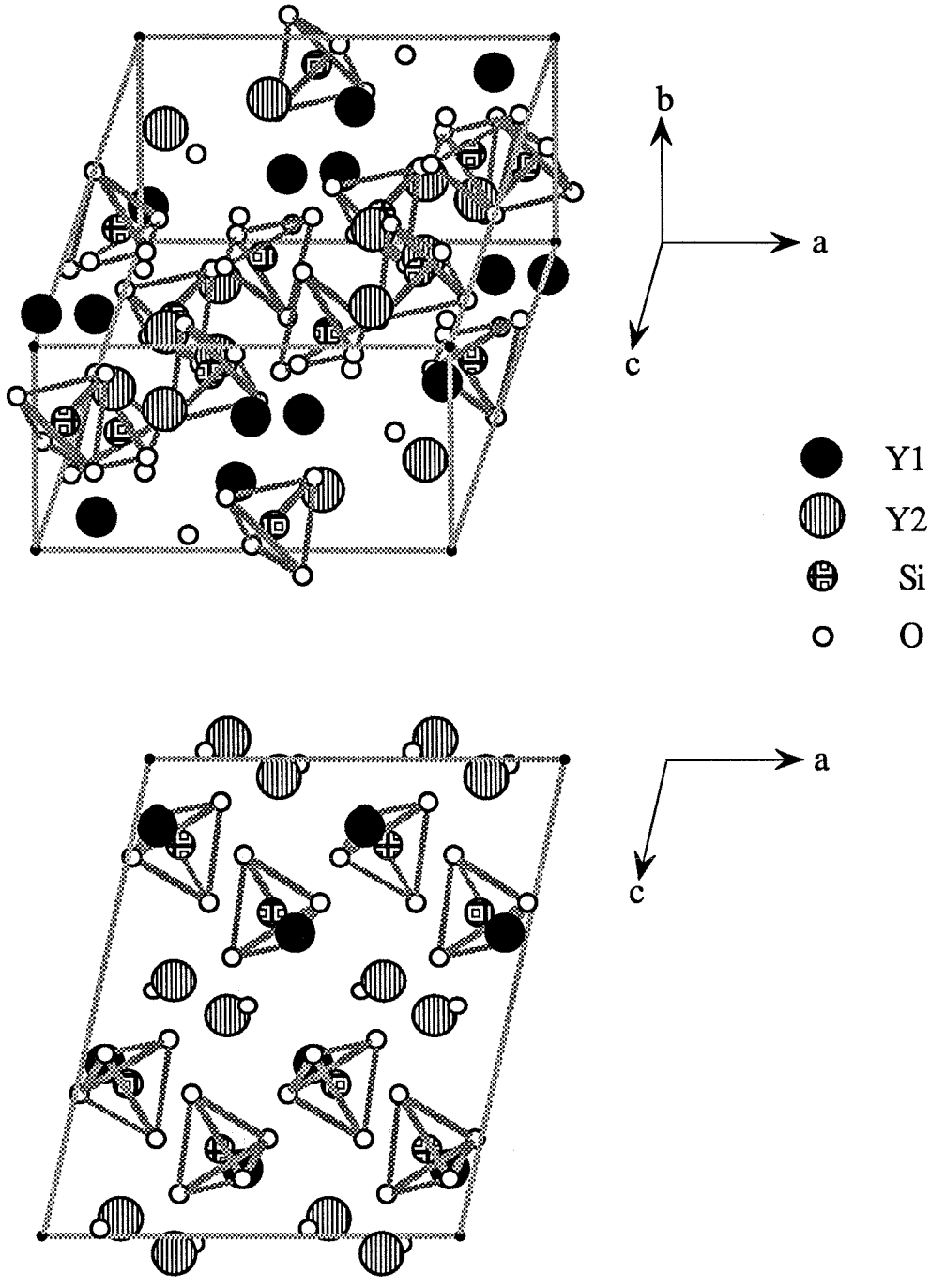

Fig. 1.2 Crystal structure of YSO (space group C2/c) [20]: a = 10.410 Å, b = 6.721 Å, c = 12.490 Å, β = 102.39°.

inductively-coupled plasma mass spectrometry; the distribution coefficient of Ce in GSO was determined to be ~0.6.

LSO and YSO crystals were grown at Schlumberger-Doll Research [23]. The 50 mm diameter iridium crucible was inductively heated, and diameter control was achieved by monitoring the weight of the crucible. Crystals were grown in a flowing atmosphere of 1 liter/min of (N_2 + 3000 ppm O_2). YSO and LSO boules were grown on iridium wires. The chemical composition of YSO and LSO was also analyzed and the distribution coefficients, of Ce in YSO and LSO were ~0.3 and ~0.2, respectively.

1.4 Light emission mechanism of Ce^{3+}

Neutral cerium has a $1s^2 2s^2 2p^6 3s^2 3p^6 3d^{10} 4s^2 4p^6 4d^{10} 4f^2 5s^2 5p^6 6s^2$ electronic configuration [24]. In liquids and solids Ce can occur in a trivalent or a tetravalent state by losing its two 6s electrons and one or both of its 4f electrons. The trivalent state with a single 4f electron is optically active. The spin-orbit interaction splits the ^2F ground state into two J states separated by $\approx$ 2253 cm^{-1} [25]. The (2J+1)-fold degeneracy of these states is reduced by the ligand field. Because the 4f electron is shielded from the ligand field by the closed 5s and 5p electron shells, the overall splitting of the ^2F_J states is small, typically only a few hundred cm^{-1}. When the 4f electron is excited to the outer 5d state, however, it experiences the full effect of the ligands. Depending upon the site symmetry, the degeneracy of the 5d state is partially or completely removed. The overall splitting of the 5d manifold is typically in the order of 5000-10000 cm^{-1}.

The transitions between the 4f ground state and the 5d excited state of Ce^{3+} are parity-allowed electric dipole transitions and thus have large oscillator strengths and short radiative lifetimes. The typical decay time of Ce^{3+} is of the order of tens of nanoseconds [26]. The Ce^{3+} in a crystal can be represented by a configuration coordinate diagram, which explains the Stokes shift (the difference in energy between absorption and emission) and the broadening of the bands (in emission and absorption) with increasing temperature

[27]. The large Stokes shift (~1800-5500 cm^{-1}) of the 4f-5d transitions is indicative of the large change in the ion-lattice coupling due to the larger radial extent of the 5d wave function compared to the 4f wave function as well as the lack of shielding of the 5d wave function. The 4f-5d transitions of Ce^{3+} typically lie in the near ultraviolet with transition energies ~30000 cm^{-1}.

The 5d $\rightarrow$ 4f fluorescence transitions of cerium doped crystals are generally thought to have a quantum efficiency near unity at low temperature. However, at elevated temperatures, nonradiative processes which depopulate the 5d level can become competitive with the radiative process and thus reduce the fluorescence lifetime.

1.5 An overview

As discussed in section 1.2, scintillator performance is characterized by detection efficiency, scintillation efficiency and speed. Among these three properties, the detection efficiency is determined by the density and atomic number of the material and is a given property once the material is chosen. Thus our efforts have been directed toward understanding and improving the latter two properties of cerium-doped rare earth oxyorthosilicates.

The scintillation properties of GSO were previously investigated [14,15]. Melcher et al. [14] discovered the existence of two decay components when GSO was excited by gamma-ray radiation. They also discovered that both primary (fast) decay and secondary (slow) decay components have strong concentration-dependence on Ce and that as the Ce concentration increases, both decay components decrease. However, the origin of these two decay components was unknown. Sekita et al. [15] observed that the emission spectrum excited by UV light at 77 K is broader than the spectrum excited at room temperature. Since the emission spectrum of Ce^{3+} should become narrower at low temperature according to the configuration coordinate model (see section 1.4), the above observation suggested the existence of an additional emission which became more evident

at low temperature.

To repeat and investigate further Sekita's low temperature measurement, we studied the optical properties of GSO at low temperature (~ 11K), using a spectrofluorometer with a refrigeration system. We also used a spectrometer, with a nitrogen flash lamp as a UV light source, to measure the decay time constant. The results are summarized in chapter 2. The results indicate that there are two types of excitation and emission spectra and two decay time constants in GSO. Since there exist two crystallographically different Gd sites, we attributed the observed two sets of optical data to two different Ce^{3+} centers occupying two gadolinium sites (Ce1 and Ce2) and proposed a two-activation-center model for GSO.

Although the structure (C2/c) of YSO and LSO is different than that ($P2_1/c$) of GSO, we also observed two types of excitation spectra and decay time constants in both YSO and LSO. We thus again attributed two types of data to Ce^{3+} centers at different rare earth sites. Thus a two-activation-center model seems to describe the scintillation mechanism of all $(RE)_2(SiO_4)O$ crystals.

However, the origins of the two decay constants observed from gamma-ray interactions in GSO could not be explained by the two-activation-center model. For example, when it is exposed to gamma rays at room temperature, 0.5 mol% GSO has two decay time constants, 56 (85~90 %) and 600 ns (10~15 %). On the other hand, the decay time constants of Ce1 and Ce2 at room temperature are 24 and 5 ns, respectively. The difference in the decay time between UV- and gamma-ray excitation suggests that there exist excitation channels which cause slow Ce^{3+} emission when GSO is exposed to gamma rays. Since for LSO and YSO, in which there is no Gd, the decay constants with gamma-ray excitation were close to the decay time constants with UV excitation, we ascribed the two kinds of slow decay time constants of GSO to the energy transfer process from Gd to Ce. Gd^{3+} shows sharp 4f-4f transitions in the UV region, and its excited states overlap Ce^{3+} absorption bands. Thus the energy of Gd^{3+} excitation can be easily transferred to Ce^{3+}. Excitation spectra of Ce1 and Ce2, in fact, contain Gd^{3+} absorption lines, which

indicates that there is energy transfer from Gd to the Ce1 and Ce2 centers.

To investigate the energy transfer from Gd to Ce, we excited Gd^{3+} absorption lines with a synchrotron light source at Brookhaven National Laboratory and monitored the Ce^{3+} emission decays. The results are summarized in chapter 3. When the absorption bands of Ce^{3+} are directly excited, the Ce^{3+} decays can be described by a single exponential. However, when ^6P_J and ^6I_J states of Gd^{3+} were excited, the decay curves of Ce^{3+} showed a long decay component and an initial build-up, which clearly indicated that the energy transfer from Gd to Ce introduces additional time dependence on the Ce emissions.

In chapter 4, energy migration through the Gd sublattice of GSO is discussed. In GSO, the Gd-Gd distance is very small (~3.57 Å), and thus the energy of the excited Gd^{3+} ion can migrate through the Gd sublattice before one of the Gd^{3+} ions near a Ce^{3+} ion transfers its energy to the Ce^{3+}. To examine the energy migration through the Gd sublattice, we grew and studied crystals in which Gd was diluted by optically inactive rare earth ions, Y^{3+} and Lu^{3+}, measuring the macroscopic transfer rate from the ^6I_J states of Gd to Ce. The dilution of the Gd is expected to increase the average Gd-Gd distance, which would result in a slower migration of energy between the Gd ions.

In chapter 5, the results of this work are summarized and suggestions are made for future work on this family of scintillators.

References

[1] D. Curie, Luminescence in Crystals (John Wiley & Sons, 1963).

[2] S. Wang, Fundamentals of Semiconductor Theory and Device Physics (Prentice Hall, 1989).

[3] J. B. Birks, The Theory and Practice of Scintillation Counting (Pergamon, 1964).

[4] C.L. Melcher, Nucl. Instr. and Meth. B40/41 (1989) 1214.

[5] A. Lempicki, A.J. Wojtowicz and E. Berman, Nucl. Instr. and Meth. A333 (1993) 304.

[6] G.F. Knoll, Radiation Detection and Measurement (John Wiley & Sons, 1979).

[7] D.J. Robbins, J. Electrochem. Soc. 127 (1980) 2694.

[8] W. van Roosbroeck, Phys. Rev. A139 (1965) 1702.

[9] A.P. Kulesskii, A.M. Korovkin, A.V. Kruzhalov, L.V. Viktorov, and B.V. Shul'gin, Zhurnal Priklanoi Spektroskopii, 48 (4) (1988) 650.

[10] C.L. Melcher, J.S. Schweitzer, A. Liberman and J. Simonetti, IEEE Trans. Nucl. Sci. NS-32 (1985) 529.

[11] K. Takagi and T. Fukazawa, Appl. Phys. Lett. 42(1) (1983) 43.

[12] B.A. Roscoe, J.A. Grau, R.A. Manente, C.L. Melcher, C.A. Peterson, J.S. Schweitzer, and C. Stroller, IEEE trans. Nucl. Sci. NS-39 (1992) 1412.

[13] C.L. Melcher, J.S. Schweitzer, R.A. Manente and C.A. Peterson, IEEE Trans. Nucl. Sci., NS-38 (2) (1991) 506.

[14] C.L. Melcher, J.S. Schweitzer, T. Utsu and S. Akiyama, IEEE Trans. Nucl. Sci., NS-37 (2) (1990) 161.

[15] M. Sekita, Y. Miyazawa, T. Akahane and T. Chiba, J. Appl. Phys. 66 (1) (1989) 373.

[16] C.L. Melcher and J.S. Schweitzer, Nucl. Instr. and Meth. A314 (1992) 212.

[17] C.L. Melcher and J.S. Schweitzer, IEEE Trans. Nucl. Sci., NS-39 (4) (1992) 502.

[18] J. Shumulovich, G. W. Berkstresser, C. D. Brandle, and A. Valentino, J. Electrochem. Soc. 135 (1988) 3141.

[19] J. Felsche, in Structure and Bonding V13, eds. Dunitz et al. (Springer-Verlag, 1973) p. 99.

[20] B.A. Maksimov, V.V. Ilyukhin, Yu.A. Kharitonov, and N.V. Belov, Sov. Phys. Crystallography 15 (1971) 806.

[21] C.D. Brandle, A.J. Valentini and G.W. Berkstresser, J. Crystal Growth 79 (1986) 308.

[22] T. Utsu and S. Akiyama, J. Crystal Growth 109 (1991) 385.

[23] C.L. Melcher, R.A. Manente, C.A. Peterson, and J.S. Schweitzer, J. Crystal Growth 128 (1993) 1001.

[24] M.J. Weber, Heavy Scintillators, eds. De Notaristefani et al. (Frontieres, 1993) p. 99.

[25] B.G. Wybourne, Spectroscopic Properties of Rare Earths (John Wiley & Sons, 1965) p. 41.

[26] L. Lyu and D.S. Hamilton, J. Lumin. 48 & 49 (1991) 251.

[27] B. Di Bartolo, Optical Interactions in Solids (John Wiley & Sons, 1968) Ch. 18.

Chapter 2

Two-activation-center model

⟨Short summary⟩

This chapter was published in Nucl. Instr. and Meth. A320 (1992) 263-272, as "UV and Gamma-Ray Excited Luminescence of Cerium-Doped Rare Earth Oxyorthosilicates."

This chapter demonstrates the existence of two different Ce^{3+} centers in cerium-doped rare earth oxyorthosilicates, $(RE)_2(SiO_4)O:Ce$ (RE = Gd, Y and Lu), and proposes the two-activation-center model.

In 1988, Sekita et al. (see ref. [3]) excited GSO by UV light at 77 K and observed a broader emission spectrum than had been observed at room temperature. However, if there is a single Ce^{3+} site, the emission spectrum of Ce^{3+} should become narrower as temperature decreases (see the configuration coordinate model of section 1.4). Thus, Sekita et al. suggested that the broadening of the emission spectrum at 77 K may be due to the existence of an additional emission band which becomes more evident at lower temperature.

To repeat and investigate further Sekita's experiment, we measured optical spectra of GSO at low temperature (~11 K), using a spectrofluorometer and spectrometer with a low-temperature refrigerator. We then discovered two types of excitation and emission spectra, and two decay time constants. Because GSO has two crystallographically different Gd sites, we attributed the two sets of optical data to two Ce^{3+} centers (Ce1 and Ce2) occupying two Gd sites leading to our proposed two-activation-center model.

We then examined this two-activation-center model by measuring the temperature-dependence of luminescent efficiency and the decay time constant for each center. At elevated temperatures, nonradiative processes which depopulate the 5d levels of Ce^{3+} can

become competitive with the radiative process and thus reduce the luminescent efficiency and lifetime. We, in fact, observed similar temperature-dependent behavior of the UV-excited decay times and the emission intensities of the two centers, which is consistent with the light emission from GSO being due to two different Ce^{3+} sites.

The confirmation of this model is that the gamma-ray excited emission spectrum, which is very different than either of the UV-excited Ce1 and Ce2 emission spectra, can be reconstructed by an appropriate combination of the Ce1 and Ce2 emission spectra.

The broadening of the emission band at low temperature is, therefore, ascribed to the increase of Ce2 emission, which becomes more evident at lower temperature.

For YSO and LSO, which have a different crystal structure than GSO but also have two different host rare earth sites, two different excitation spectra and decay time constants were similarly observed. This observation supports the existence of two Ce^{3+} centers in both YSO and LSO.

2.1 Introduction

Most of the rare-earth (RE) oxyorthosilicates, $(RE)_2(SiO_4)O$ have been successfully grown in single crystal form by the Czochralski technique [1]. Among these, $Gd_2(SiO_4)O$, $Y_2(SiO_4)O$ and $Lu_2(SiO_4)O$ have no absorption lines at visible wavelengths and thus have been examined as potential single crystal scintillators by doping with cerium. The scintillation properties of these three materials are listed in table 2.1. Because of their high density and average atomic number, reasonably high scintillation emission intensities, and fast scintillation decay times, they all show good potential as gamma-ray detectors. The purpose of this research is to understand better the light emission mechanisms of $(RE)_2(SiO_4)O$:Ce, in order to help realize their high potential as scintillators.

Ce-doped gadolinium oxyorthosilicate (GSO) was described by Takagi and Fukazawa [2] in 1983 and subsequently studied by others [3-6]. It has seen limited application in such fields as oil-well logging [7] and positron emission tomography [8,9]. Although there have been some investigations into the scintillation mechanism of GSO, some questions remain, whose answers could potentially improve GSO's scintillation properties. The existence of the two decay time components (56 and 600 ns) [4] and the broadening of the emission spectrum at 77 K compared with that at room temperature [3]

Table 2.1 Scintillation properties

	GSO	YSO	LSO
Relative emission intensity *	25	25	75
Peak wavelength (nm)	430	420	420
Decay constant (ns)	56 and 600	37 and 82	12 and 40
Density (g/cm^3)	6.7	4.54	7.4
Effective atomic no.	59	39	66

* Relative to NaI(Tl) = 100.

have not been explained. In addition, the strong dependence of the decay times and the emission intensity on Ce concentration remains to be explained [4].

The recently introduced Ce-doped lutetium oxyorthosilicate (LSO) [10] has much higher light output, faster decay time, and higher density and average atomic number than GSO and thus also has high potential as a scintillator for gamma-ray detection.

The light emission properties of Ce-doped yttrium oxyorthosilicate (YSO) have been analyzed for cathode ray tube applications [11], but due to its low effective atomic number, YSO has attracted less interest as a scintillator. However, because its crystal structure is the same as LSO, YSO also contributes to an understanding of the scintillation mechanism of $(RE)_2(SiO_4)O$:Ce.

Ce^{3+} ions can substitute for the rare-earth ions (Y^{3+}, Gd^{3+}, Lu^{3+}) in the rare-earth oxyorthosilicates and act as scintillation centers. The light emission is based on the electronic transition of a Ce^{3+} ion from excited 5d levels to the 4f ground state levels, typically with decay times of tens of nanoseconds. The Ce^{3+} ion fluoresces in the blue region in these host materials, which allows these scintillators' light output to be effectively converted by the photocathodes in most photomultiplier tubes. Because of the apparent simplicity of the light emission mechanism of the Ce^{3+} ion, the scintillation mechanism of $(RE)_2(SiO_4)O$:Ce was expected to be resolved by simply applying the emission model of a single Ce^{3+} site. However, this model does not explain the broadening of the emission spectrum at low temperature or the existence of two decay components, which is especially dramatic in GSO.

Most previous investigations into the scintillation properties of $(RE)_2(SiO_4)O$:Ce have used relatively high-energy excitations like gamma rays and fast electrons [10,12]. At these excitation energies, which are well above the band gap of the host rare-earth oxyorthosilicates, it has been difficult to analyze the energy band structure. In addition, most measurements have been made at room temperature; thus, the emission, excitation, and absorption bands display significant thermal broadening. In the current work the

emission spectra and the decay times were measured with UV-excitation in order to excite directly selected 5d energy levels and at temperatures as low as 11 K to reduce thermal broadening.

In previous studies the fact that the Ce^{3+} activator ion can occupy two different crystallographically independent sites in $(RE)_2(SiO_4)O$ has been overlooked in considering the light emission mechanism. Felsche [13] shows that $Gd_2(SiO_4)O$ has the monoclinic structure of space group $P2_1/c$. The Gd^{3+} ions occupy two distinct sites. One site is surrounded by 7 oxygen ligands; the other site is surrounded by 9 oxygen ligands. On the other hand, the crystal structure of space group B2/b has been defined for $Y_2(SiO_4)O$ and $Lu_2(SiO_4)O$. The rare earth ions occupy two sites with 6 and 7 oxygen ligands. This fact that the Ce^{3+} ions occupy two independent sites and experience two different crystal fields will be reflected in the experimental results and plays a key role in supporting the two-activation-center model which will be proposed.

2.2 Experimental techniques

All the crystals used in this study were grown by the Czochralski technique using raw materials with purities of at least 99.99%. GSO crystals were purchased from Hitachi Chemical Co., Ltd. YSO and LSO single crystals were grown in our laboratory. The Ce concentration in the melts from which the crystals were grown was 0.25% relative to the rare earth content. However, the Ce concentration in the crystals depends on the distribution coefficient of Ce in each host material. The structure of these crystals was analyzed by the powder x-ray diffraction method. The results confirmed that GSO had a monoclinic P structure and that both YSO and LSO had monoclinic C structures.

The excitation and emission spectra were measured with a SPEX Fluorolog-2 spectrofluorometer (fig. 2.1). A CTI-CRYOGENICS refrigeration system (Model 21) could maintain samples at temperatures as low as 11 K. The temperature of the sample was controlled by a nichrome heater wire (NC-32, Lakeshore Electronics) and monitored by a

silicon diode sensor (CY7-CU4, OMEGA Electronics) which was mounted on the copper sample holder. The stability of the temperature was ±1 K. The light source was an ozone-free 450 W xenon lamp. Double monochrometers were used in both the excitation and the emission light paths. The bandpass was 0.18 nm for the UV-excitation and 12.6 nm for the gamma-ray excitation experiment. The crystals (1 x 1 x 1 cm^3) were mounted on the cold station of the refrigerator. In UV experiments, the excitation beam was normal to the front face of the crystal, and the emission optics were collimated at 22.5° from the normal as shown in the figure. For gamma-ray excited measurements, the geometry was the same except that an uncollimated ^{241}Am source was placed 1.8 cm in front of the sample.

Absorbance measurements were performed with a spectrophotometer (Model U-3210, Hitachi Instruments), using the same refrigeration system as in the excitation and emission measurements, but with a ladder containing multiple samples replacing the single crystal holder shown in fig. 2.1.

The measurements of the decay time with UV-excitation were performed with a nanosecond flash lamp system (LS-100, Photon Technology International, Inc.). This flash lamp uses nitrogen as the plasma gas, and the excitation pulses have a duration of

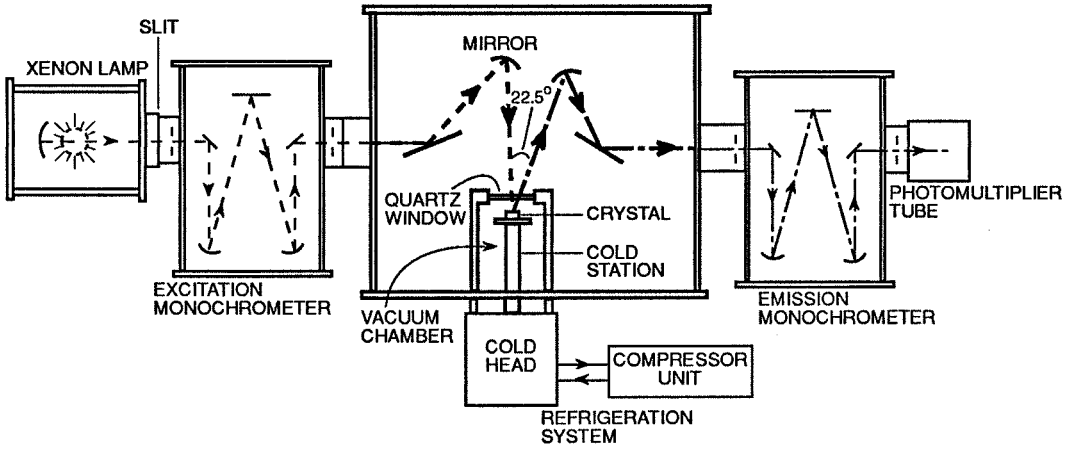

Fig. 2.1 Optical configuration of the spectrofluorometer with the refrigeration system.

about 6 ns. The wide range of excitation wavelength (294-407 nm) of this N_2 flash lamp made it possible to excite the scintillators at various UV wavelengths. Monochrometers were used to select the excitation and emission wavelengths. The bandpass was 2 nm for the excitation measurements and 8 nm for the emission measurements. The emitted light was detected at a right angle to the direction of the incident light. Decay measurements were made at temperatures from 77 K to 300 K by immersing the sample in various organic solvents which were cooled to their freezing points by mixing with liquid nitrogen in a quartz dewar flask [14]. The temperature of the two-component mixture was monitored by the same CY7-CU4 silicon diode sensor. The stability of the temperature was ±2 K.

Measurements of the gamma-ray excited decay were made, using the time-correlated single photon technique [15]. The decay data were deconvoluted and analyzed with a least squares fitting technique for both UV and gamma-ray excitation.

2.3 Results

2.3.1. GSO

A configuration coordinate model is often used to explain the luminescence properties of crystals, including those doped with Ce [16]. In the case of crystals doped with the Ce^{3+} ion, such a model predicts excitation bands corresponding to the excited 5d states of the ion and emission bands corresponding to transitions from the lowest 5d level to the $^2F_{5/2}$ and $^2F_{7/2}$ ground states. The model also predicts that both the excitation and emission bands will become narrower as the temperature is lowered. In contrast to the predictions of this model, Sekita et al. [3] observed a broadening of the emission of Ce-doped GSO at 77K, compared to the room temperature spectrum, which suggested the existence of an additional emission which became more evident at low temperature.

We measured the excitation spectrum of GSO at 11K in order to reduce thermal broadening and to investigate the 5d levels of Ce^{3+} in more detail. The solid curve (marked "1") in fig. 2.2a is the excitation spectrum measured at 11K for an emission wavelength of

420 nm. Essentially this same spectrum has been reported previously [3,4], although at higher temperatures, and the bands have been identified with the 5d levels of Ce^{3+}. The lowest energy 5d level corresponds to the excitation band at 345 nm. Surprisingly, however, we found that when the emission wavelength is changed to 500 nm, a markedly different excitation band structure is observed which is shown as the dashed curve (marked "2") in fig. 2.2a. In this case, the lowest energy excitation band appears at 378 nm. This spectrum already suggests the existence of a second luminescence center.

We measured the emission spectrum of GSO using excitation wavelengths corresponding to the strongest excitation bands in spectra "1" and "2" of fig. 2.2a, i.e., 345 and 378 nm. As shown in fig. 2.2b, two distinct emission spectra are observed. Exciting the 345 nm band gives rise to the well known GSO emission at ~430 nm (marked "1"), while exciting the 378 nm band gives rise to a previously unobserved emission at ~ 480 nm (marked "2"). Note that the shapes of both emission spectra are consistent with a doublet structure indicating transitions to a split ground state as expected for Ce^{3+}.

Fig. 2.3a and 2.3b show the excitation and emission spectra at 296 K. As can be seen in these figures, emission 1 is dominant at this temperature. Only at very low temperature do emission 1 and emission 2 have comparable intensities. This explains why previous studies, which were conducted mostly at room temperature, have observed evidence of only one luminescence center.

Fig. 2.4 shows absorbance spectra of a 0.27 mm thick GSO crystal at 11 K and at 299 K. At 299 K there are two bands located at 284 and 345 nm which correspond to bands in the 296 K excitation spectrum in fig. 2.3a and to curve 1 in fig. 2.2a. These absorption bands are also seen at 11 K along with a band at 378 nm, and a possible band near 300 nm, which correspond to bands in the curve 2 excitation spectrum in fig. 2.2a. (The lines at 247, 252 and 275 nm are due to absorption by Gd^{3+}.)

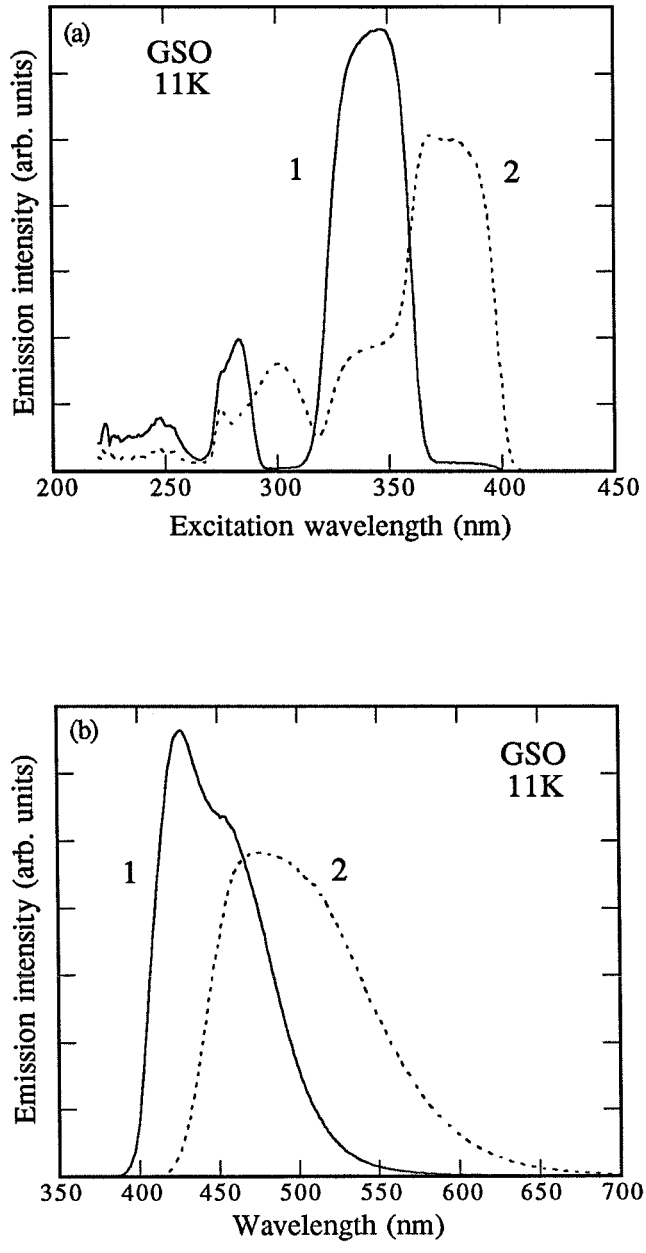

Fig. 2.2 Excitation (a) and emission (b) spectra of GSO at 11 K. The excitation spectra were measured at the two emission wavelengths of 420 nm (solid line) and 500 nm (dashed line). The two emission spectra have excitation wavelengths of 345 nm (solid line) and 378 nm (dashed line).

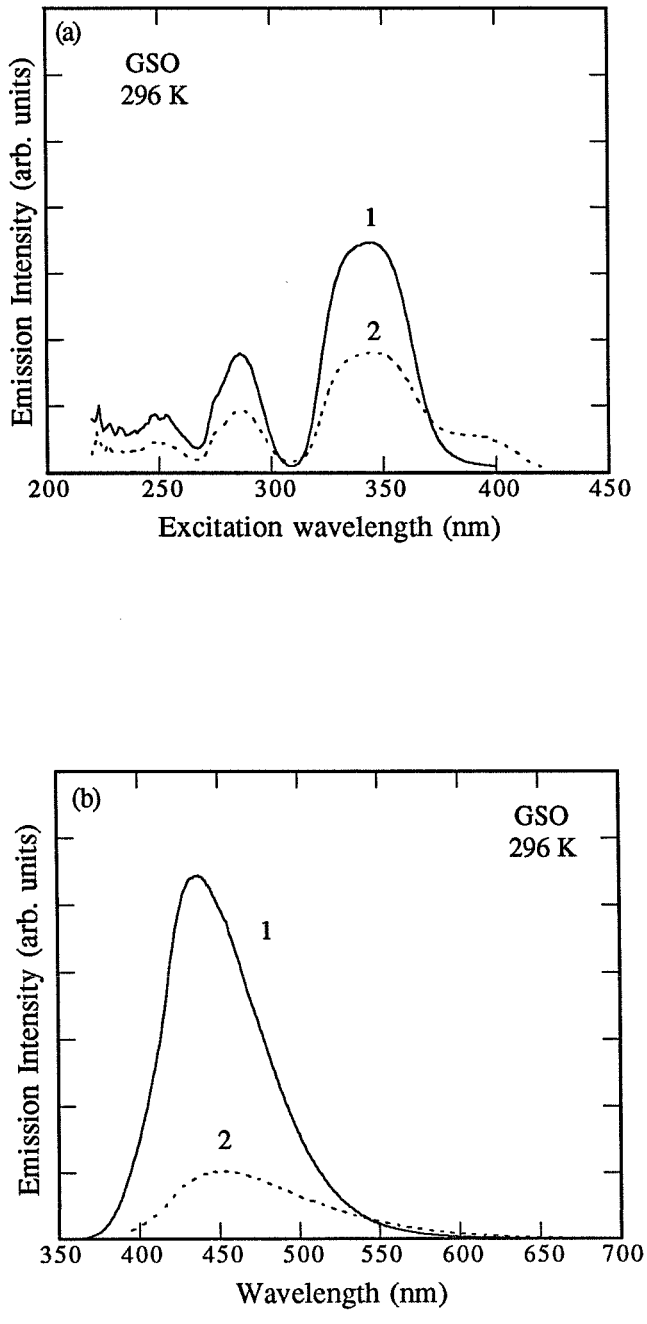

Fig. 2.3 Excitation (a) and emission (b) spectra of GSO at 296 K. The monitored emission wavelengths and excitation wavelengths are the same as in fig. 2.2 for each spectrum.

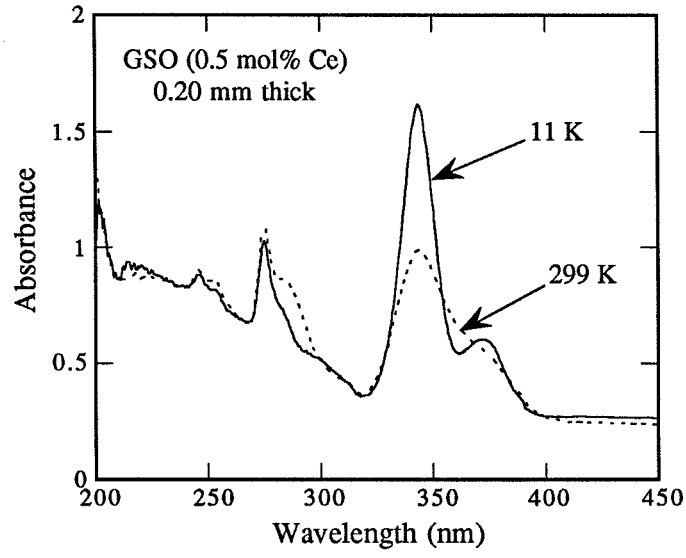

Fig. 2.4 Absorbance spectra of GSO at 11 K (solid line) and 299 K (dashed line).

Although the excitation and absorption spectra taken near 300 K might be explained by the existence of a single Ce^{3+} site, the spectra at 11 K clearly reveal the existence of a second site. A similar phenomenon has been previously observed in Ce-Mn activated Fluorophosphate FAP:Ce, Mn [17], for which two series of Ce^{3+} emission spectra corresponding to two excitation wavelengths were found. Our emission spectra of GSO at 11 K are, in fact, very similar to those of FAP:Ce, Mn. In light of the existence of two sets of excitation and emission spectra, and since we know that the Ce^{3+} ions can occupy two distinct crystallographic sites, it is reasonable to assume the existence of two distinct Ce^{3+} luminescence centers in GSO:Ce. For convenience, we will refer to these centers as Ce1 and Ce2. We arbitrarily designate Ce1 as the center responsible for excitation bands at 284 and 345 nm (curve 1 in figs. 2.2 and 2.3) and Ce2 as the center responsible for excitation bands at 300 and 378 nm (curve 2 in figs. 2.2 and 2.3). It follows that the emission at 425 nm is due to Ce1, and the emission at 480 nm is due to Ce2. Similarly, the absorption

Table 2.2 The emission, excitation, and absorption bands of two Ce^{3+} centers in GSO

	Ce 1	Ce2
Emission band [nm]	425	480
Excitation band [nm]	284 345	300 378
Absorption band [nm]	284 345	300(?) 378

bands at 284 and 345 nm are due to Ce1 while the absorption bands at 300 and 378 nm are due to Ce2. At room temperature the excitation, absorption, and emission spectra are dominated by the Ce1 center, while at 11 K luminescence from each of the two centers is easily observed. The excitation, absorption, and emission bands associated with each center are summarized in table 2.2.

If we examine the two-activation-center model by considering that only transitions from the lowest excited 5d level to the ground 4f levels are induced to prevent any complications rising from photoionization of the Ce^{3+} ion, the total decay rate $1/\tau$ for each Ce^{3+} site is given by

$$1/\tau_1 = 1/\tau_{1r} + 1/\tau_{1nr} \qquad \text{for Ce1} \qquad (2.1)$$

$$\text{and} \quad 1/\tau_2 = 1/\tau_{2r} + 1/\tau_{2nr} \qquad \text{for Ce2,} \qquad (2.2)$$

where $1/\tau_r$ and $1/\tau_{nr}$ are the radiative and nonradiative decay rates, respectively. Though the radiative decay rate $1/\tau_r$ includes both a purely radiative transition (temperature-independent) and a phonon-assisted transition (temperature-dependent), it is assumed that the contribution of the latter to the radiative decay rate is negligible in the temperature range of interest (< 300 K), and that the radiative decay is temperature-independent. It is also assumed that the functional form of $1/\tau_{nr}$ is the Arrhenius equation [18]:

$$1/\tau_{1nr} = s_1 \exp(-\Delta E_1/kT) \quad (2.3)$$

and $$1/\tau_{2nr} = s_2 \exp(-\Delta E_2/kT), \quad (2.4)$$

where s is a frequency factor and ΔE is an activation energy. Thus the measured fluorescence lifetime, τ, has the following temperature dependence:

$$\tau_1 = [1/\tau_{1r} + s_1 \exp(-\Delta E_1/kT)]^{-1} \quad (2.5)$$

and $$\tau_2 = [1/\tau_{2r} + s_2 \exp(-\Delta E_1/kT)]^{-1}. \quad (2.6)$$

When the absorption cross section and radiative transition probabilities are assumed to be independent of temperature, it can be shown [19] that the temperature dependence of the luminescence quantum efficiency, Q(T), is given by:

$$Q(T) = [1/\tau_r] / [1/\tau_r + 1/\tau_{nr}], \quad (2.7)$$

which shows that the temperature dependence of the emission intensity is expected to be identical with that of the luminescence decay time.

Fig. 2.5a and 2.5b show the emission spectra of Ce1 and Ce2 as a function of temperature. The longest wavelength peaks (345 and 378 nm) in the excitation spectra were chosen for exciting the two Ce^{3+} centers (Ce1 and Ce2) to distinguish clearly the two emission spectra. The emission spectra of Ce1 and Ce2 become broad with increasing temperature, in good agreement with the configuration coordinate model. The two emission peaks of Ce1 merge and the emission intensity decreases with increasing temperature (fig. 2.5a). Thus at room temperature, two separate peaks from decays to the two 4f levels can no longer be resolved. Compared with Ce1, the temperature dependence of the Ce2 emission above 200 K is striking (fig. 2.5b). The peak position of the Ce2 emission shifts to shorter wavelengths above 250 K. This peak shift implies that there is a contribution from Ce1 in these spectra. This contribution increases with increasing

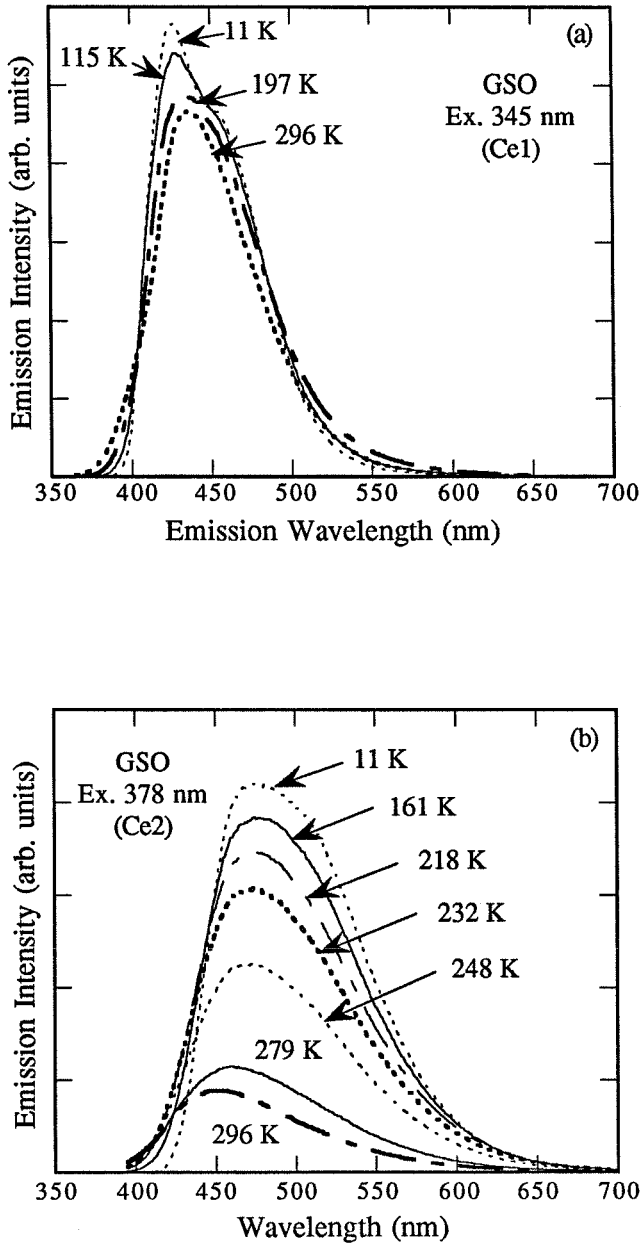

Fig. 2.5 Emission spectra of GSO as a function of temperature (between 11 and 296 K) for excitation of Ce1 at 345 nm (a) and of Ce2 at 378 nm (b).

temperature. The luminescence efficiency of the two Ce^{3+} sites are shown as a function of temperature in fig. 2.6.

Fig. 2.7 shows both a typical decay curve of GSO together with the pulse from the N_2 flashlamp, which has about a 6 ns duration and a long decaying tail. This GSO decay curve was obtained at an excitation wavelength of 337 nm (Ce1) at 299 K. The excitation and emission wavelengths for Ce1 and Ce2 were carefully chosen to minimize overlap of the emission curves of the two Ce^{3+} sites. The excitation and emission wavelengths are 337 and 420 nm for Ce1, and 381 and 500 nm for Ce2, respectively. Fig. 2.8 shows the temperature dependence of the lifetimes of the Ce1 and Ce2 centers. The intrinsic (77 K) lifetimes of Ce1 and Ce2 are 27 ns ($= \tau_{1r}$) and 43 ns ($= \tau_{2r}$), respectively. The rollover point of the lifetime of Ce1 is near 270 K and that of Ce2 is near 200 K. This trend in the temperature-dependence of the two lifetimes is identical with the behavior of the emission intensity (fig. 2.6), as expected from the Arrhenius equation. Thus, all of the data obtained are consistent with the light emission from GSO being due to two different crystal sites for the Ce^{3+} activator.

2.3.2. YSO

Since excitation and emission spectra of YSO have only been reported at room temperature [11], the existence of the two Ce^{3+} sites has been overlooked in analyzing the light emission. Fig. 2.9 shows the excitation spectrum of YSO at 11 K. The emission wavelengths for the two excitation spectra are 400 nm (solid) and 500 nm (dashed). Although the crystal structure of YSO is different than that of GSO, it also has two independent rare-earth sites resulting in two luminescence centers as in GSO.

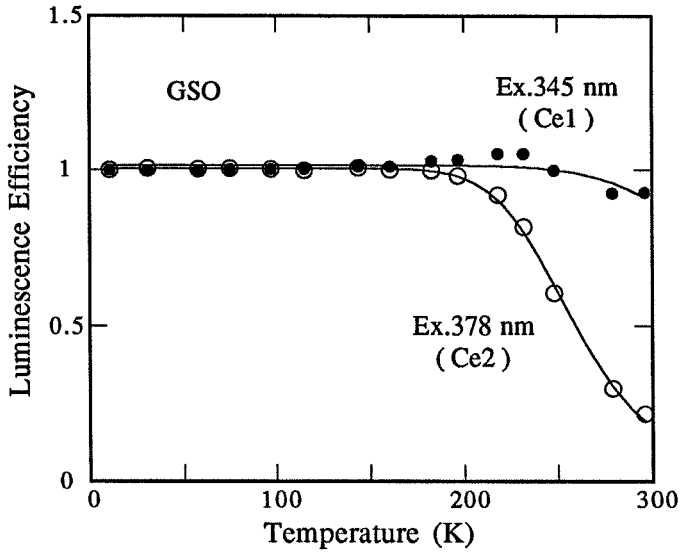

Fig. 2.6 The luminescence efficiency of Ce1 (solid line, excited at 345 nm) and Ce2 (dashed line, excited at 378 nm) in GSO as a function of temperature. The emission intensity obtained at each temperature was normalized to the intensity at 11 K.

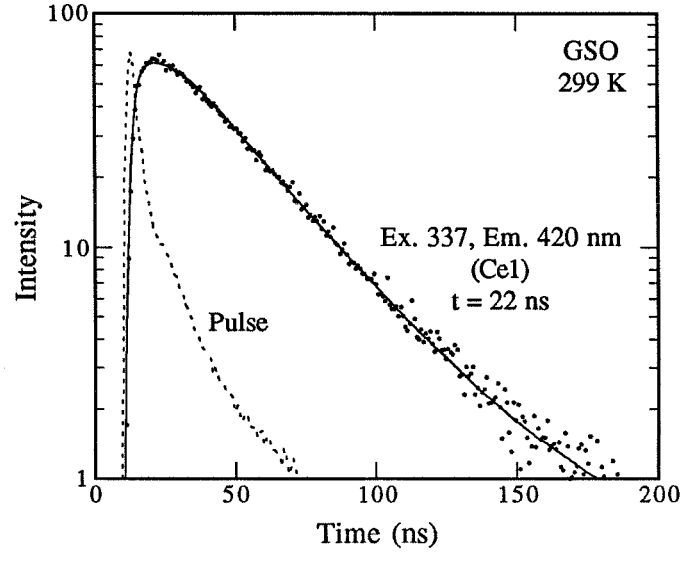

Fig. 2.7 Typical UV-excited decay curve of GSO for excitation at 337 nm and emission at 420 nm (Ce1). The dashed line indicates the nitrogen flash pulse. The scattered points are the measured data. The solid curve is a fit to the data with a single exponential (22 ns decay).

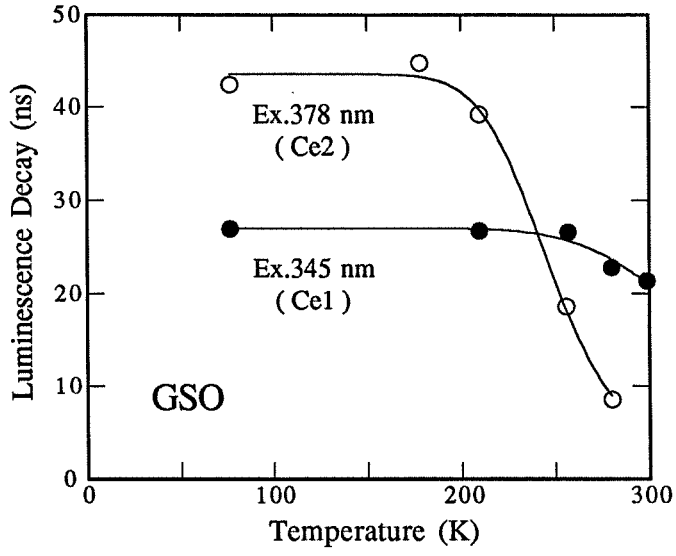

Fig. 2.8 UV-excited luminescent decay of Ce1 (solid line) and Ce2 (dashed line) in GSO as a function of temperature. The excitation and emission wavelengths were 337 and 420 nm for Ce1, and 381 and 500 nm for Ce2, respectively.

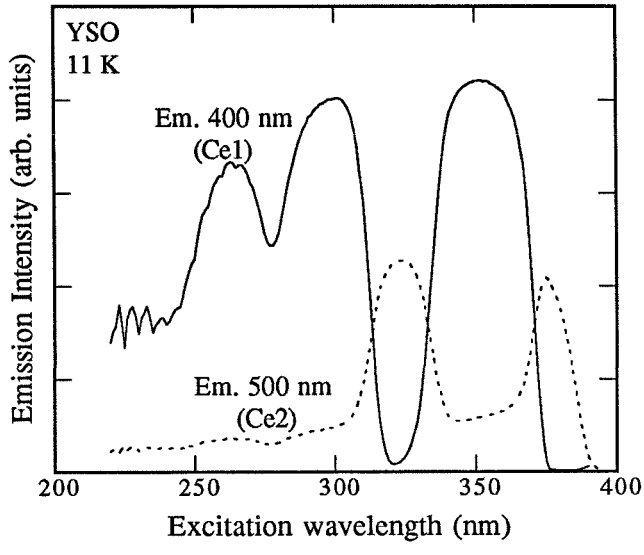

Fig. 2.9 Excitation spectra of YSO at 11 K. The solid line is the spectrum monitored at an emission wavelength of 400 nm (Ce1), and the dashed line is the spectrum monitored at an emission wavelength of 500 nm (Ce2).

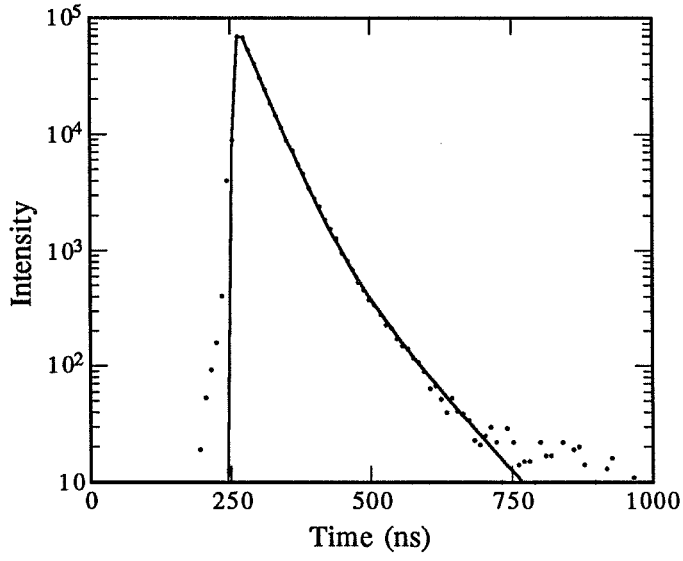

Fig. 2.10 The gamma-ray excited decay curve of YSO at room temperature determined with a single photon counting technique. ^{137}Cs was used as the gamma-ray source.

Table 2.3 Gamma-ray and UV-excited luminescent decay times (in ns) of GSO, YSO and LSO near room temperature. The UV-excited luminescent decay times were measured with the excitation of the lowest excited 5d level of the Ce^{3+} ion.

	GSO	YSO	LSO
Gamma-ray excited decay	56 and 600	37 and 82	12 and 40
UV-excited decay	22 (Ex. 337, Em. 420 nm) <6 (Ex. 381, Em. 500 nm)	39 (Ex. 358, Em. 400 nm) 59 (Ex. 381, Em. 500 nm)	34 (Ex. 358, Em. 400 nm) 42 (Ex. 381, Em. 480 nm)

The gamma-ray excited decay curve at room temperature is shown in fig. 2.10. The measured lifetimes from a double exponential fit are 37 and 82 ns. The measurement of the decay time with UV-excitation was made at excitation wavelengths of 358 and 381 nm and emission wavelengths of 400 and 500 nm for the Ce1 and Ce2 sites, respectively (at 298 K, table 2.3). Each UV-excited decay spectrum was fit with a single exponential. Time constants of 39 ns for Ce1 and 59 ns for Ce2 were obtained.

2.3.3 LSO

This newly invented scintillator has the same monoclinic C structure as YSO and thus it is expected that the light emission mechanism of LSO would be similar to that of YSO. The excitation spectrum of LSO at 11 K is shown in fig. 2.11. The monitored emission wavelengths for the two excitation spectra are 420 nm (solid) and 480 nm (dashed). The existence of two Ce^{3+} luminescence centers is also clear for LSO.

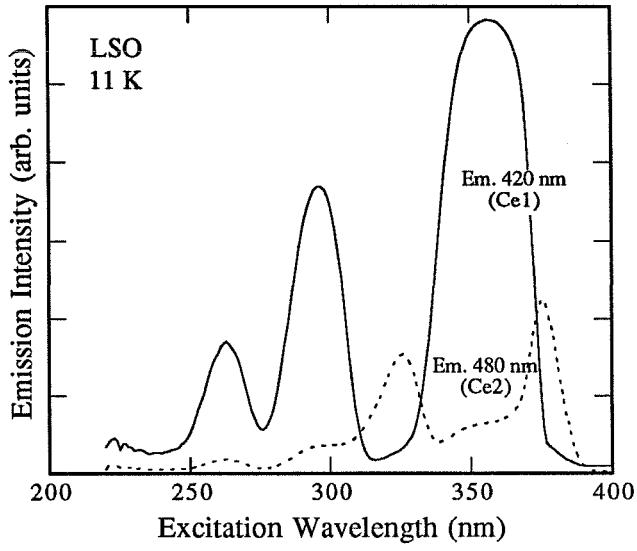

Fig. 2.11 Excitation spectra of LSO at 11 K. The solid line is the spectrum monitored at an emission wavelength of 420 nm (Ce1), and the dashed line is the spectrum monitored at an emission wavelength of 480 nm (Ce2).

The decay time is given in table 2.3 for both gamma-ray and UV-excited emission. The decay times with gamma-ray excitation were 12 and 40 ns from a double exponential fit. The excitation and emission wavelengths for Ce1 were 358 and 400 nm and were 381 and 480 nm for Ce2. The decay time from the UV-excitation of Ce1 was 34 ns and that of Ce2 was 42 ns.

2.4 Discussion

A significant confirmation of the two-activation-center model is that the gamma-ray excited emission can be duplicated by adding the appropriately weighted UV-excited emissions of Ce1 and Ce2. Fig. 2.12 shows the gamma-ray excited emission, the UV-excited emissions of Ce1 and Ce2, and a weighted combination of the Ce1 and Ce2 emissions for GSO at 11 K. This calculated emission spectrum was obtained by adding the

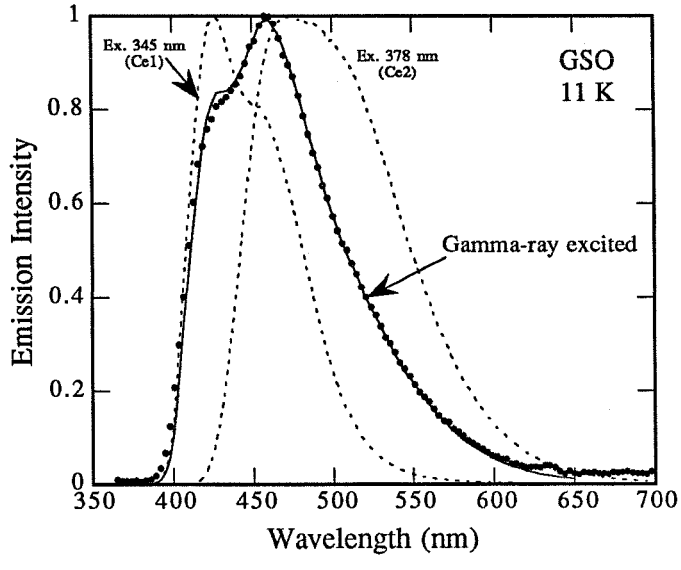

Fig. 2.12 The gamma-ray excited emission (filled circles), the UV-excited emissions of Ce1 (excited at 345 nm) and Ce2 (at 378 nm) (dashed lines), and a weighted combination of the Ce1 and Ce2 emissions (solid line) for GSO at 11 K. All the measured spectra are normalized to their peak intensity.

emission spectra of Ce1 (Ex. 345 nm) and Ce2 (Ex. 378 nm) in a ratio of 58:42. It is clear from fig. 2.12 that the gamma-ray excited emission at 11 K, which is very different from either the UV-excited emissions of Ce1 or Ce2, is well fit by a weighted combination of the Ce1 and Ce2 emission spectra. This agreement between the gamma-ray excited emission and the weighted combination of Ce1 and Ce2 emissions implies that, at 11 K, both Ce1 and Ce2, which have very different energy band structures (fig. 2.2a), contribute to the gamma-ray excited emission. It was also confirmed that at all temperatures (between 11 and 300 K) the gamma-ray excited emission can be obtained from a weighted combination of Ce1 and Ce2 emission spectra. Fig. 2.13 shows the temperature dependence of the normalized gamma-ray excited emission. The decrease in the emission intensity at longer wavelengths above 200 K can thus be attributed to a decrease in the intensity of the Ce2 emission.

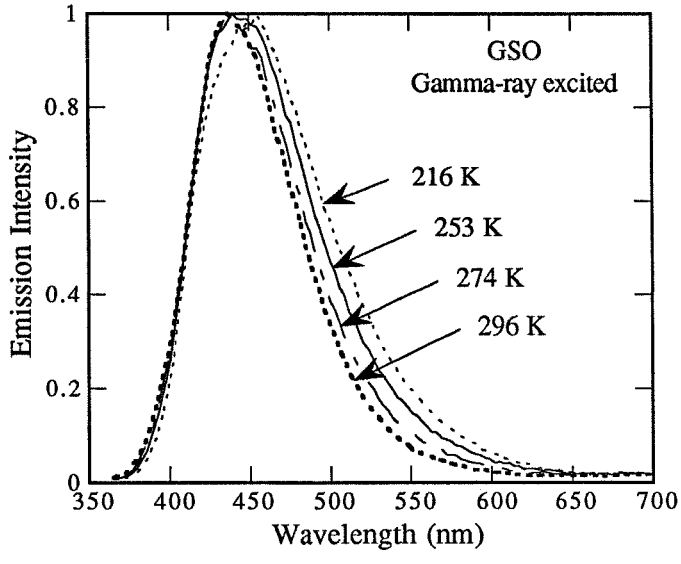

Fig. 2.13 Gamma-ray excited emission spectra of GSO at temperatures between 200 and 300 K. All the spectra are normalized to their peak intensity.

The UV-excited emission spectra of Ce1 and Ce2 discussed above were all obtained by exciting the lowest 5d level, and a simple configuration coordinate model was used to analyze the temperature-dependence of the spectra. In fig. 2.14 the luminescence efficiency from the second excited 5d level of Ce1 and Ce2, and that of gamma-ray excited emissions are shown as a function of temperature. The excitation wavelengths for Ce1 and Ce2 are 284 nm and 310 nm, which correspond to the lower wavelength bands in the excitation spectra shown in fig. 2.2. The shape of the UV-excited luminescence spectra from the second excited 5d level of Ce1 and Ce2 were identical with those from the lowest excited 5d level at all temperatures. The luminescence efficiency from the second excited 5d level of Ce1 rises to a maximum at about 230 K. The intensity of Ce2 begins to decrease at about 180 K. The results, particularly for Ce1, cannot be described by the Arrhenius' equation, implying that the simple model used to describe the emissions from the lowest energy excitation bands is not appropriate, and other factors must be taken into

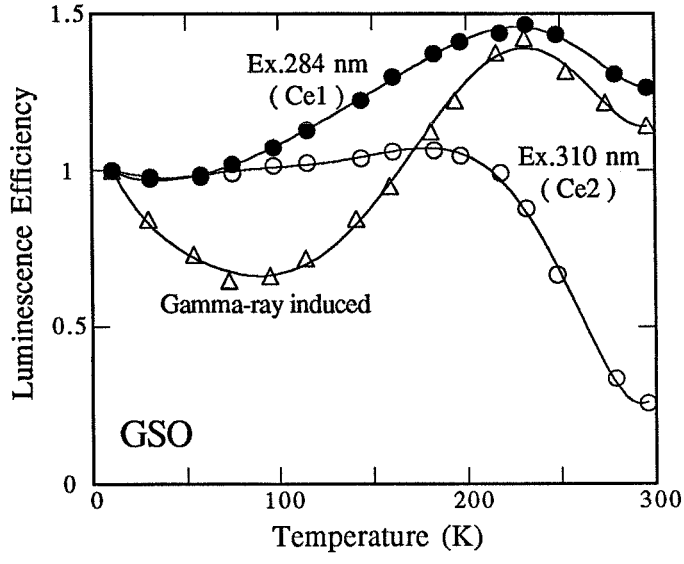

Fig. 2.14 The luminescence efficiency from the UV-excitation of the second 5d level of Ce1 (solid line) and Ce2 (dashed line), and that from gamma-ray excitation (dot-dash line), as a function of temperature. The intensity obtained at each temperature was normalized to the emission intensity at 11 K.

account to describe the UV-excited emission from the second excited 5d level of Ce^{3+} ion. The temperature dependence of the gamma-ray excited emission intensity, shown in fig. 2.14, is difficult to explain from the dependence of the UV-excited responses shown in this figure and in fig. 2.6.

In fig. 2.2a, three peaks were observed at 247, 252 and 275 nm in the excitation spectra of each Ce^{3+} site for GSO. Since the position of these peaks correspond to absorption lines of the Gd^{3+} ion, it is clear that energy absorbed at these wavelengths by the Gd^{3+} ion is transferred to the Ce^{3+} ion. This fact is important in considering the energy transfer mechanism in the gamma-ray excited response, as the gamma rays lose energy primarily through interactions with the Gd^{3+} ions. GSO has two gamma-ray excitation decay components, 56 (85 - 90 %) and 600 ns (10 - 15 %), but the UV-excited luminescence decay times are 22 ns for Ce1 and < 6 ns for Ce2 from the excitation of the lowest 5d level near room temperature. Even at 77 K, the UV-excited decay times of Ce1 and Ce2 (fig. 2.8) are only 27 and 43 ns. This significant difference in decay times between the UV-excited and the gamma-ray excited emissions, as well as the temperature-dependent behavior of the gamma-ray excited emission intensity, suggest an energy transfer mechanism from Gd^{3+} to Ce^{3+} which is strongly temperature-dependent.

The difference of the decay constants between gamma-ray and UV-excitation in GSO can be contrasted with the behavior in YSO and LSO, in which the decay times for both types of excitation are closer. In the cases of YSO and LSO the gamma-ray excited decay times are, near room temperature, 37 and 82 ns for YSO, and 12 and 40 ns for LSO. UV-excited luminescence decay times are 39 and 59 ns for YSO and 34 and 42 ns for LSO. The agreement of the gamma-ray excited decay times with the UV-excited ones in YSO and LSO indicates that the gamma-ray excited luminescence decay is primarily determined by the luminescence of the Ce^{3+} ion in those crystals, though the short component (12 ns) of gamma-ray excited decay in LSO remains to be investigated. However, this assumption must be examined more carefully, for instance, by comparing the gamma-ray excited decay

times with UV-excited ones as a function of temperature.

The previously observed broadening effect of the emission spectrum of GSO at 77 K compared with that at room temperature in Sekita's paper [3] can be explained by the existence of the Ce2 emission band at low temperature. Although in his paper the excitation wavelength for the UV-excited emission was not stated, it is likely that both Ce1 and Ce2 were excited in his emission measurement at 77K.

Future experiments and calculations will attempt to address the explanation for the relative contributions of Ce1 and Ce2 emissions to the gamma-ray excited emission (fig. 2.12).

2.5 Conclusion

The absorption, excitation, and emission spectra, and crystallographic data on GSO, lead to the conclusion that GSO has two luminescence centers. The existence of these two luminescence centers in GSO is supported by the agreement of the temperature-dependent behavior of the UV-excited decay times and the emission intensities of the two centers. Excitation spectra for both YSO and LSO also indicate two luminescence centers, which is consistent with the fact that these crystals also have two rare-earth sites, despite their having a different structure than GSO. The gamma-ray excited emission can be reconstructed from weighted combinations of the Ce1 and Ce2 emission spectra in GSO, but the gamma-ray excited temperature response is difficult to explain from the measured UV-excited temperature responses. The long gamma-ray excited decay times of GSO, as compared with the UV-excited decay times, as well as the dependence of the gamma-ray excited decay times and emission intensity on the Ce^{3+} concentration in GSO remain to be explained.

Acknowledgments

We are grateful to Ralph Manente and Carl Peterson for their assistance in growing

the crystals and in obtaining the data, and to Oliver Mullins and Yifu Zhu for many valuable discussions.

References

[1] G. V. Anan'eva, A. M. Korovkin, T. I. Merkulyaeva, A. M. Morozova, M. V. Petrov, I. R. Savinova, V. R. Startsev, and P. P. Feofilov, Izvestiya Akademii Nauk SSSR, Neorganicheskie Materialy, 17(6) (1981) 1037.

[2] K. Takagi and T. Fukazawa, Appl. Phys. Lett. 42(1) (1983) 43.

[3] M. Sekita, Y. Miyazawa, T. Akahane, and T. Chiba, J. Appl. Phys. 66(1) (1989) 373.

[4] C. L. Melcher, J. S. Schweitzer, T. Utsu, and S. Akiyama, IEEE Trans. Nuc. Sci. 37(2) (1990) 161.

[5] M. Kobayashi and M. Ishii, Nucl. Instr. and Meth. B61 (1991) 491.

[6] T. Utsu and S. Akiyama, J. Crystal Growth 109 (1991) 385.

[7] B. Roscoe, J. Grau, R. Manente, C. L. Melcher, C. Peterson, J. Schweitzer, and C.Stoller, IEEE Trans. Nucl. Sci. NS-39(5) (1992) 1412.

[8] M. Dahlbom, M. A. Mandelkern, E. J. Hoffman, A. R. Ricci, J. B. Barton, J. S. Iwanczyk, and A. J. Dabrowski, IEEE Trans. Nucl. Sci. 32(1) (1985) 533.

[9] A.A. Abramov et al., Pribory i Tekhnika Eksperimenta, 5 (1990) 78.

[10]C. L. Melcher and J. S. Schweitzer, Nucl. Instr. and Meth. A314 (1992) 212.

[11] J. Shumulovich, G. W. Berkstresser, C. D. Brandle, and A. Valentino, J. Electrochem. Soc. 135 (1988) 3141.

[12] H. Ishibashi, Nucl. Instr. and Meth. A294 (1990) 271.

[13] J. Felsche, in Structure and Bonding V13, eds. Dunitz et al. (Springer-Verlag, 1973) p. 99.

[14] R. E. Rondeau, J. Chem. Eng. Data 11 (1966) 124.

[15] L. M. Bollinger and G. E. Thomas, Rev. Sci. Instr. 32 (1961) 1044.

[16] B. Di Bartolo, Optical Interactions in Solids (John Wiley & Sons, 1968) Chap. 18.

[17] J. Zhou, M. Tang, and X. Luo, J. Lumin. 40 & 41 (1988) 381.

[18] L. Lyu and D. S. Hamilton, J. Lumin. 48 & 49 (1991) 251.

[19] J. B. Birks, The Theory and Practice of Scintillation Counting (Pergamon, 1964) Chap. 4.

Chapter 3

Energy transfer from Gd to Ce in $Gd_2(SiO_4)O:Ce$

⟨Short summary⟩

This chapter was submitted to Nucl. Instr. and Meth. (1994) as "The Role of Gadolinium in the Scintillation Processes of Cerium-doped Gadolinium Oxyorthosilicate."

This chapter investigates the origins of the two decay time constants observed by Melcher et al. (see ref. [2]) when GSO is exposed to gamma radiation and to describe the overall scintillation mechanism of GSO.

When the $Ce1^{3+}$ absorption band is directly excited by UV light, the $Ce1^{3+}$ decay is a single exponential (~24 ns). However, when GSO is excited by gamma rays, the $Ce1^{3+}$ decay shows a build-up and a long decay component, both of which strongly depend on Ce concentration. This build-up and long decay in $Ce1^{3+}$ decay suggest the existence of excitation channels which transfer energy to $Ce1^{3+}$ and cause slow emission decay.

Since a slow decay component is detrimental to the timing capability of GSO, it is important to know the origins of this slow decay component.

As a possible explanation for an excitation channel which transfers energy to $Ce1^{3+}$, we considered the Gd^{3+} ions. Gd^{3+} shows very sharp 4f-4f transitions in the UV and its emission bands overlap the $Ce1^{3+}$ absorption bands. In fact, the excitation spectrum of $Ce1^{3+}$ contains the Gd^{3+} absorption bands, which indicates the existence of energy transfer from Gd^{3+} to $Ce1^{3+}$.

To investigate this energy transfer between Gd and Ce, Gd^{3+} absorption bands were excited by a synchrotron light source and the emission decay from $Ce1^{3+}$ was monitored. When the ^6P_J and ^6I_J states of Gd^{3+} in 2.5 mol% GSO were excited, a long decay component and a build-up were observed in the $Ce1^{3+}$ emission, supporting our assumptions about the energy transfer from Gd^{3+} to $Ce1^{3+}$.

This observation, obtained with UV excitation, leads to the speculation that the initial build-ups and the long decay components of gamma-ray excited decay curves are also due to the energy transfer from Gd^{3+} to $Ce1^{3+}$. We were able to fit successfully the gamma-ray excited decay curves using three terms which represent the $Ce1^{3+}$ prompt emission, the energy transfer from the excited ^6I_J multiplets to $Ce1^{3+}$, and the energy transfer from the excited ^6P_J multiplets to $Ce1^{3+}$. The fraction of the $Ce1^{3+}$ prompt emission (a single exponential decay of ~23 ns) in the total emission increases linearly with the total Ce concentration in GSO. The decay rates of the ^6I_J multiplets obtained from the gamma-ray excited decay curves agree with those obtained from the decay curve excited at 275 nm (into the ^6I_J multiplets) for various GSO samples, supporting our assumption that the build-ups of the gamma-ray excited decay curves are due to the energy transfer from ^6I_J state of Gd^{3+} to $Ce1^{3+}$. It is shown that the long decay component in the gamma-ray excited decay is due to the energy transfer from the ^6P_J multiplets of Gd^{3+} to $Ce1^{3+}$.

3.1 Introduction

The scintillation properties of Ce-doped gadolinium oxyorthosilicate $Gd_2(SiO_4)O$:Ce (GSO) are characterized by a relatively high emission intensity (25% of NaI(Tl)), two decay constants (~56 and ~600 ns for 0.5 mol% Ce-doped GSO), an emission peak at 430 nm [1,2] and emission intensities and decay times that depend on the Ce concentration. The blue emission of GSO entirely originates from the Ce^{3+} activator, which has parity allowed electric-dipole transitions between the excited 5d states and the spin-orbit split 4f ground state.

When GSO is excited with high energy particles such as gamma rays or x-rays, the scintillation processes of GSO can be separated into two parts: primary and secondary processes [3]. The primary process is the transfer of energy from ionizing radiation to the luminescent centers (Ce^{3+}). The secondary process is that by which excited luminescent centers lose their energy. The secondary process of GSO has been studied independently as a function of temperature (11 K to 300 K) by direct excitation of the luminescent centers, with ultraviolet excitation instead of with ionizing radiation [4]. The existence of two activation centers (Ce1 and Ce2) has been proposed because $Gd_2(SiO_4)O$ has two crystallographically independent Gd^{3+} sites [5,6]. We showed that these two Ce centers have different excitation and emission bands, different decay constants, and different temperature-dependence.

The Ce1 center has its two lowest energy absorption bands at 284 and 345 nm, and an emission band at 425 nm. The decay constant of $Ce1^{3+}$, which is obtained by a direct excitation into the $Ce1^{3+}$ absorption bands, is 27 ns at 77 K, and it becomes faster (22 ns) at room temperature due to an increase in the non-radiative transition rate (as a result of thermal quenching). On the other hand, the two lowest absorption bands of $Ce2^{3+}$ are located at 300 and 378 nm and the emission band is at 480 nm. The $Ce2^{3+}$ has a decay constant of 43 ns at 77 K; this decay constant becomes much faster (< 6 ns) at room temperature because of strong thermal quenching. Thus the emission of GSO following

gamma-ray excitation at room temperature is dominated by the emission from the $Ce1^{3+}$ luminescent center.

The emission peak of GSO with room temperature gamma-ray excitation agrees well with the emission peak of Ce1 and it supports the assumption that most emission comes from the Ce1 center. However, the two decay constants, ~56 and ~600 ns, obtained with gamma-ray excitation are much slower than the decay constant of the Ce1 center itself (22 ns). This difference in the decay time between UV excitation and gamma-ray excitation suggests that the primary scintillation process of GSO is slower than the secondary process and that there are at least two types of primary processes which produce two decay constants. Thus the existence of two decay constants observed in gamma-ray excited GSO can be attributed to the primary excitation process.

To investigate the primary excitation process of GSO, Gd^{3+} absorption lines in the UV region were excited by a synchrotron light source and the decay of the emissions from Ce^{3+} were monitored. When the Gd^{3+} absorption lines were excited, the Ce^{3+} decays showed a build-up and a slow decay component, which is clearly caused by the energy transfer from Gd^{3+} to Ce^{3+}.

The decomposed gamma-ray excited decay curve of GSO showed that the emission from GSO consists of prompt Ce emission and delayed Ce emission (transfer of energy through Gd).

Crystallographically, $Gd_2(SiO_4)O$ has a monoclinic structure of space group $P2_1/c$. There are two Gd sites in $Gd_2(SiO_4)O$: one Gd site has a ninefold oxygen coordination, and the other site has a sevenfold oxygen coordination. The mean distance from the former Gd site to the nine oxygen ligands is 2.49 Å, while that from the latter site to the seven oxygen ligands is 2.39 Å. Due to the different interactions with the crystal field and the lattice, the two Gd^{3+} ions are expected to show slightly different optical properties in interacting with the two Ce^{3+} ions (Ce1 and Ce2). However, in the discussion below where the interaction of Gd^{3+} with Ce^{3+} is macroscopically treated, no distinction will be

made between the two Gd^{3+} ion sites, as we do not propose to describe the details of the spectroscopic properties of GSO. Rather we attempt to understand the primary process to provide a comprehensive explanation of the scintillation processes of GSO.

3.2 Experimental measurements

The GSO crystals used for this study were purchased from Hitachi Chemical Co., Ltd., which grew the GSO crystals by the Czochralski technique. The Ce concentration in the melts from which the crystals were grown varied from 0.1 to 2.5 mol%. However, the Ce concentration in the crystals depends on the distribution coefficient of Ce in the host material $Gd_2(SiO_4)O$. The Ce concentration in the crystals were analyzed by X-ray Assay Laboratories and the distribution (or segregation) coefficient of Ce was determined to be ~0.6, in reasonably good agreement with previous studies [7]. Six GSO samples ($(Gd_{1-x}Ce_x)_2(SiO_4)O$) were used in this study. Their Ce concentrations relative to Gd are: sample #1 (nominal 0.1 mol%, x=0.00035), #2 (0.5 mol%, 0.0018), #3 (1.0 mol%, 0.0036), #4 (1.5 mol%, 0.0051), #5 (2.0 mol%, 0.0074) and #6 (2.5 mol%, 0.0098).

The absorption spectra were measured with a spectrophotometer (Model U-3210, Hitachi Instruments). The emission spectra were obtained with a SPEX Fluorolog-2 spectrofluorometer. The details of these optical measurements as well as those of the gamma-ray excited decay curve at room temperature have been described elsewhere [4].

The low-temperature measurements of the gamma-ray excited decay curves were made with the configuration shown in fig. 3.1. Temperatures as low as 15 K were achieved with a CTI-Cryogenics refrigeration system (Model 21). The decay data were taken using the time-correlated single-photon technique [8], with a ^{22}Na source and a second crystal to provide a timing reference [9]. The reference signal was produced by cerium-doped lutetium oxyorthosilicate $Lu_2(SiO_4)O$:Ce (LSO), which has a very high light output and a primary decay constant of 40 ns [10,11]. The GSO crystal was excited from the side. Two 511 keV gamma rays, simultaneously produced by annihilation of a positron

and an electron, were used to excite both GSO and the reference LSO scintillator. All the gamma-ray excited decay curves shown here were measured without correcting for the wavelength dependence of the photocathode on the photomultiplier tube. One of two filters, S40-400 and LL-600 (CORION), was placed between the GSO crystal and its photomultiplier tube to select either Ce1 or Ce2 emission. The bandpass filter S40-400 has a peak at ~400 nm and transmits only Ce1 emission. The long wave pass filter LL-600 transmits photons which have wavelengths longer than 600 nm and is suitable for selecting only Ce2 emission.

The measurements of UV-excited decay curves as well as those of UV-excited excitation spectra were made by using the U9B beam line of the National Synchrotron Light Source at Brookhaven National Laboratory. For the former measurements, we used the single bunch mode, whose duration time is ~1.0 ns. This light source has a repetition rate of ~5.88 MHz, i.e., a beam repetition period of ~170 ns. Because of the short beam period, longer decay constants than the beam period could not be measured. For the measurements on the UV-excited excitation spectra, we used the normal periodic bunch

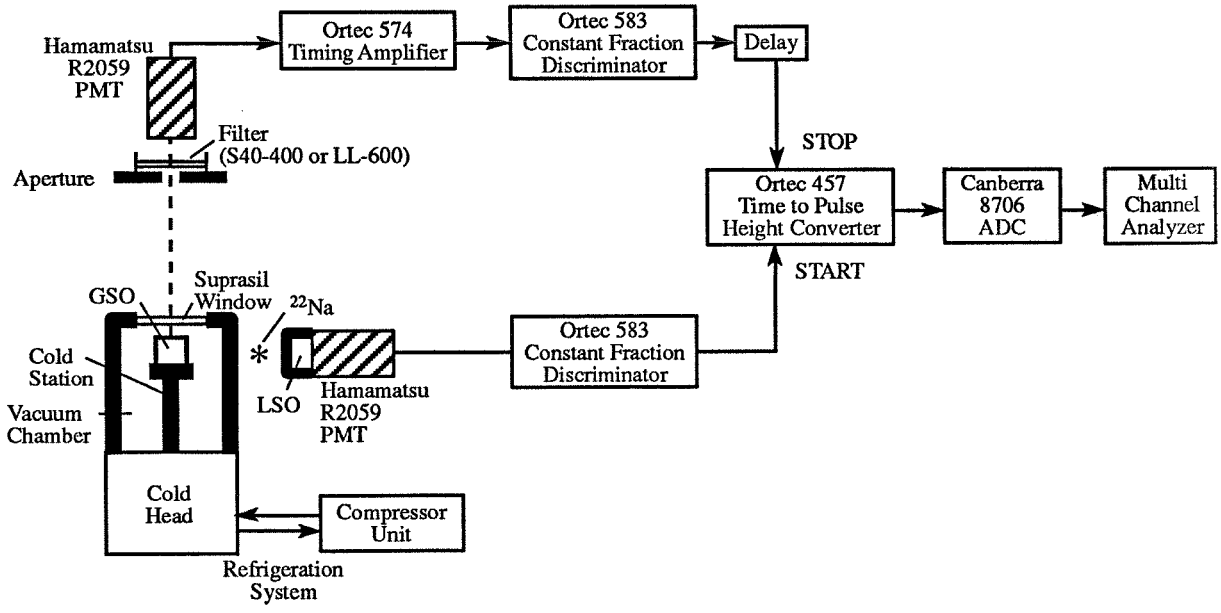

Fig. 3.1 Equipment and electronics used to measure gamma-ray excited decay curves at 15 K.

mode to get enough intensity from the light source. Monochrometers were used to select the excitation and emission wavelengths. The bandpasses of excitation and emission monochrometers were 1.7 and 10 nm, respectively. The UV-excited decay data were also taken using the time-correlated single-photon technique and were analyzed with a least-squares-fitting technique.

In the discussion below each GSO sample is labeled by its sample name, its Ce concentration in the melt or its Ce concentration in the crystal (e.g., #1, 0.1 mol% or 0.00035). However, neither the charge state of Ce in the crystal nor the exact concentration of each Ce center (Ce1 and Ce2) has been determined.

3.3 Results

3.3.1 Comparison between UV and gamma-ray excitation

Fig. 3.2 shows the decay curves of $Ce1^{3+}$ on a relatively short time scale for various GSO samples excited by gamma rays. Counts are plotted on a logarithmic scale. To choose Ce1 emission, whose emission peaks at 425 nm, the S40-400 bandpass filter was placed between the crystal and the stop photomultiplier tube (see fig. 3.1). This bandpass filter transmits only Ce1 emission, eliminating Ce2 emission, whose emission peak is at 480 nm. The Ce1 decay from 2.5 mol% GSO obtained with direct UV excitation into the $Ce1^{3+}$ band is also displayed in fig. 3.2. The excitation and emission wavelengths were 284 and 420 nm. As can be seen, the Ce1 decays with gamma-ray excitation are much slower than the decay of Ce1 itself (22 ns). The decay constants with gamma-ray excitation decrease as Ce concentration increases from 0.1 to 2.5 mol%. Note that the gamma-ray excited decay curves of all GSO samples, when viewed with this time resolution, contain initial build-ups, indicating that the decay curve obtained with gamma-ray excitation cannot be described by a simple summation of two exponentials. The extent of this build-up, in addition, strongly depends on the Ce concentration.

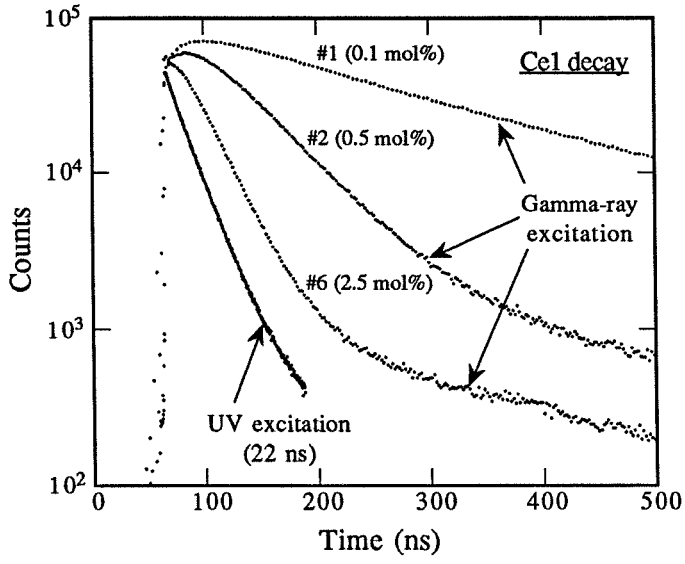

Fig. 3.2 Gamma-ray excited decay curves of three GSO samples and the UV excited decay curve of 2.5 mol% GSO. The latter curve has an excitation wavelength of 284 nm and an emission wavelength of 420 nm.

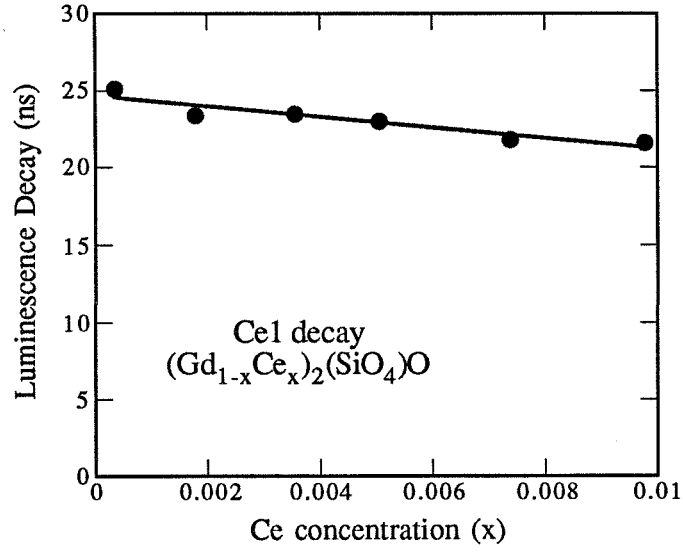

Fig. 3.3 UV-excited luminescent decay of Ce1 as a function of the total Ce concentration (x). The emission and excitation wavelengths were 284 and 420 nm, respectively.

Fig. 3.3 shows the Ce1 decay constant for various GSO samples with different Ce concentrations. The decay data were obtained with an excitation wavelength of 284 nm and an emission wavelength of 420 nm. The decay constants were calculated from a single exponential fit. The decay constant of Ce1 changes slightly from 25 ns for 0.1 mol% GSO to 22 ns for 2.5 mol% GSO. This trend of the Ce1 decay constant, i.e., a weak concentration-dependence of the decay, has been previously reported [12]. Note that the strong dependence of the gamma-ray excited Ce1 decay on Ce concentration differs from that of the UV-excited (at 284 nm) Ce1 decay, which shows only a weak dependence on Ce concentration.

Since the observed decay constants of GSO with gamma-ray excitation are much longer than the decay constant of Ce1 itself, the primary process must be relatively slow. By analogy with thallium-doped sodium iodide NaI(Tl) [3], five processes in exciting the luminescent center (Ce^{3+}) following the interaction of high energy particles are possible:

<1> Luminescence by the lattice centers (Gd^{3+}) and absorption by the luminescent center (Ce^{3+}) (radiative transfer);
<2> Non-radiative energy transfer from the excited lattice centers (Gd^{3+}) to the luminescent centers (Ce^{3+}) (including resonant transfer);
<3> Non-radiative transfer from vacancies or traps to the luminescent center (Ce^{3+});
<4> Exciton diffusion to the luminescent center (Ce^{3+}); and
<5> Binary (independent) diffusion of electrons and holes to the luminescent center (Ce^{3+}).

Processes <1> and <2> will be discussed below. The possibility of the other processes will be discussed in the next section.

The Gd^{3+} ion has 7 electrons in the 4f shell, which is well shielded from the crystalline environment by two electronic shells with larger radial extension ($5s^25p^6$) [13].

As a result, Gd^{3+} shows very sharp 4f-4f transitions in the UV, with wavelengths that are relatively independent of the particular Gd compound [14-19]. The transition between two 4f states of Gd^{3+} depends on both forced electric dipole radiation and magnetic dipole radiation. The electric dipole radiation is forbidden in first order and it occurs only as a consequence of a perturbation. The magnetic dipole radiation, which is about six orders of magnitude weaker than the electric dipole radiation in free atoms, is observed in the Gd^{3+} spectra from crystals with about the same intensity as the electric dipole radiation.

The absorption data for undoped $Gd_2(SiO_4)O$ is shown in fig. 3.4a. The thickness of the sample was 0.040 cm. The absorption coefficients α (cm^{-1}) are calculated using the formula $I = I_0 \exp(-\alpha \ell)$, where I and I_0 indicate the intensity of the transmitted and incident light, respectively, and ℓ is the thickness of the crystal (cm). The undoped GSO spectrum has absorption lines at 313, 308 and 302 nm, which are ascribed to the transitions from the ground $^8S_{7/2}$ state to the three excited states $^6P_{7/2}$, $^6P_{5/2}$ and $^6P_{3/2}$. The absorption line at 275 nm is due to transitions from the ground $^8S_{7/2}$ state to the ^6I_J multiplets (J = 7/2, 9/2,17/2, 11/2, 15/2, and 13/2). The excitation into the $^6D_{9/2}$ state from the ground $^8S_{7/2}$ state is seen at 254 nm, and the excitations into the other ^6D_J multiplets (J = 1/2, 7/2, 3/2 and 5/2) are observed at 247 nm. The small peak at 203 nm is due to the absorption of ^6G_J (J = 7/2, 9/2, 11/2 and 5/2) multiplets [20]. The lattice absorption begins at ~200 nm.

The emission lines of Gd^{3+} in undoped GSO were observed at 278 (from the ^6I_J) and 314 nm (from the ^6P_J) with gamma-ray excitation (500 μCi ^{241}Am source) (fig. 3.4b). The emission bandpass was 7.2 nm. Note that the emission wavelengths are almost identical with the absorption wavelengths. The ground state emissions from higher excited states were not seen. This is probably because the non-radiative decay rates from the higher excited states to the lower excited states (^6I_J and ^6P_J) are much greater than the radiative decay rate to the ground state and deplete the higher excited states.

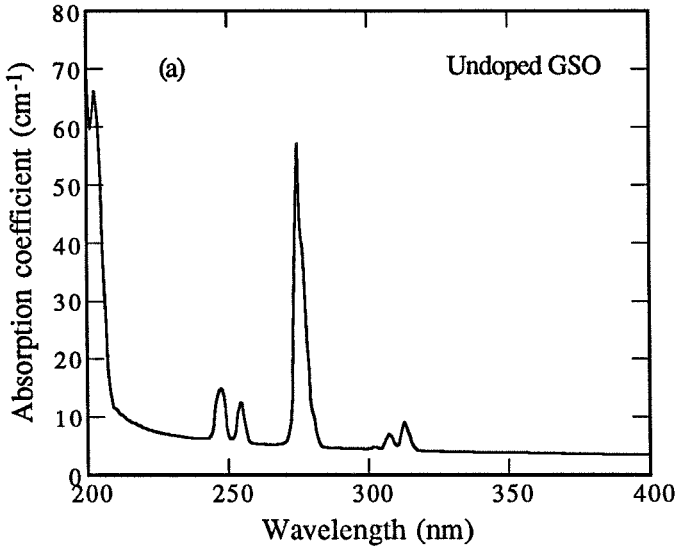

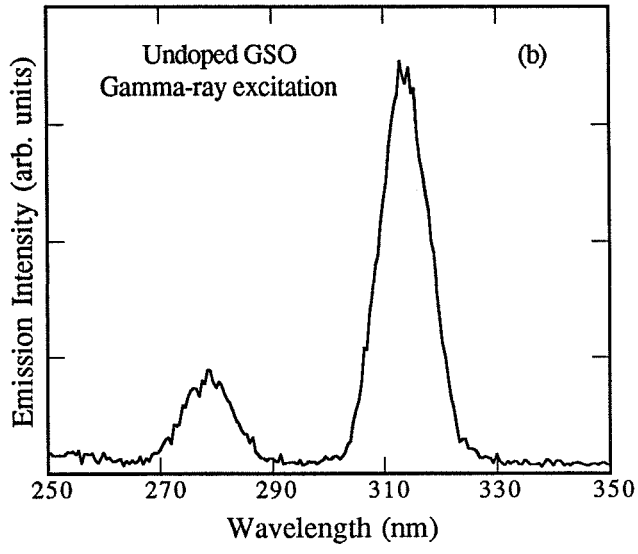

Fig. 3.4 a) Absorption and b) emission spectra of undoped GSO.

The excitation spectra of 0.1 and 2.5 mol% GSO were measured for both the Ce1 and Ce2 centers, with thin GSO samples (0.20 and 0.18 mm thick, respectively) at 11K (figs. 3.5a and 3.5b). One excitation spectrum has a monitored emission wavelength of 420 nm (near the Ce1 emission peak), and the other excitation spectrum has a monitored emission wavelength of 550 nm (near the Ce2 emission peak). The peaks at 203, 247, 254, 275, 308 and 313 nm in fig. 3.5a correspond to the Gd^{3+} absorption lines, which indicates that energy is transferred from Gd to Ce1 and Ce2 centers either by process <1> or process <2>. As stated above, the excitation peaks at 284 and 345 nm are due to direct absorption by the Ce1 center, and the peaks at 300 and 378 nm are due to direct absorption by the Ce2 center. The excitation spectra of 2.5 mol% GSO (fig. 3.5b) do not show as many Gd^{3+} absorption lines as in fig. 3.5a since the intensities of Gd^{3+} absorption are small compared with the intensities of Ce^{3+} absorption. Note that the peak at 250 nm is observed for the first time and ascribed to the third-lowest 5d state of Ce1 center.

Fig. 3.6 displays the energy levels of Gd^{3+} within the $4f^7$ configuration [21-23] and the absorption bands of $Ce1^{3+}$ and $Ce2^{3+}$ for the transitions between the ground 4f states and the excited 5d states. The energy levels of Gd^{3+} are based on the data shown in fig. 3.4a and previous work [20]. The energy levels of $Ce1^{3+}$ and $Ce2^{3+}$ are based on the excitation spectra of GSO at 11 K (figs. 3.5a and 3.5b). As can be seen, the three $^6P_{7/2}$, $^6P_{5/2}$ and $^6P_{3/2}$ excited states overlap absorption bands of the lowest excited state of $Ce1^{3+}$ and the second excited state of $Ce2^{3+}$. The ^6I_J multiplets of Gd^{3+} mainly overlap the absorption band of the second excited state of $Ce1^{3+}$.

3.3.2 Model

As observed in fig. 3.6, the excited states of Gd^{3+} overlap absorption bands of $Ce1^{3+}$ and $Ce2^{3+}$. In addition, the excited states of Gd^{3+} overlap each other. Thus, in the case of high donor concentration such as in GSO, donor-donor (Gd-Gd) and donor-acceptor (Gd-Ce) interactions between two ions must be taken into account in describing

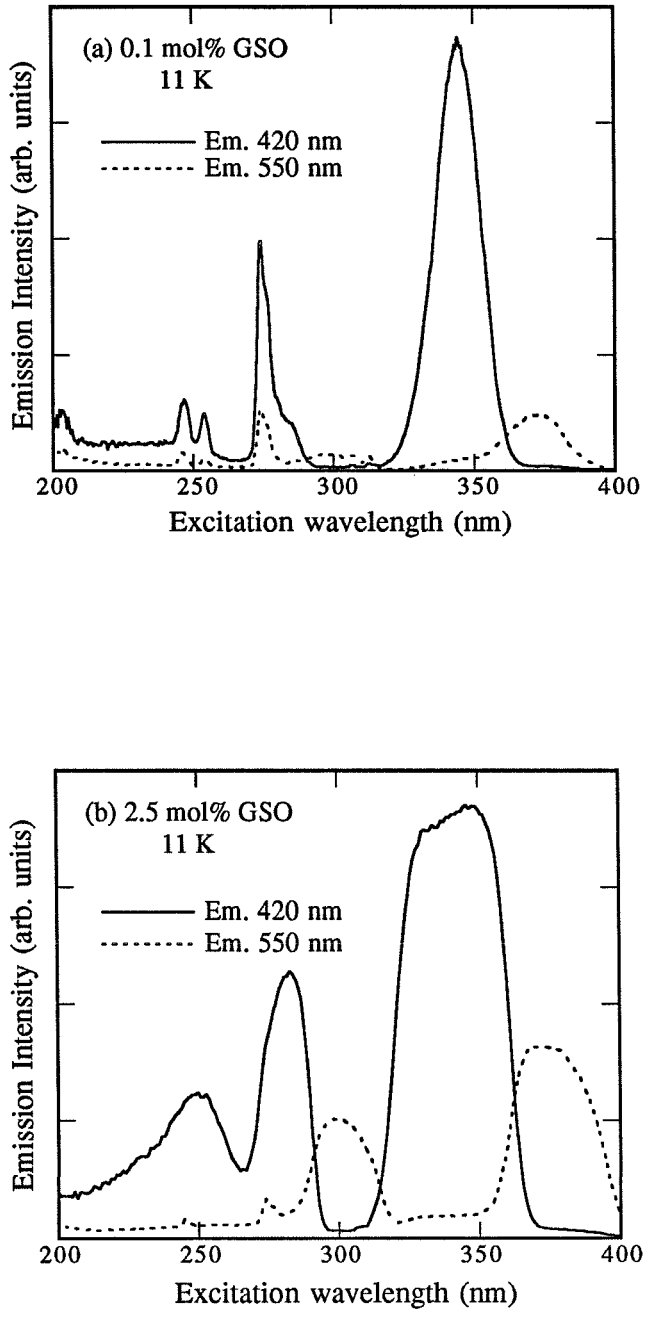

Fig. 3.5 a) Excitation spectrum of 0.1 mol% GSO (0.2 mm thick sample), b) Excitation spectrum of 2.5 mol% GSO (0.18 mm) at 11 K. The excitation spectra were measured at the two emission wavelengths of 420 nm (solid line) and 550 nm (dashed line).

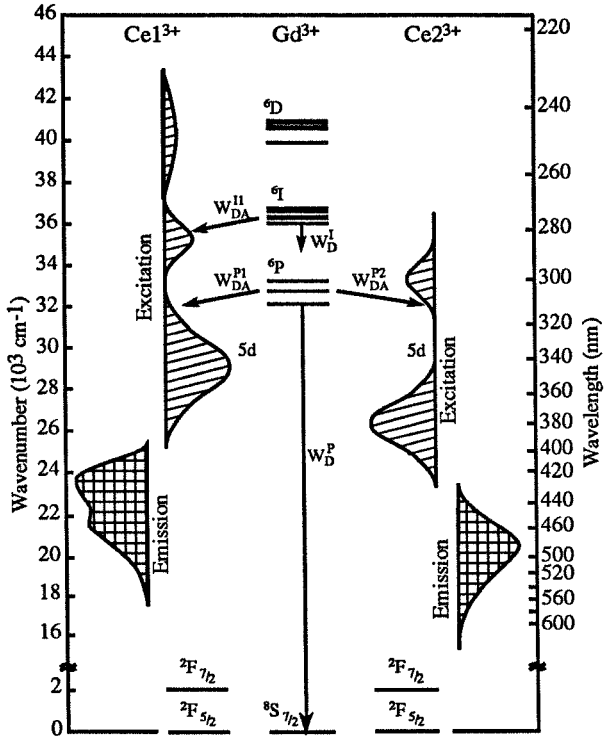

Fig. 3.6 Energy levels of Gd^{3+}, $Ce1^{3+}$ and $Ce2^{3+}$ in GSO.

the decay of the excited donor $(Gd^{3+})^*$. As one possible energy transfer mechanism between donor and acceptor, and between donors, let us consider resonant energy transfer. For example, between a donor and an acceptor the resonant energy transfer is given by [24]:

$$W_{da} = \frac{(2\pi)^2}{h} |\langle D, A^*|H'|D^*, A\rangle|^2 \int g_D(E) g_A(E) dE = C_{da}\, f(R), \qquad (3.1)$$

where an asterisk indicates the excited state of the ion, H' is the interaction Hamiltonian, $g_D(E)$ and $g_A(E)$ are the normalized lineshape functions for the transitions D*--->D and A--->A*. C_{da} is a microscopic parameter for the D-A interaction, and f(R) is the function

whose form is determined by the nature of the D-A interaction. This energy transfer is non-radiative; it does not involve the emission of a photon by D and the subsequent absorption by A. Rather, it is a simultaneous deexcitation of D and excitation of A. The interactions which cause energy transfer are electrostatic coupling, magnetic coupling, and/or exchange coupling between ions. Similarly, the rate of resonant energy transfer between donors is expressed by

$$W_{dd} = C_{dd}\, f(R). \qquad (3.2)$$

where C_{dd} is a microscopic parameter for the D-D interaction.

When one of the Gd^{3+} ions (donors) is excited, the energy of this Gd^{3+} ion can migrate through the Gd^{3+} sublattice, since in GSO the Gd-Gd distance is very small (table 3.1), and the acceptor concentration is low. We assume energy to migrate through the Gd^{3+} sublattice before one of the excited Gd^{3+} ions spontaneously (radiatively) emits a photon or resonantly transfers its energy to a nearby Ce^{3+} or to a quenching center. This resonant energy transfer can accelerate the decay process of the excited Gd^{3+} by the energy transfer to Gd^{3+} centers with the shortest lifetime. The details of this energy migration through the Gd^{3+} sublattice is discussed elsewhere [25].

Table 3.1 The number of Gd^{3+} neighbor sites and the corresponding Gd^{3+} - Gd^{3+} distances.

Starting point	Distance (Å)	Site of neighbor	Number of neighbors
Gd1	3.360	Gd1	1
	3.671	Gd1	2
	3.724	Gd2	1
	3.791	Gd2	1
	4.176	Gd2	1
Gd2	3.520	Gd2	1
	3.573	Gd2	2
	3.724	Gd1	1
	3.791	Gd1	1
	3.803	Gd2	2
	4.128	Gd2	1
	4.176	Gd1	1

Process <1> - Radiative energy transfer

Process <1>, that is, the radiative transfer from excited Gd^{3+} to Ce^{3+} can occur since the emission lines (^6P_J and ^6I_J) of the Gd^{3+} (donor) overlap the absorption bands of the Ce^{3+} (acceptor) (fig. 3.4b). However, it will be shown that process <1> is not important on the time scale of interest. As observed for many Gd compounds [14-16,18,26] where Gd is either an activator or a lattice constituent, the decay constants of the strongly light-emitting states, $^6P_{7/2}$ and $^6I_{7/2}$, are usually of the order of μs to ms. Thus, it is reasonable to assume that the Gd^{3+} in GSO also has very slow radiative decay constants from these fluorescent states. If the radiative transfer from the Gd^{3+} to the Ce^{3+} occurs, that is, the Ce^{3+} ion absorbs the photons emitted by the Gd^{3+} without influencing the emission ability of Gd^{3+} [27], then the observed decay curve of $Ce1^{3+}$ in fig. 3.2 must have very slow decay constants, of the same order of the Gd^{3+} decay. However, the observed decay constants of $Ce1^{3+}$ are much shorter. Thus, it is unlikely that process <1> contributes to the emission of GSO on the time scale observed from gamma-ray excitation (< 1 μs). Even on a long time scale, however, we expect that the radiative transfer from Gd^{3+} to Ce^{3+} does not play an important role, since the intensities of the Gd^{3+} emission from undoped GSO with gamma-ray excitation are very weak compared with the intensities of the Ce^{3+} emission from doped GSO. Thus, process <1> can be ignored in considering the excitation process of Ce^{3+}.

Process <2> - Non-radiative (including resonant) energy transfer

As the energy of the excited Gd^{3+} migrates through the Gd^{3+} sublattice, the Gd^{3+} system senses the average environment of acceptor ions. The average energy transfer from the donor to the acceptor is then expressed by a macroscopic (or an effective) transfer rate, W_{eff}, which is a function of four parameters (C_{da}, C_{dd}, N_A and N_D). N_A and N_D are the ion densities of the acceptor and the donor, respectively; C_{da} and C_{dd} were defined earlier. W_{eff} depends linearly on N_A regardless of the nature of interactions between ions.

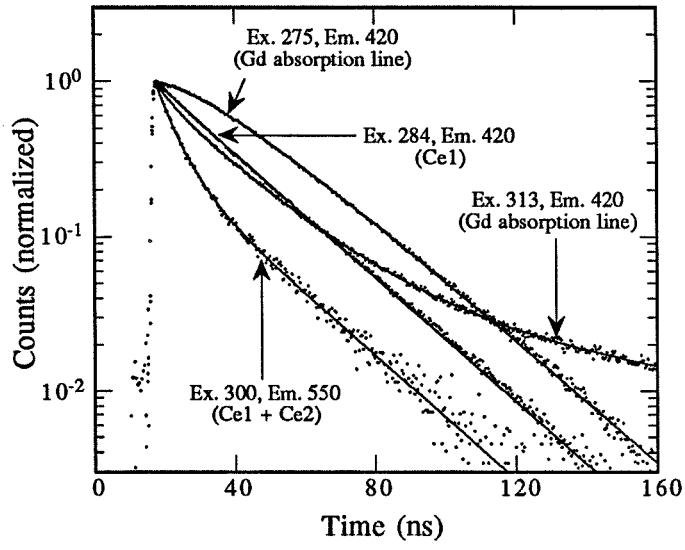

Fig. 3.7 The UV-excited decay curves of 2.5 mol% GSO.

To analyze the non-radiative energy transfer process from Gd^{3+} to $Ce1^{3+}$, the decay curves of 2.5 mol% GSO were measured by exciting the Gd^{3+} absorption lines (fig. 3.7). The decay curves observed with 275 and 313 nm excitation correspond to excitations of the excited ^6I_J multiplets and the $^6P_{7/2}$ states of Gd^{3+}, respectively. The decay curve excited at 284 nm is a direct excitation of the Ce1 absorption band, and the decay curve excited at 300 nm is mainly exciting the Ce2 absorption band. The decay curve excited at 284 nm is the emission of the $Ce1^{3+}$ and can be fit with a single exponential (22 ns). The decay curve excited at 300 nm contains the emission of both $Ce1^{3+}$ and $Ce2^{3+}$ and can be fit with an appropriate combination of two exponentials that have decay constants of 22 and 5 ns. On the other hand, the decay curve excited at 275 nm shows a build-up, and the decay excited at 313 nm contains a slow component. Since both wavelengths (275 and 313 nm) correspond to Gd^{3+} absorption lines, it is reasonable to assume from these data that the energy is non-radiatively transferred from the Gd^{3+} to the two Ce^{3+} luminescent centers.

The excited Ce^{3+} emits photons at much longer wavelengths than the absorption wavelengths (due to the large Stokes shift). Thus, the back transfer from Ce^{3+} to Gd^{3+} is

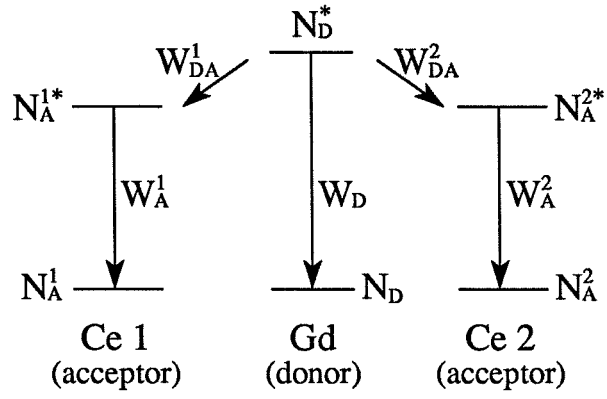

Fig. 3.8 Modes of decay and energy transfer in GSO.

unlikely to occur in GSO. If we ignore the difference between the two types of Gd^{3+} ions, as discussed above, the transfer process from Gd^{3+} to $Ce1^{3+}$ and $Ce2^{3+}$ can be illustrated as in fig. 3.8. N stands for the population of the ion. The effective transfer rate from the donor to the acceptor is written as $W_{DA}{}^i$, where the superscript i indicates the type of the Ce^{3+} (acceptor). W_D, $W_A{}^1$ and $W_A{}^2$ represent the radiative decay rate of the excited Gd^{3+} state and the decay rate (including both radiative and non-radiative transitions) of the excited $Ce1^{3+}$ and $Ce2^{3+}$ states, respectively. Then the rate equation for each excited state can be given by:

$$\frac{dN_D^*}{dt} = - W_D N_D^* - W_{DA}^1 N_D^* - W_{DA}^2 N_D^*; \tag{3.3}$$

$$\frac{dN_A^{1*}}{dt} = W_{DA}^1 N_D^* - W_A^1 N_A^{1*}; \tag{3.4}$$

$$\frac{dN_A^{2*}}{dt} = W_{DA}^2 N_D^* - W_A^2 N_A^{2*}. \tag{3.5}$$

The solutions in the case where $N_D^*(0)$ excited donors are created at t=0 and where no

acceptors are excited, are:

$$N_D^*(t) = N_D^*(0) \exp[- (W_D + W_{DA}^1 + W_{DA}^2) t] ; \quad (3.6)$$

$$N_A^{1*}(t) = N_D^*(0) \frac{W_{DA}^1}{W_A^1 - (W_D + W_{DA}^1 + W_{DA}^2)} \{\exp[- (W_D + W_{DA}^1 + W_{DA}^2) t] - \exp[- W_A^1 t]\} ; \quad (3.7)$$

$$N_A^{2*}(t) = N_D^*(0) \frac{W_{DA}^2}{W_A^2 - (W_D + W_{DA}^1 + W_{DA}^2)} \{\exp[- (W_D + W_{DA}^1 + W_{DA}^2) t] - \exp[- W_A^2 t]\} . \quad (3.8)$$

In the case of GSO, for which the emission of the acceptor $Ce1^{3+}$ has been measured, eq. (3.7) can be used to fit the decay curves.

3.3.3 Energy Transfer from Gd to Ce

3.3.3.1 Transfer from the ^6P_J states to Ce^{3+}

First, consider the energy transfer from the excited $^6P_{7/2}$ state of Gd to $Ce1^{3+}$ and $Ce2^{3+}$. The transition from the excited $^6P_{7/2}$ state to the ground $^8S_{7/2}$ state occurs only by radiative decay since the energy gap between these two states is too large to be compensated by multiphonon emission. The radiative decay rate ($1/\tau_R$) of the excited $^6P_{7/2}$ state has been measured for many Gd compounds [15,18,23,28,29] and has been reported to be of the order of μs to ms. Thus the decay of the excited $^6P_{7/2}$ state can be expressed by the summation of the radiative decay and the effective transfer rate to the two Ce^{3+} ions. The excitation wavelength of 313 nm overlaps to the absorption band of the lowest excited 5d state of $Ce1^{3+}$, the second lowest excited 5d state of $Ce2^{3+}$, and the excited $^6P_{7/2}$ state of Gd. Thus the decay curve excited at 313 nm (emission at 420 nm) can be fit with the following expression:

$$N_A^{1*}(0)\exp\left(-\frac{t}{22}\right)+N_A^{2*}(0)\exp\left(-\frac{t}{5}\right)$$

$$+N_D^{P*}(0)\frac{W_{DA}^{P1}}{\frac{1}{22}-(W_D^P+W_{DA}^{P1}+W_{DA}^{P2})}\{\exp[-(W_D^P+W_{DA}^{P1}+W_{DA}^{P2})t]-\exp[-\frac{1}{22}t]\}\quad , \qquad (3.9)$$

where the first and the second terms represent the direct emission from $Ce1^{3+}$ and $Ce2^{3+}$ centers, respectively. The decay constants for the $Ce1^{3+}$ (22 ns) and $Ce2^{3+}$ (5 ns) emission are taken from the decay constant obtained from the decay curve excited at 284 and at 300 nm (fig. 3.7). The third term is taken from eq. (3.7) and represents the energy transfer from the $^6P_{7/2}$ state of Gd^{3+} to $Ce1^{3+}$. The $Ce2^{3+}$ emission produced by the transfer from the $^6P_{7/2}$ state is ignored. As shown in fig. 3.9, the decay excited at 313 nm is well fit with eq. (3.9), which can be decomposed into three curves, each of which represents a term in eq. (3.9). From the fit with this equation, a decay rate for the excited $^6P_{7/2}$ state of Gd^{3+}, $W_D^P + W_{DA}^{P1} + W_{DA}^{P2}$, of ~160 ns is obtained.

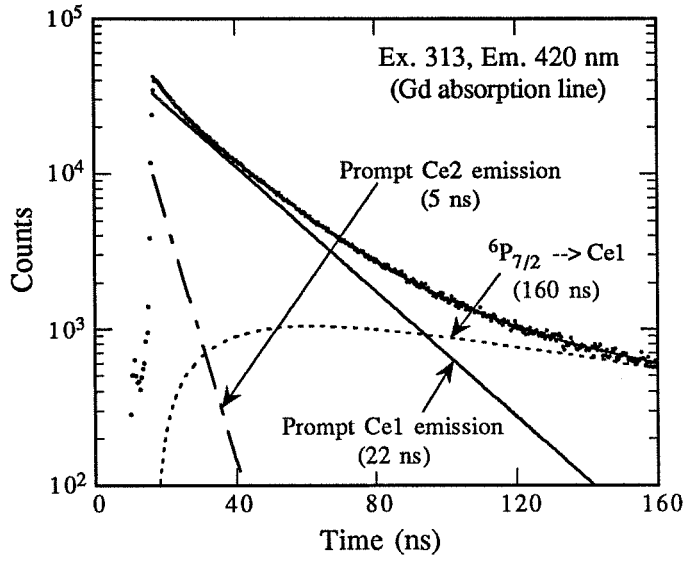

Fig. 3.9 The decay curve of 2.5 mol% GSO (closed circle). The excitation and emission wavelengths are 313 and 420 nm. The data were fit with eq. (3.9) (solid line through the data points). The decay was decomposed into three curves, each of which represents a term in eq. (3.9).

Two other excited states, $^6P_{5/2}$ and $^6P_{3/2}$, were excited at 308 and 302 nm for 2.5% GSO. When exciting at 308 and 302 nm, not only the $^6P_{5/2}$ and $^6P_{3/2}$ states of Gd^{3+} but also the excitation bands of $Ce1^{3+}$ and $Ce2^{3+}$ are excited. The decay curves excited at 308 and 302 nm did not show long components and are composed of $Ce1^{3+}$ and $Ce2^{3+}$ decays. This is probably because the absorption intensities of $Ce1^{3+}$ and $Ce2^{3+}$ at 308 and 302 nm are much stronger than the absorption of these excited states of Gd^{3+}, and as a result it was difficult to observe the transfer effect due to these two excited states on our short time scale.

3.3.3.2 Transfer from the ^6I_J states to Ce^{3+}

Next consider the energy transfer from the excited ^6I_J states of Gd^{3+} to Ce^{3+}. Because of our energy resolution (~1.7 nm), each state of the ^6I_J multiplets, which usually have much smaller energy separation [20], could not be excited separately. Here we treat the ^6I_J multiplets as a group. The ^6I_J multiplets decay radiatively to the $^8S_{7/2}$ ground state and non-radiatively to the ^6P_J multiplets by phonon emission. The non-radiative decay rate from the ^6I_J multiplets to the ^6P_J multiplets is a little faster than the radiative decay rate from the ^6I_J multiplets to the ground state, as has been shown for YOCl:Gd and $LiYF_4$:Gd [30]. However, the total decay rate of the ^6I_J multiplets of Gd^{3+} is much longer than our time scale (< 1 μs) for gamma-ray excitation. Based on the assumption that the decay rate of the ^6I_J multiplets of Gd^{3+} is much longer than our times of interest, a similar equation to eq. (3.9) can be used to fit the decay curve excited at 275 nm (emission at 420 nm):

$$N_A^{I*}(0)\exp\left(-\frac{t}{22}\right)+N_D^{I*}(0)\,\frac{W_{DA}^{II}}{\frac{1}{22}-(W_D^{I}+W_{DA}^{II})}\left\{\exp\left[-(W_D^{I}+W_{DA}^{II})\,t\right]-\exp\left[-\frac{t}{22}\right]\right\}\ ; \qquad (3.10)$$

where the first term represents the direct emission of $Ce1^{3+}$ since the wavelength of 275 nm corresponds to the absorption band of the second excited 5d state of $Ce1^{3+}$. The second

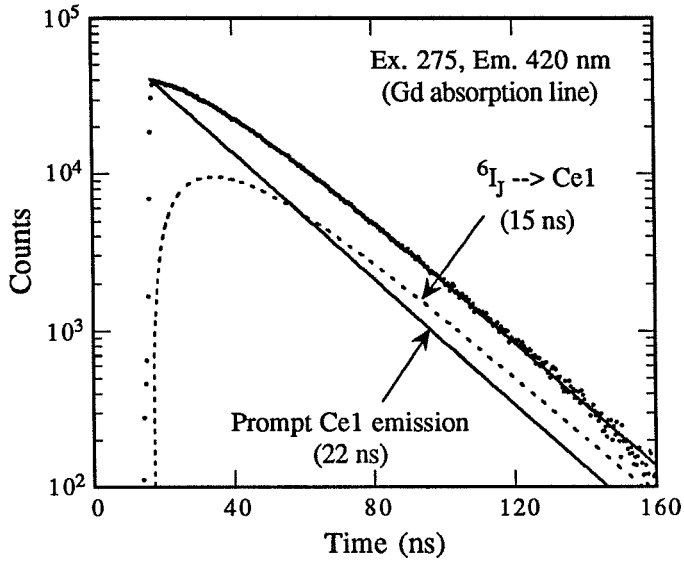

Fig. 3.10 The decay curve of 2.5 mol% GSO excited at 275 nm (closed circles). The data are fit with eq. (3.10) (solid line) and decomposed into two curves, representing each term in eq. (3.10).

term represents the transfer from the ^6I_J multiplets to $Ce1^{3+}$. The transfer from the ^6I_J multiplets to $Ce2^{3+}$ is ignored because the spectral overlap between the excited ^6I_J multiplets and the absorption band of the second excited 5d state of $Ce2^{3+}$ is small.

Fig. 3.10 shows the decay curve excited at 275 nm together with the curve fit by using eq. (3.10). Two decomposed curves, each of which represents the individual terms in eq. (3.10), are also shown. The decay rate of the excited ^6I_J multiplets, $(W_D^I + W_{DA}^{I1})^{-1}$, is obtained as 15 ns.

3.3.3.3 Concentration-dependence of the transfer rate

The amount of the build-up observed for the gamma-ray excited decay curves shows a concentration-dependence on Ce (fig. 3.2). As the Ce concentration increases, the degree of the build-up decreases. Similarly, build-up is observed (for 2.5% GSO) with UV excitation (at 275 nm). The long component in the gamma-ray decay was also

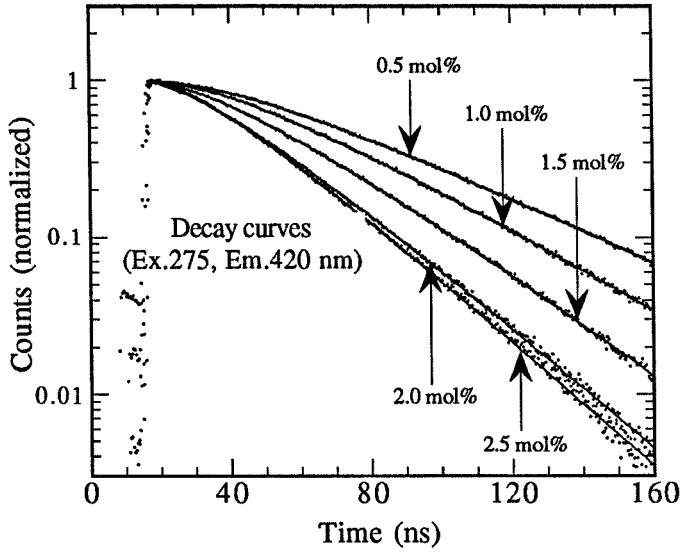

Fig. 3.11 The decay curve of five GSO samples excited at 275 nm. All curves have an emission wavelength of 420 nm.

observed with UV excitation into the $^6P_{7/2}$ states at 313 nm and this UV-excited, long decay component was found to be similar to the long decay component of the gamma-ray excited decay curve. This agreement suggests that the build-ups and slow components of gamma-ray excited decay curves could be associated with the energy transfer from Gd^{3+} to Ce^{3+}. Here we attempt to study the concentration-dependence of the transfer rate for the ^6I_J states. The concentration-dependence of the ^6P_J excited states could not be examined because of the short beam period (~170 ns) with the synchrotron source.

To study the concentration-dependence of the transfer rate, the decay curves excited at 275 nm were measured for various GSO samples. Fig. 3.11 shows the decay curves of five GSO samples (closed circle) excited at 275 nm. Also shown with each decay curve is a curve fit with eq. (3.10). The decay constant of $Ce1^{3+}$ for each sample was obtained from the data in fig. 3.3. The decay curves of these five GSO samples are well fit with eq. (3.10). The transfer rates from the excited ^6I_J multiplets to the $Ce1^{3+}$ were determined

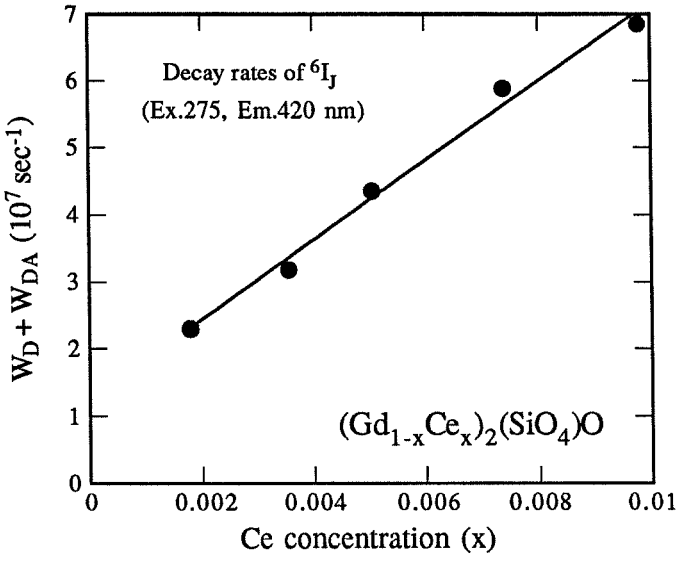

Fig. 3.12 Transfer rates from the ^6I_J multiplets of Gd^{3+} to $Ce1^{3+}$. The horizontal axis is the total Ce concentration.

for each GSO sample (table 3.2, column 3).

The decay rates of the excited ^6I_J states, that is $(W_D^I + W_{DA}^{I1})^{-1}$, are displayed in fig. 3.12 as a function of Ce concentration. Although the concentration of trivalent Ce concentration was not measured, we assume that $Ce1^{3+}$ concentration is proportional to the total Ce concentration obtained from chemical analysis. As expected, the decay rate, $(W_D^I + W_{DA}^{I1})^{-1}$, depends linearly on the total Ce concentration. The straight line intercepts the vertical axis at about 1×10^7 sec^{-1}. This implies that W_D^I, which is independent of Ce concentration, is about 1×10^7 sec^{-1}. However, in many other Gd compounds, W_D^I is much slower than 1×10^7 sec^{-1} [14,18,23,30]. Thus, the fast rate of W_D^I might be due to the energy transfer from the ^6I_J states to quenching centers such as Gd traps or other impurities, whose contribution was not taken into account in deriving eq. (3.10). The possibility of energy transfer to the Gd traps is discussed elsewhere [25].

3.3.3.4 Transfer from the ^6D_J state to Ce^{3+}

A sample of 2.5 mol% GSO was excited at 254 and 247 nm into the excited ^6D_J states. The two wavelengths correspond to the excitation of the ^6D_J multiplets and the absorption band of $Ce1^{3+}$ located at 250 nm. Since the $Ce1^{3+}$ absorption intensity at 250 nm is much stronger than the Gd absorption intensities at 247 and 254 nm, the decay curves excited at 254 and 247 nm were the same as the decay curve excited at 284 nm and no effect due to the transfer from Gd to Ce1 was observed on our short time scale.

3.4 Discussion

In the last section data on the decay of Ce^{3+} from the excitation of the ^6P_J, ^6I_J and ^6D_J states of the Gd^{3+} ion were analyzed. A build-up and a long component were observed in the Ce^{3+} decays when ^6I_J and ^6P_J states of Gd^{3+} were excited. This observation suggests that the build-up and the long component seen in the gamma-ray excited decays may be associated with the energy transfer from ^6I_J and ^6P_J states of Gd^{3+} to Ce^{3+}.

To test this speculation, we attempted to explain the gamma-ray excited decays. We assume that Ce^{3+} is excited either by the energy transfer from Gd^{3+} (delayed emission, process <2>) or excited promptly (< 1 ns) [31] by any of several mechanisms including exciton capture (process <4>) or a prompt electron-hole recombination process (process <5>). We also assume that the excited state, $(Gd^{3+})^*$, of ^6I_J and ^6P_J states are promptly created and then energy is transferred mostly to the Ce^{3+}. The energy transfer from the higher excited states of Gd^{3+} to Ce^{3+} is ignored since the spectral overlaps between those states and Ce^{3+} are relatively small. The time required for the $(Gd^{3+})^*$ and $(Ce^{3+})^*$ to be created is very short (1 < ns) on our time scale and it is assumed that $(Gd^{3+})^*$ and $(Ce^{3+})^*$ are formed at t = 0. The non-radiative energy transfer from vacancies or traps to the Ce^{3+} (process <3>) is ignored.

Using these assumptions, the $Ce1^{3+}$ decays of various GSO samples excited by

gamma rays were fit with the following:

$$N_A^{1*}(0)\exp\left(-\frac{t}{\tau_1}\right)+N_D^{I*}(0)\frac{W_{DA}^{I1}}{\frac{1}{\tau_1}-(W_D^I+W_{DA}^{I1})}\{\exp[-(W_D^I+W_{DA}^{I1})t]-\exp[-\frac{t}{\tau_1}]\}$$

$$+N_D^{P*}(0)\frac{W_{DA}^{P1}}{\frac{1}{\tau_1}-(W_D^P+W_{DA}^{P1}+W_{DA}^{P2})}\{\exp[-(W_D^P+W_{DA}^{P1}+W_{DA}^{P2})t]-\exp[-\frac{t}{\tau_1}]\} \quad ,(3.11)$$

where τ_1 represents the decay constant of $Ce1^{3+}$ and is taken from the data of fig. 3.3. The first term of eq. (3.11) represents the prompt emission from $Ce1^{3+}$ created by processes <4> and <5>, the second term represents the $Ce1^{3+}$ emission populated through the ^6I_J multiplets of Gd^{3+} and the third term represents the $Ce1^{3+}$ emission populated through the ^6P_J multiplets. $N_A{}^1*(0)$, $N_D{}^I*(0)$ and $N_D{}^P*(0)$ are the populations of excited $Ce1^{3+}$, of the excited ^6I_J multiplets, and of the excited ^6P_J multiplets, at t = 0. The curve from fitting the

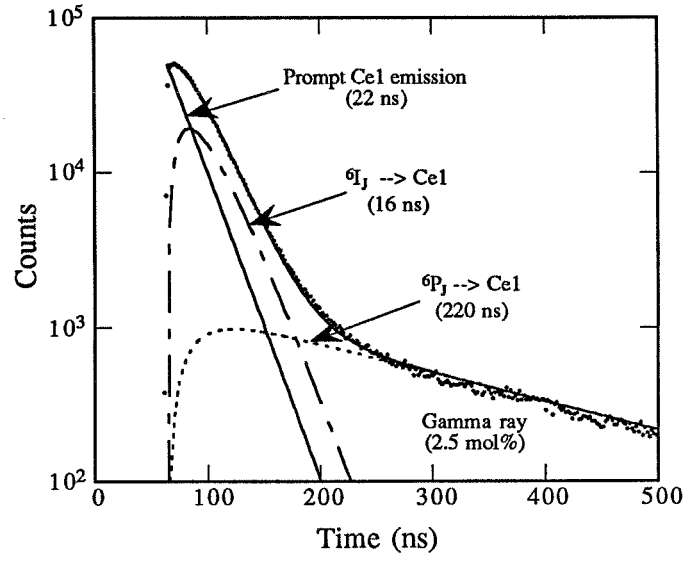

Fig. 3.13 The gamma-ray excited decay curve of 2.5 mol% GSO (closed circles). The data are fit with eq. (3.11) (solid line through the data) and decomposed into three curves, representing each term in eq. (3.11).

data for 2.5 mol% GSO is shown by the solid line through the data in fig. 3.13. The decay curve is also decomposed into the three separate terms of eq. (3.11) in fig. 3.13. As seen in fig. 3.13, the gamma-ray excited decay curve is reasonably well fit. Without the first term of eq. (3.11), the decay curve could not be well fit. The best fit parameters are given in table 3.2. Columns 4 and 5 in table 3.2 show the decay rates of the ^6I_J multiplets and of the ^6P_J multiplets calculated from the decay curves excited by gamma radiation, respectively. The values in column 3 agree well with those in column 4, suggesting that the initial build-ups of the gamma-ray excited decay curves are due to the non-radiative transfer from the ^6I_J multiplets of Gd^{3+} to $Ce1^{3+}$.

The $N_A{}^1{}^*(0)$ and $N_D{}^{I*}(0)$ can be calculated from the fitting curves. The $N_A{}^1{}^*(0)$ is the coefficient of the first term of eq. (3.11) and the $N_D{}^{I*}(0)$ is calculated from the coefficient of the second term of eq. (3.11). An interesting comparison is made by taking the ratio of the $N_A{}^1{}^*(0)$ to the $N_D{}^{I*}(0)$. These ratios are displayed against Ce concentration in fig. 3.14. The $N_D{}^{I*}(0)$ denotes the population of the excited ^6I_J multiplets which transfer energy to the $Ce1^{3+}$ and is used as a denominator in calculating the ratios, assuming that the excitation probability of the ^6I_J multiplets of the Gd^{3+} is essentially

Table 3.2 Decay rates for different GSO samples. Decay rates of the ^6I_J states of the Gd^{3+} (column 3) were calculated from the UV-excited decays by fitting eq. (3.10). Decay rates of the ^6I_J (column 4) and ^6P_J (column 5) states were also obtained from the gamma-ray excited decays using eq. (3.11). All the decay rates are given by their reciprocals (in ns).

Sample #	Nominal Ce concn (mol%)	$(W_D^I + W_{DA}^{I1})^{-1}$ (UV) (ns)	$(W_D^I + W_{DA}^{I1})^{-1}$ (Gamma) (ns)	$(w_D^P+w_{DA}^{P1}+w_{DA}^{P2})^{-1}$ (Gamma) (ns)
1	0.1	—	194	736
2	0.5	43	52	397
3	1.0	31	29	340
4	1.5	23	23	308
5	2.0	17	18	232
6	2.5	15	16	220

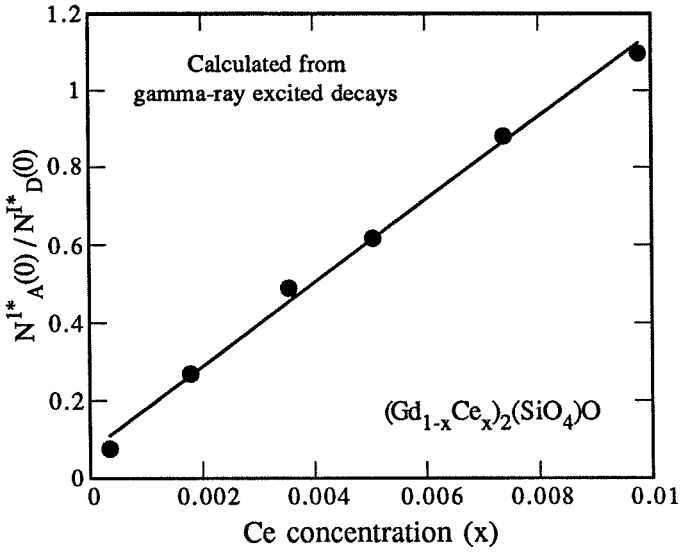

Fig. 3.14 The ratio of Ce1 population to Gd population (^6I_J state) at time t = 0 as a function of total Ce concentration.

constant from sample to sample. This assumption is reasonable since the Gd concentration is almost the same for each of the measured GSO samples. As can be seen in fig. 3.14, the ratio of $N_A{}^{1*}(0)$ to $N_D{}^{I*}(0)$ depends linearly on the total Ce concentration. This linear dependence shows that the probability of prompt exciton capture or prompt electron-hole recombination at $Ce1^{3+}$ is constant. It also shows that the rates of prompt exciton capture or prompt electron-hole recombination at $Ce1^{3+}$ increase linearly with the increase in the Ce concentration in GSO.

The gamma-ray excited decay curve of each center was measured at 15 K (fig. 3.15). The decay of $Ce1^{3+}$ contains both the build-up and the long decay component, similar to the data taken at room temperature. The decay of $Ce2^{3+}$, however, does not show the build-up. The Ce2 decay seems to contain a fast decay component, probably due to the prompt emission, and the long decay component, which is similar to the long decay component of Ce1 decay. Thus, these results support our assumption that the ^6I_J states do

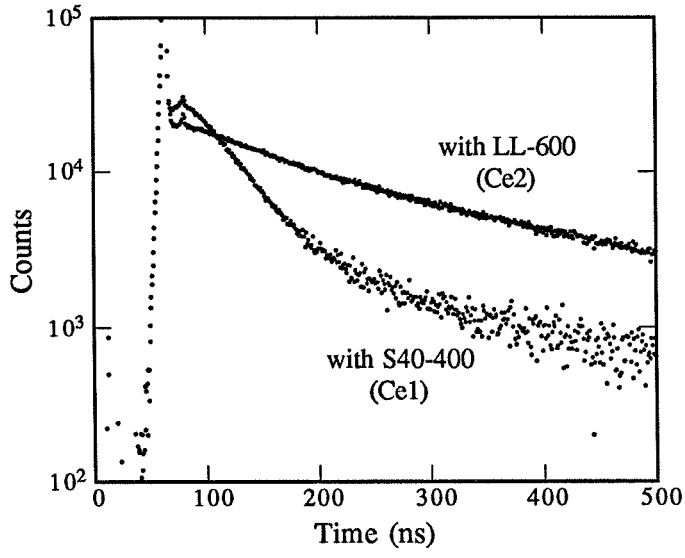

Fig. **3.15** The gamma-ray excited decay curves of Ce1 and Ce2 emissions at 15 K (from 2.5 mol% GSO).

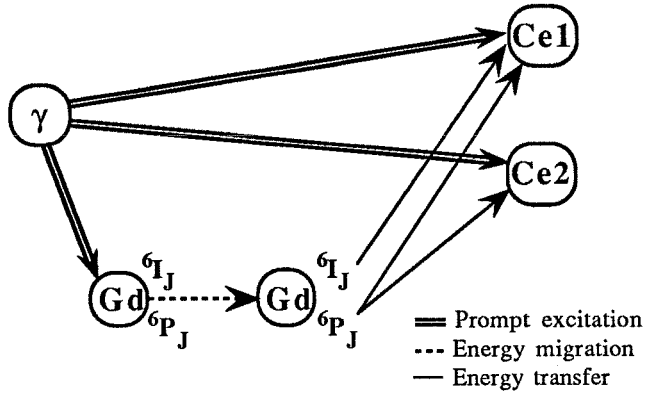

Fig. 3.16 Scintillation processes in GSO.

not feed the Ce2 center.

In analyzing these gamma-ray excited decay curves, the effect of the non-radiative transfer from the vacancies or traps to $Ce1^{3+}$ (process <3>) were ignored. Nonetheless, the gamma-ray excited decay curves have been successfully reproduced. These results suggest that the non-radiative energy transfer from Gd^{3+} to $Ce1^{3+}$ and the prompt $(Ce^{3+})^*$ creation by any of several mechanisms are the main processes in exciting $Ce1^{3+}$ at room temperature where all the gamma-ray excited decay data were taken. The origins of the two decay constants previously observed with gamma-ray excitation [2] can be attributed to the non-radiative transfer from Gd^{3+} to $Ce1^{3+}$. Among the five probable processes for exciting the Ce^{3+} (discussed in section 3.1), processes <2>, <4> and <5> seem important. The overall scintillation mechanism for GSO can be summarized in fig. 3.16. The role of Gd is to capture energy from ionizing radiation and to transfer it to Ce^{3+} ions. However, the energy transfer from Gd^{3+} to Ce^{3+} causes slow scintillation decays, which is not desirable for applications involving fast timing. The details of the prompt creation process of the excited states, $(Gd^{3+})^*$ and $(Ce^{3+})^*$, have yet to be investigated.

3.5 Summary

We have shown that the gamma-ray excited decay curves of GSO have initial build-ups as well as long decay components. We also have shown that the amount of build-up in the gamma-ray excited decay curve decreases as the Ce concentration increases.

As a possible explanation for the build-ups and the long decay components of gamma-ray excited decay curves, the non-radiative transfer from Gd^{3+} to Ce^{3+} was investigated using a UV light source. The UV-excited decay curves of GSO showed that the energy transfer from the excited ^6I_J multiplets of Gd^{3+} to Ce^{3+} produces the initial build-ups and that the energy transfer from the excited ^6P_J multiplets of Gd^{3+} to Ce^{3+} creates the long decay components. This observation for the UV-excited decay curves leads to the speculation that the initial build-ups of gamma-ray excited decay curves from

GSO are also due to the energy transfer from Gd^{3+} to Ce^{3+}.

We successfully fit the gamma-ray excited decay curves using three terms, which represent the $Ce1^{3+}$ prompt emission, the energy transfer from the excited ^6I_J multilets to $Ce1^{3+}$ and the energy transfer from the excited ^6P_J multiplets to $Ce1^{3+}$. The decay rates of the ^6I_J multiplets obtained from the gamma-ray excited decay curves agree with those obtained from the decay curve excited at 275 nm for various GSO samples, supporting our assumption.

The population of initially excited $Ce1^{3+}$, $N_A{}^1*(0)$, was compared with the population of initially excited ^6I_J multiplets of Gd^{3+}, $N_D{}^{I*}(0)$. This comparison showed that the ratio, $N_A{}^1*(0) / N_D{}^{I*}(0)$, linearly increases as the total Ce concentration increases.

The origin of the two decay constants observed with gamma-ray excitation in GSO can be ascribed to non-radiative energy transfer from Gd^{3+} to Ce^{3+}.

Acknowledgments

We are grateful to Drs. John Sutherland, John Trunk and Krzysztof Polewski in the Biology Department, Brookhaven National Laboratory, for their help in obtaining the decay data. We would like to thank Drs. John J. Simonetti and Stefan Vajda at EMR Photoelectric for their valuable comments and Dr. Hiroyuki Ishibashi and Takeshi Utsu at Hitachi Chemical Co., Ltd., for providing GSO samples. We also would like to thank Dr. Oliver Mullins, Dr. Yifu Zhu and Ralph Manente for useful discussions.

References

[1] K. Takagi and T. Fukazawa, Appl. Phys. Lett. 42 (1) (1983) 43.

[2] C.L. Melcher, J.S. Schweitzer, T. Utsu and S. Akiyama, IEEE Trans. Nuc. Sci. NS-37 (2) (1990) 161.

[3] J.B. Birks, The Theory and Practice of Scintillation Counting (Pergamon, 1964) Chap. 4.

[4] H. Suzuki, T.A. Tombrello, C.L. Melcher and J.S. Schweitzer, Nucl. Instr. and Meth. A320 (1992) 263.

[5] J. Felsche, in: Structure and Bonding V13, eds. Dunitz et al. (Springer-Verlag, 1973) p. 99.
[6] V.G. Baryshevskii et al., Vestsi Akad. Navuk BSSR, Ser. Fiz. Energet. Navuk 4 (1991) 114 (or The Proceedings of the BSSR Academy of Science, Power Engineering Physical Series 4 (1991) 114).
[7] C.L. Melcher, R.A. Manente, C.A. Peterson and J.S. Schweitzer, J. Cryst. Growth 128 (1993) 1001.
[8] L.M. Bollinger and G.E. Thomas, Rev. Sci. Instr. 32 (1961) 1044.
[9] M. Moszynski, C. Gresset, J. Vacher and R. Odru, Nucl. Instr. and Meth. 188 (1981) 403.
[10] H. Suzuki, T.A. Tombrello, C.L. Melcher and J.S. Schweitzer, IEEE Trans. Nuc. Sci. 40 (4) (1993) 380.
[11] C. L. Melcher and J.S. Schweitzer, Nucl. Instr. and Meth. A314 (1992) 212.
[12] V.A. Voloshin et al., Preprint ISC-91-8. Kharkov: Institute for Single Crystals-1991.
[13] S. Hufner, Optical Spectra of Transparent Rare Earth Compounds (Academic Press, Inc., 1978).
[14] P.J. Alonso, V.M. Orera, R. Cases and R. Alcala, J. Lumin. 39 (1988) 275.
[15] C.T. Garapon, B. Jacquier, J.P. Chaminade and C. Fouassier, J. Lumin. 34 (1985) 211.
[16] A.J. de Vries, M.F. Hazenkamp and G. Blasse, J. Lumin. 42 (1988) 275.
[17] H.S. Kiliaan, A. Meijerink and G. Blasse, J. Lumin. 35 (1986) 155.
[18] A.J. de Vries and G. Blasse, J. Chem. Phys. 88 (1988) 7312.
[19] L.H. Brixner and G. Blasse, Eur. J. Solid State Inorg. Chem. 27 (1990) 581.
[20] H.M. Crosswhite and R.L. Schwiesow, J. Chem. Phys. 50 (1969) 5032.
[21] B. Di Bartolo, Optical Interactions in Solids (John Wiley & Sons, 1968) p. 470.
[22] H.M. Crosswhite and H.W. Moos (Eds.), Optical Properties of Ions in Crystals (Interscience, 1967) p. vi.
[23] P.P. Yaney, D.M. Schaeffer and J.L. Wolf, Phys. Rev. B11 (1975) 2460.
[24] B. Henderson and G.F. Imbusch, Optical Spectroscopy of Inorganic Solids (Oxford University, 1989) Chap. 10.
[25] H. Suzuki, T.A. Tombrello, C.L. Melcher and J.S. Schweitzer, submitted to IEEE Trans. Nuc. Sci. (1994).
[26] D.W. Hall and M.J. Weber, Phys. Rev. B27 (1983) 1903.
[27] N.J. Turro, Modern Molecular Photochemistry (The Benjamin/Cummings, 1978) Chap. 9.

[28] J. Chrysochoos, B. Kumar and S.P. Sinha, J. Less-Commom Met. 126 (1986) 195.

[29] A.J. de Vries and G. Blasse, J. Phys., Colloq. C7 (1985) 109.

[30] J. Sytsma, G.F. Imbusch and G. Blasse, J. Phys. Condens. Matter 2 (1990) 5171.

[31] R.B. Murray, IEEE Trans. Nucl. Sci. 22 (1975) 54.

Chapter 4

Energy migration through the Gd sublattice in $Gd_2(SiO_4)O:Ce$

⟨Short summary⟩

This chapter was submitted to IEEE Trans. Nucl. Sci. (1994) as "Energy Transfer Mechanism in $Gd_2(SiO_4)O:Ce$ scintillators."

The energy transfer from Gd to Ce discussed in chapter 3 is considered to be a macroscopic transfer: the energy initially localized at a particular Gd^{3+} ion migrates through the Gd^{3+} sublattice until one of the Gd^{3+} ions transfers its energy to an energy sink, a Ce^{3+} ion. That is, the transfer from Gd to Ce is preceded by energy migration among the Gd^{3+} ions. Thus it is not a transfer from an initially excited Gd^{3+} ion to a Ce^{3+} ion. The rationale for believing the migration process through Gd is the following: the Gd-Gd distance in GSO is very close (~3.57 Å), while the average Gd-Ce distance is very large, since Ce concentration in these samples is very low compared with the Gd concentration. As a result, the initially excited Gd^{3+} ion is unlikely to directly transfer its energy to a Ce^{3+} ion without the energy migrating through the Gd sublattice.

In general, the best way to investigate the decay kinetics of the excited donor ion, in this case Gd, is to measure the emission decay of the donor ion. The actual donor emission decay reveals the stages of the donor decay, the nature of donor-donor and donor-acceptor interactions, and the migration mechanism among donor ions. However, because of the weak Gd^{3+} emission, the Gd^{3+} decay could not be measured directly. Therefore, we had to extract the decay kinetics of Gd^{3+} through the emission decay of Ce^{3+}.

To examine energy migration through the Gd sublattice, the Gd in GSO was diluted by partial substitution with optically inactive rare earths, Y and Lu, and the decay kinetics of Ce^{3+} emission was analyzed. The substitution of Y and Lu increases the average Gd-Gd distance and reduces the strength of the resonant energy transfer between Gd^{3+} ions. This

dilution of the Gd^{3+} slows the migration of the energy and lengthens the time required to reach the Ce^{3+}, to which the energy of the excited Gd^{3+} is then transferred irreversibly. The net result of the dilution is that the lifetime of the excited Gd^{3+} increases monotonically as the Gd^{3+} concentration decreases, and that the decay of Ce^{3+} emission is slowed.

We chose the excited ^6I_J state of Gd^{3+} to examine the energy migration systematics through the Gd sublattice. The diluted GSO samples were excited at 275 nm (into the ^6I_J states) by a synchrotron light source and the decay of Ce^{3+} emission was monitored at 420 nm. The decay curves of the Ce^{3+} emission showed different amounts of build-up, depending on the Gd concentrations. The diluted GSO samples with lower Gd concentration have slower build-ups, which suggests slower migration through the Gd^{3+} sublattice. This observation agrees with our assumption that the dilution of Gd would slow the migration of the excitation energy and would lengthen the macroscopic transfer rate of the energy from Gd to Ce.

The gamma-ray excited decay curves were also measured with the diluted GSO samples. As the Gd concentration decreases, the decay time constant of Ce^{3+} becomes slower, which again agrees with our assumption.

4.1 Introduction

Gadolinium oxyorthosilicate $Gd_2(SiO_4)O$ [1] has a high density (6.7 g/cm^3) and a high effective atomic number (59) for the efficient detection of x- and γ-radiation. Therefore, if $Gd_2(SiO_4)O$, which has an energy gap of ~6 eV, is used as a scintillator, it is expected to be optically transparent and be an ideal environment to an efficient and fast light emitting activator, the Ce^{3+} ion. However, the 4f-4f transitions of Gd^{3+} ions are of an energy where energy localized in Gd^{3+} can be transferred to the Ce^{3+} activator [2]. This energy transfer from Gd (donor or "D") to Ce (acceptor or "A") lengthens the light emission time of the Ce^{3+}, which produces limits for timing applications of $Gd_2(SiO_4)O$:Ce (GSO) [3]. Although the light emission mechanism of the Ce^{3+} in GSO is well understood [4], the overall scintillation processes of GSO are still not clear. Previously, the dependence of scintillation properties on Ce concentration was investigated [5]. To examine the role of the Gd in the scintillation processes, we diluted Gd with optically inactive rare earth elements, Y and Lu, and analyzed the decay kinetics of Ce^{3+} emission using UV- and gamma-ray excitations. The Gd^{3+} emission could not be measured because of its weak intensity; this limits our understanding of the stages of the Gd^{3+} decay, the nature of donor-donor and donor-acceptor interactions, and the migration mechanism among Gd^{3+} ions. The dilution of the Gd is expected to increase the average Gd-Gd distance and cause the migration of energy between Gd ions to be slowed. Hence, the transfer from Gd to Ce also will be slowed. Our results confirm that the transfer from Gd to Ce becomes slower, that is, the decay of the Gd^{3+} becomes longer, as the Y (or Lu) concentration increases.

When GSO absorbs the energy of the incident radiation, many electrons, holes and excitons are created. Some electrons, holes and excitons migrate through the GSO crystal to excite the Ce^{3+} and recombine. We can thus separate the scintillation mechanism into two parts: primary and secondary processes [6]. The primary processes are the transfer of energy from the ionizing radiation to the luminescent centers (Ce^{3+}); the secondary

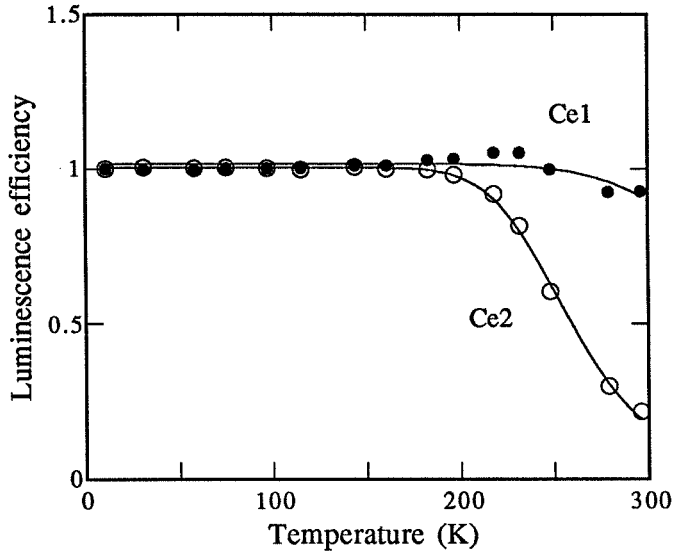

Fig. 4.1 Luminescence efficiency of Ce1 and Ce2 centers between 11 K and 300 K. The luminescence intensity at each temperature is normalized to the intensity at 11 K.

processes are the processes by which excited Ce^{3+} ions lose their energy.

We studied the secondary processes independently by direct excitation of the Ce^{3+} using UV excitation [4]. We proposed that GSO has two different activation centers (Ce1 and Ce2) because the host rare earth, Gd, occupies two different crystallographic sites in GSO [7], which is based on our observation of two types of excitation and emission spectra and two decay constants. We also investigated the temperature-dependence of the two Ce centers. At room temperature most of the Ce2 emission is thermally quenched and the Ce1 emission dominates (fig. 4.1). At temperatures < 300 K the gamma-ray excited emission can be reconstructed by an appropriate combination of Ce1 and Ce2 emissions.

We also investigated the primary processes [2], [5]. The gamma-ray excited decay curve of GSO at room temperature has build-up and slow decay components. Since $Ce1^{3+}$, which dominates the emission at room temperature, has a single exponential decay (22~25 ns), the observed slow decay with gamma-ray excitation is attributed to the slow energy transfer from the ionizing radiation to the Ce^{3+}, i.e., due to slow primary processes. A possible explanation for these slow primary processes is the resonant energy transfer

from Gd^{3+} to Ce^{3+}. This may occur because the excited states of Gd^{3+} ion overlap the absorption bands of Ce^{3+} (fig. 4.2). We measured the decay rates of the ^6I_J multiplets of Gd^{3+} as a function of Ce1 concentration and showed that the decay rates linearly depend on Ce1 concentration, which agrees well with theoretical predictions for resonant transfer. We also showed that the gamma-ray excited decay curves are composed of prompt Ce1 emission and delayed Ce1 emission (transfer of energy through Gd).

GSO has a monoclinic structure of space group $P2_1/c$ [7]. Gd has two different sites (Gd1 and Gd2) in GSO. We designate two Gd sites by Felsche's definition. Gd1 has the first three nearest neighbor Gd ions at Gd1 sites with an average distance of

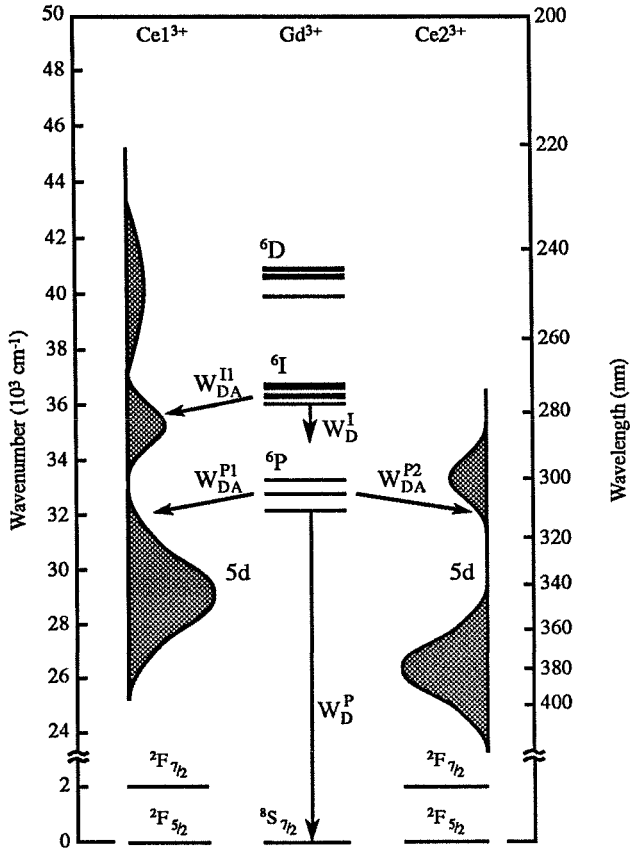

Fig. 4.2 Energy levels of Gd^{3+}, $Ce1^{3+}$ and $Ce2^{3+}$. W_{DA}^{I1} indicates the effective transfer rate from the ^6I_J multiplets of Gd^{3+} to $Ce1^{3+}$, W_{DA}^{P1} represents the rate from the ^6P_J multiplets of Gd^{3+} to $Ce1^{3+}$, and W_{DA}^{P2} indicates the rate from the ^6P_J multiplets of Gd^{3+} to $Ce2^{3+}$.

3.57 Å [5]. Gd2 has, on the other hand, the first three nearest neighbor Gd ions at the Gd2 site with an average distance of 3.56 Å. Since the Gd-Gd distances are very small, we expect very fast energy migration through the donor, Gd^{3+} ion [8]. In considering the energy transfer from Gd to Ce, we make no distinction between Gd1 and Gd2.

4.2 Model

We follow the theory of the energy transfer developed by Burshtein and co-workers [9-11] and apply their theory to GSO. We assume that the energy transfer from Gd to Ce in GSO is dominantly non-radiative (resonant) and that the back transfer from Ce to Gd can be neglected [5].

When donor-donor (Gd-Gd) energy transfer exists in addition to donor-acceptor (Gd-Ce) transfer, the donor decay becomes complex. After short-pulse excitation of the donor system (Gd^{3+}), the decay processes of the excited donor can be divided into three stages [12]:

(1) Static ordered decay; (2) Static disordered decay; (3) Migration-limited decay.

In stage (1), the excited donors, which have nearby acceptors, decay with a high transfer probability, and the donor decay becomes exponential. This is followed by stage (2) in which the excited donors transfer their energy to the acceptors located farther from them, and the donor decay becomes non-exponential. In both stages (1) and (2), the D-A transfer probabilities are independent of donor density, N_D. In stage (3), the D-A energy transfer is preceded by the energy migration among Gd^{3+} ions. That is, the energy initially localized at a particular Gd^{3+} ion migrates through the Gd^{3+} sublattice until one of the Gd^{3+} ions transfers its energy to an energy sink, a Ce^{3+} ion. In this stage the Gd^{3+} decay again becomes exponential.

Since the Gd-Gd nearest neighbor distance is small, the Gd-Gd transfer rate must

be very high; thus, the decay of the excited donors becomes exponential at an early time. Here we assume that stage (3) dominates on our time scale. As the Gd concentration decreases by partial substitution of the Y or Lu, the separation between the Gd increases, and the strength of the resonant energy transfer between Gd^{3+} ions is reduced. This dilution of the Gd^{3+} slows the migration of the excitation and lengthens the time required to reach the Ce^{3+}, to which the energy of the excited Gd^{3+} is then transferred irreversibly. The net result of the dilution is that the lifetime of the excited Gd^{3+} increases monotonically as the Gd^{3+} concentration decreases.

For a particular pair of ions, let us define the D-D transfer rate as W_{dd} and the D-A transfer rate as W_{da}. The notation for the transfer rates are [9]:

$W_{dd} = C_{dd}\, f(R)$ and

$W_{da} = C_{da}\, f(R)$,

where R is the distance between the interacting ions and f(R) are the functions whose forms are determined by the nature of the D-D and D-A interactions. C_{dd} and C_{da} are the microscopic parameters for the D-D and D-A interactions, respectively. In stage (3), the macroscopic transfer rate from Gd^{3+} to Ce^{3+} can be described by an effective transfer rate (W_{eff}). If the ion densities of the donors and the acceptors are defined as N_D and N_A, the effective transfer rate W_{eff} at stage (3) can be a function of four parameters [9]: C_{dd}, C_{da}, N_D, and N_A. W_{eff} linearly depends on N_A regardless of the type of interaction (multipolar or exchange) between the donors, and between the donor and the acceptor. If both D-D and D-A interactions are dipole-dipole in nature, W_{eff} also linearly increases with the donor density N_D; that is, W_{eff} depends linearly on the product $N_A \times N_D$. The exact form of W_{eff}, however, varies depending on whether the migration is hopping-limited or diffusion-limited [11].

We choose the excited ^6I_J multiplets of Gd^{3+} in analyzing the energy transfer mechanism from Gd to Ce. The different multiplets of ^6I_J states are treated together since we are not concerned with the detailed optical properties. The transfer rate from ^6P_J multiplets of Gd^{3+} to $Ce1^{3+}$ in GSO is low [2] and is difficult to analyze on the relatively short time scale (< 170 ns) of our UV excitation experiments. Transfer from the higher excited states of Gd^{3+} (e.g., ^6D_J and ^6G_J) was not considered in the present analysis. When we analyze the energy transfer from the ^6I_J multiplets of Gd^{3+} to Ce^{3+}, we ignore the transfer from Gd^{3+} to $Ce2^{3+}$ since the spectral overlap between Gd^{3+} emission band and $Ce2^{3+}$ absorption band is very small (fig. 4.2). The rate equations for Gd^{3+} and $Ce1^{3+}$, after initial sharp excitation, are given by [13]:

$$\frac{dN_D^{I*}}{dt} = -W_D^I N_D^{I*} - W_{DA}^{I1} N_D^{I*} \quad \text{and} \tag{4.1}$$

$$\frac{dN_A^*}{dt} = -W_A N_A^* + W_{DA}^{I1} N_D^{I*} \ , \tag{4.2}$$

where N_D^{I*} and N_A^* are the number of excited ^6I_J multiplets and of excited acceptors ($Ce1^{3+}$), respectively. W_{DA}^{I1} is the effective transfer rate from the ^6I_J multiplets of Gd^{3+} to $Ce1^{3+}$, W_D^I is the decay rate of the lowest ^6I_J multiplets including transitions to both ground $^8S_{7/2}$ state and the excited ^6P_J multiplets in an isolated Gd^{3+} ion, and W_A is the decay rate of the excited 5d level of $Ce1^{3+}$. The solution for N_A^* then becomes:

$$N_A^*(t) = N_D^{I*}(0) \frac{W_{DA}^{I1}}{W_A - (W_D^I + W_{DA}^{I1})}$$

$$\times \{\exp[-(W_D^I + W_{DA}^{I1})\, t] - \exp[-W_A\, t]\} \ , \tag{4.3}$$

where $N_D^{I*}(0)$ is the number of excited donors (^6I_J multiplets) created at t=0. Eq. (4.3) describes the $Ce1^{3+}$ decay in the case where no $Ce1^{3+}$ ions are created at t=0. In the current study of diluted GSO, we measured the decay of $Ce1^{3+}$ emission (N_A^*) and examined the decay rate of the excited ^6I_J multiplets of Gd^{3+} ($W_D^I + W_{DA}^{I1}$) as a function of N_A and N_D using UV- and gamma-ray excitations.

4.3 Experiment

The crystals used in this experiment were grown by the Czochralski technique using raw materials (Gd_2O_3, Y_2O_3, Lu_2O_3, and CeO_2), which have purities of at least 99.99%. GSO crystals were used as seeds. The starting melt material had chemical compositions $(Gd_{1-x-y}Ce_xY_y)_2(SiO_4)O$ or $(Gd_{1-x-y}Ce_xLu_y)_2(SiO_4)O$. The structure of all the crystals was analyzed with the x-ray diffraction method. The exact chemical composition of all the crystals was analyzed by X-ray Assay Laboratory using inductively-coupled plasma mass spectrometry.

The structure of the crystals changes from $P2_1/c$ to C2/c by partially substituting the smaller rare earths, Y^{3+} (0.910 Å) and Lu^{3+} (0.848 Å), into the Gd^{3+} (0.938 Å) site. The change of the lattice structure produces an entirely different crystal field and space group, and changes the energy splitting of the 4f-5d transitions of Ce^{3+}. In this study we, therefore, focused only on 10 diluted GSO samples, which have the monoclinic structure $P2_1/c$ with relatively low Y (or Lu) concentration ($y \leq 0.28$) (table 4.1). The ratio of the Gd, Y, and Lu in the crystals were approximately (within 12%) the same as that in the melt. The distribution coefficient of Ce varied from ~0.55 to ~0.81. The data obtained from undiluted GSO samples, $(Gd_{1-x}Ce_x)_2(SiO_4)O$ [5], were also used in this study.

The measurements of emission and excitation spectra were made with a SPEX Fluorolog-2 spectrofluorometer. The sample was cooled to 11 K using a CTI-CRYOGENICS refrigeration system (Model 21). The optical configuration of the

spectrofluorometer with the refrigeration system has been described previously [4]. The UV excited decay curves of the diluted GSO crystals were measured using the U9B beam line of National Synchrotron Light Source at Brookhaven National Laboratory. The duration of the excitation pulse was ~1.0 ns. The details of the experimental set up are described elsewhere [5]. The gamma-ray excited decay curves were measured with a ^{137}Cs source. Both UV- and gamma-ray excited decay curves were obtained with the time-correlated single photon technique [14], and the data were analyzed with a least squares fitting routine. When diluted GSO crystals are excited by gamma rays, both Ce1 and Ce2 emit photons at room temperature. To measure selectively the decay curve of Ce1, which has an emission peak at 425 nm, a bandpass filter (CORION S40-400) was placed between the crystal and the stop photomultiplier. This filter is transparent at ~400 nm and eliminates Ce2 emission, which has an emission peak at 480 nm.

Table 4.1 Chemical compositions of the rare earths in diluted GSO and decay rates of the excited Gd^{3+} states (^6I_J and ^6P_J) calculated from the decay curves by fitting the eqs. (4.4) and (4.5). The fifth column indicates the decay rate ($W_D^I + W_{DA}^{II}$) of the excited ^6I_J multiplets obtained from the UV-excited decay curve. The sixth and seventh columns show the decay rates of the excited ^6I_J and ^6P_J multiplets calculated from the gamma-ray excited decay curves. All the decay rates are given by their reciprocals (in ns).

no.	Chemical composition $[Gd_{1-x-y}Ce_x(Y \text{ or } Lu)_y]_2SiO_5$			^6I_J (ns) (UV)	^6I_J (ns) (γ)	^6P_J (ns) (γ)
	1-x-y	x	y			
1	0.96	0.0015	0.044(Y)	51	57	440
2	0.94	0.0038	0.056(Y)	33	34	395
3	0.94	0.0061	0.055(Y)	21	23	300
4	0.78	0.0016	0.22(Y)	60	74	538
5	0.72	0.0032	0.28(Y)	45	53	527
6	0.72	0.0054	0.28(Y)	30	37	370
7	0.95	0.0014	0.049(Lu)	60	61	485
8	0.84	0.0017	0.16(Lu)	59	67	567
9	0.76	0.0015	0.24(Lu)	73	85	634
10	0.75	0.0034	0.25(Lu)	48	61	491

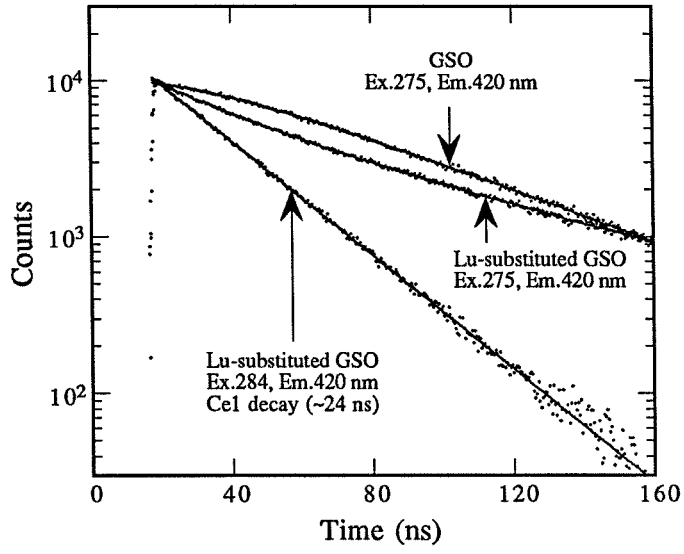

Fig. 4.3 UV-excited decay curves of $(Gd_{0.99}Ce_{0.0018})_2(SiO_4)O$ and $(Gd_{0.76}Ce_{0.0015}Lu_{0.24})_2(SiO_4)O$ (Lu-substituted GSO, crystal no. 9). The data are fit with a single exponential (~24 ns) or eq. (4.4) (solid line).

4.4 Results and discussion

First, the emission and excitation spectra of 10 diluted GSO crystals were investigated using UV-excitation at room temperature. Although the emission and excitation bands of Ce2 were not well resolved because of thermal quenching, the bands of Ce1 were observed at almost the same wavelengths as observed for undiluted GSO (containing neither Y nor Lu). That is, the excitation bands of Ce1 were at 250, 284, and 345 nm (fig. 4.2). The emission band of Ce1 was at 425 nm [4].

The decay curves of the 10 diluted GSO samples were measured with excitation wavelengths of 275 nm (into ^6I_J multiplets) and 284 nm (directly into $Ce1^{3+}$ band) and an emission wavelength of 420 nm. All the decay curves excited at 284 nm could be fit with a single exponential (~24 ns) (fig. 4.3). That is, $W_A^{-1} = 24ns$. On the other hand, the decay curves excited at 275 nm show different amounts of build-up. Fig. 4.3 shows the decay curves of two GSO samples (excited at 275 nm) which have approximately the same Ce concentration but have different Gd concentrations. As we expected, Lu-substituted GSO

has a slower build-up, which suggests slower migration through the Gd^{3+} sublattice. Since at 275 nm both Gd^{3+} and $Ce1^{3+}$ are excited, the decay curves excited at 275 nm were fit with the following equation:

$$N_A^*(t) = N_A^*(0) \exp\left(-\frac{t}{24}\right)$$

$$+ N_D^{I*}(0) \frac{W_{DA}^{I1}}{\frac{1}{24} - (W_D^I + W_{DA}^{I1})}$$

$$\times \{\exp[-(W_D^I + W_{DA}^{I1})\, t] - \exp[-\frac{t}{24}]\} \quad , \tag{4.4}$$

where the first term represents the direct emission from the Ce1 center (prompt Ce emission), and the second term represents the energy transfer from Gd to Ce (delayed Ce emission). $N_A^*(0)$ is the number of excited acceptors at t=0.

The decay rates $(W_D^I + W_{DA}^{I1})$ of the ^6I_J multiplets of Gd^{3+} for 10 samples are displayed with the data previously taken for undiluted GSO (y = 0) as a function of Ce concentration (fig. 4.4). Although the concentration of trivalent Ce was not measured, we

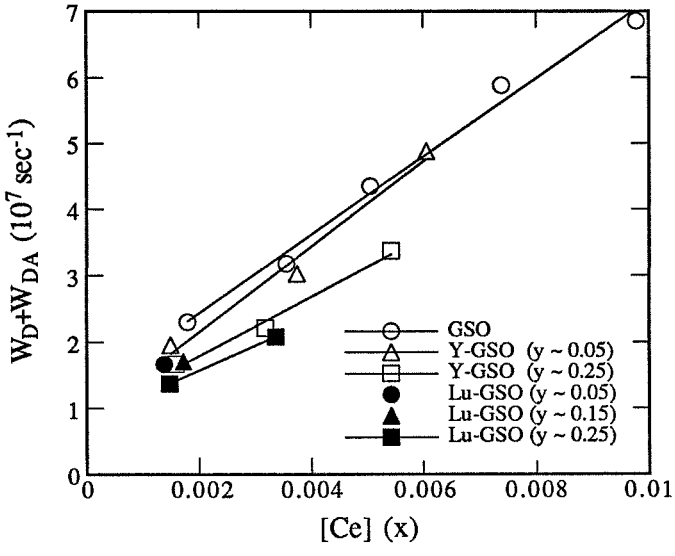

Fig. 4.4 The decay rates of the ^6I_J multiplets obtained from UV-excited decay curves. The measured samples are undiluted GSO (y = 0 and x varies from 0.0018 to 0.0098) and diluted GSO (crystal no. 1 ~ 10).

assume that the $Ce1^{3+}$ concentration is proportional to the total Ce concentration obtained from chemical analysis. The decay rates ($W_D^I + W_{DA}^{I1}$) are fit with a straight line for a group of samples which have approximately the same Gd concentration. The decay rates of the diluted GSO samples which have the same Gd concentration linearly increase as the Ce concentration increases, in agreement with the functional dependence of the effective transfer rates W_{DA}^{I1}. All the straight lines intercept the vertical axis at about 1×10^7 sec^{-1}. This indicates that W_D^I, which is independent of Ce concentration, is about 1×10^7 sec^{-1}. Since the lowest state of the ^6I_J multiplets, i.e., $^6I_{7/2}$, usually has a decay rate of the order of $10^3 \sim 10^4$ sec^{-1} [15], the large value of W_D^I obtained from the fitting may represent the energy transfer rate from Gd to impurity centers or to quenching centers, whose contribution is not taken into account in deriving eq. (4.4). The existence of quenching centers such as Gd^{3+} traps (or perturbed Gd^{3+} ions) in Gd compounds has been previously reported [16], [17]. In fact, when a lightly Ce-doped GSO crystal was cooled to 11 K, we observed very strong emission at 318 nm (fig. 4.5). This wavelength is slightly longer than the peak wavelength of unperturbed Gd^{3+} ions (excited $^6P_{7/2}$ level) and can be attributed to the perturbed Gd^{3+} ions or Gd^{3+} traps. The emission at 318 nm disappeared when the temperature was raised above 60 K.

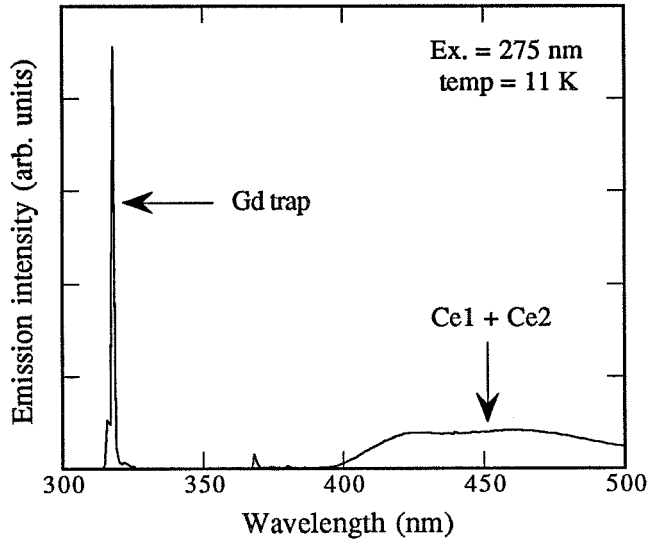

Fig. 4.5 Emission spectrum of $(Gd_{0.99}Ce_{0.00035})_2(SiO_4)O$.

For the same Ce concentration, the decay rates ($W_D^I + W_{DA}^{II}$) decrease as the Gd concentration decreases (fig. 4.4). This dependence of the decay rates on the Gd concentration, as previously stated, suggests that the donor decay is in stage (3), since the transfer rates from Gd to Ce in stages (1) and (2) are independent of the Gd concentration. This dependence also suggests that the dilution of Gd causes the longer migration time through the Gd and results in the slower energy transfer to Ce. Although we do not know the nature of the Gd-Gd and the Gd-Ce interactions in GSO, we attempted to correlate the decay rates with Gd concentration by plotting the decay rates vs. the product of Ce concentration and Gd concentration, [Ce]×[Gd] (fig. 4.6). The decay rates depend linearly on the [Ce]×[Gd] product, suggesting that both Gd-Gd and Gd-Ce interactions for the excited ^6I_J multiplets are dipole-dipole in nature.

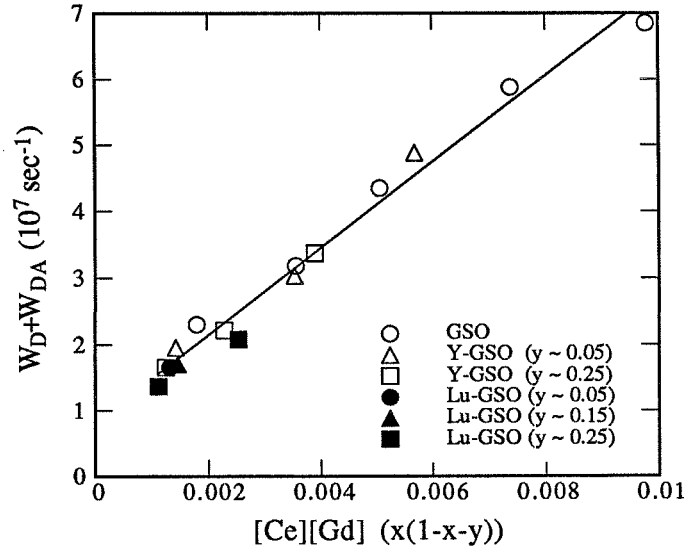

Fig. 4.6 The same decay rates as in fig. 4.4, but displayed as a function of [Ce]×[Gd].

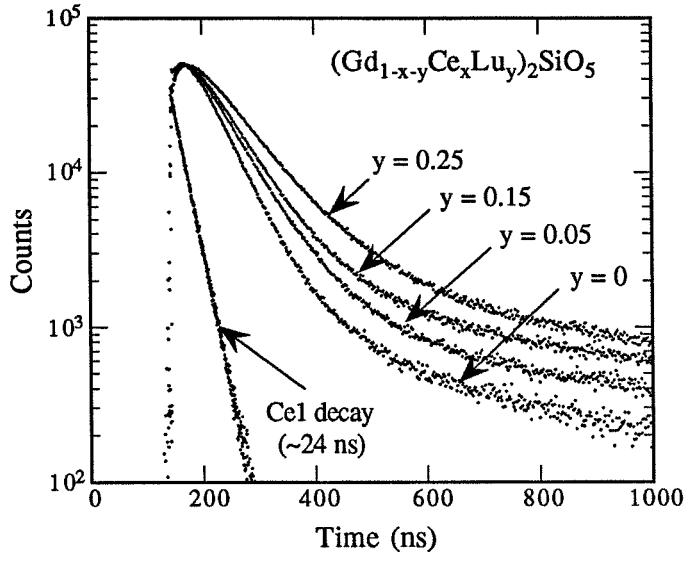

Fig. 4.7 Gamma-ray excited decay curves of crystals (no. 7 ~ 9) and undiluted GSO, which has a chemical composition of $(Gd_{0.99}Ce_{0.0018})_2(SiO_4)O$. The Ce1 decay from crystal (no. 9) is also shown.

The gamma-ray excited decay curves were also measured for the 10 diluted GSO samples. The Ce2 emission, which is weak but has a fast decay constant (~5 ns) [2], is eliminated with the bandpass filter. Fig. 4.7 shows the decay curves of three Lu-substituted GSO samples and of an undiluted GSO sample. The decay curve of the Ce1 emission (~24 ns) is also displayed. These four samples have approximately the same Ce concentration, i.e., x slightly varies from 0.0014 to 0.0018. As Gd concentration decreases with the partial substitution of Lu, the decay of $Ce1^{3+}$ becomes slower, which again agrees with our assumption. We fit the gamma-ray excited decay curves [5] with the following equation:

$$N_A^*(t) = N_A^*(0) \exp\left(-\frac{t}{24}\right)$$

$$+ N_D^{I*}(0) \frac{W_{DA}^{I1}}{\frac{1}{24} - (W_D^I + W_{DA}^{I1})}$$

$$\times \{\exp[-(W_D^I + W_{DA}^{I1})\,t] - \exp[-\tfrac{t}{24}]\}$$

$$+ N_D^{P*}(0)\,\frac{W_{DA}^{P1}}{\frac{1}{24} - (W_D^P + W_{DA}^{P1} + W_{DA}^{P2})}$$

$$\times \{\exp[-(W_D^P + W_{DA}^{P1} + W_{DA}^{P2})\,t] - \exp[-\tfrac{t}{24}]\} \qquad (4.5)$$

which is based on the assumption that after gamma rays are absorbed in the crystal, excited Ce^{3+} ions, $(Ce^{3+})^*$, and excited Gd^{3+} ions, $(Gd^{3+})^*$, are immediately created. We assume that the build-up of the gamma-ray excited decay is due to the energy transfer from ^6I_J multiplets of Gd^{3+} to $Ce1^{3+}$, and that the slow decay is due to the transfer from ^6P_J multiplets of Gd^{3+} to $Ce1^{3+}$ and $Ce2^{3+}$, whose decay equation is not shown. We thus ignore the energy transfer from other excited states of Gd^{3+} to Ce^{3+} in this simple model of the scintillation processes. Thus, the first term in eq. (4.5) indicates the prompt emission from Ce1, the second term represents the Ce1 emission through the ^6I_J multiplets of Gd^{3+}, and the third term represents the Ce1 emission through the ^6P_J multiplets. $N_A^*(0)$, $N_D^{I*}(0)$, and $N_D^{P*}(0)$ are the populations of excited Ce1, of the excited ^6I_J multiplets, and of the excited ^6P_J multiplets, at t=0. The last two terms indicate the delayed Ce1 emission. The fitting curve for the decay of crystal (no. 8) is shown (fig. 4.8). The decay rates of the ^6I_J multiplets $(W_D^I + W_{DA}^{I1})$ and those of the ^6P_J multiplets $(W_D^P + W_{DA}^{P1} + W_{DA}^{P2})$ calculated from the gamma-ray excited decay curves are shown (table 4.1). The decay rates of the ^6I_J multiplets agree well with the decay rates obtained with UV excitation for lightly diluted GSO ($y \leq 0.16$) (table 4.1). However, the differences in the decay rates between UV- and gamma-ray excitation become larger for more heavily diluted crystals ($y \sim 0.25$). The reasons for this difference are not clear.

The decay rates of the ^6I_J multiplets calculated from the UV-excited decay curves

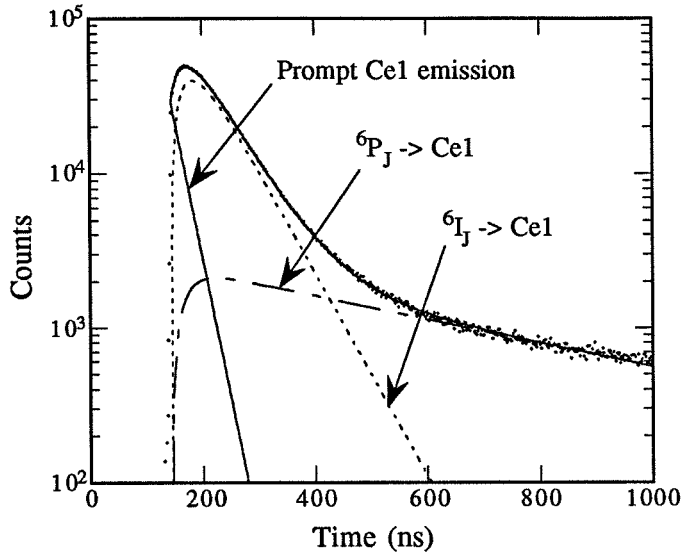

Fig. 4.8 The gamma-ray excited decay curve of crystal (no. 8). The data are fit with eq. (4.5) and decomposed into three curves.

depend linearly on the [Ce]×[Gd] product (fig. 4.6), which agrees with our assumption that the Y^{3+} and Lu^{3+} ions are optically inactive in this UV region and simply increases the average Gd-Gd distances. However, the decay rates of the ^6I_J multiplets obtained from the gamma-ray excited decay curves of the heavily diluted GSO are much longer than the decay rates from UV-excited decay curves. Since for undiluted GSO the decay rates between UV- and gamma-ray excitation agree [5], the longer decay rates obtained with gamma-ray excitation for diluted GSO must be related to the substitution of Y and Lu. Lempicki et al. [18] reported the presence of the slow energy transfer to the Ce^{3+} in the gamma-ray excited decay curve of YPO_4:Ce. Although they didn't observe slow decay components for $LuPO_4$:Ce, the substitution of Y and Lu into GSO may introduce other channels which slowly transfer energy to either Gd^{3+} or Ce^{3+} when diluted GSO is exposed to ionizing radiation.

4.5 Summary

The decay rate of the ^6I_J multiplets of Gd^{3+} was investigated for Y- or Lu-

substituted GSO using UV- and gamma-ray excitations. The decay rates obtained with two different excitation methods for lightly diluted GSO samples agree and suggest that the migration through the Gd slows down with the substitution of Y or Lu and leads to a delay in the overall transfer rate from Gd to Ce. The decay rates obtained from UV excitation have a linear dependence on the product [Ce]×[Gd], which suggests that both Gd-Gd and Gd-Ce interactions for the excited ^6I_J multiplets have dipole-dipole character. The decay rates obtained with UV excitation have a term independent of the Ce concentration, which suggests the existence of impurity centers or quenching centers. We, in fact, observe strong emission which is different than regular Gd^{3+} emission and attribute it to a Gd trap. A large difference in the decay rates between UV- and gamma-ray excitation was observed for heavily diluted GSO, which suggests that the substitution of Y and Lu introduces other channels of energy transfer when the diluted GSO is excited by gamma-ray radiation.

Acknowledgment

We would like to thank Drs. John C. Sutherland, John G. Trunk, and Krzysztof Polewski, Brookhaven National Laboratory, for assistance with decay measurements. We also would like to thank Drs. Marvin J. Weber at Lawrence Livermore National Laboratory and Rogier Visser at Delft University of Technology for useful discussions on the donor-donor transfer. The crystals for these studies were grown by T. Utsu and S. Akiyama at Hitachi Chemical. Co., Ltd.

References

[1] K. Takagi and T. Fukazawa, Appl. Phys. Lett. 42 (1) (1983) 43.

[2] H. Suzuki, T. A. Tombrello, C. L. Melcher and J. S. Schweitzer, J. Lumin. in press.

[3] C. L. Melcher, J. S. Schweitzer, T. Utsu and S. Akiyama, IEEE Trans. Nuc. Sci. NS-37 (2) (1990) 161.

[4] H. Suzuki, T. A. Tombrello, C. L. Melcher and J. S. Schweitzer, Nucl. Instr. and Meth. A320 (1992) 263.

[5] H. Suzuki, T. A. Tombrello, C. A. Peterson, C. L. Melcher and J. S. Schweitzer, submitted to Nucl. Instr. and Meth. (1994).

[6] J. B. Birks, The theory and practice of scintillation counting (Pergamon, 1964) p. 55.

[7] J. Felsche, The crystal chemistry of the rare-earth silicates, in: Structure and Bonding V13, eds. Dunitz et al. (Springer-Verlag, 1973) p. 99.

[8] H. S. Kiliaan, A. Meijerink and G. Blasse, J. Lumin. 35 (1986) 155.

[9] I. A. Bondar, A. I. Burshtein, A. V. Krutikov, L. P. Mezentseva, V. V. Osiko, V. P. Sakun, V. A. Smirnov and I. A. Shcherbakov, Sov. Phys. JETP 54 (1) (1981) 45.

[10] A. I. Burshtein, J. Lumin. 34 (1985) 167.

[11] A. I. Burshtein, Sov. Phys. Usp. 27 (8) (1984) 579.

[12] A. J. de Vries, B. P. Minks and G. Blasse, J. Lumin. 39 (1988) 153.

[13] B. Henderson and G. F. Imbusch, Optical Spectroscopy of Inorganic Solids (Clarendon, 1989) Chap. 10.

[14] L. M. Bollinger and G. E. Thomas, Rev. Sci. Instr. 32 (9) (1961) 1044.

[15] J. Sytsma, G. F. Imbusch and G. Blasse, J. Phys.: Condens. Matter 2 (1990) 5171.

[16] A. J. de Vries and G. Blasse, J. Phys. (Paris) C7 (1985) 109.

[17] C. T. Garapon, B. Jacquier, J. P. Chaminade and C. Fouassier, J. Lumin. 34 (1985) 211.

[18] A. Lempicki, E. Berman, A. J. Wojtowicz, M. Balcerzyk and L. A. Boatner, IEEE Trans. Nuc. Sci. 40 (1993) 384.

Chapter 5

Conclusions and important/promising directions for future work

5.1 Conclusion

The important results of this work are reviewed with their impact on the three processes (conversion, transfer and luminescence, see section 1.2.2) which affect the overall scintillation efficiency of these rare earth oxyorthosilicate scintillator crystals.

In chapter 2, the evidence for the existence of two activation centers (Ce1 and Ce2) in GSO was presented. The intrinsic (at 77 K) lifetimes of Ce1 and Ce2 are 27 ns and 43 ns, respectively. However, when temperature increases above 200 K, the lifetimes of Ce2 becomes shorter due to enhanced non-radiative transitions. Thus, at room temperature the lifetime of Ce2 becomes ~5 ns and its fluorescence intensity becomes weak. On the other hand, for the Ce1 center the radiative process is still dominant at room temperature and a lifetime of 22 ns is observed. The emission of GSO following gamma-ray excitation at room temperature is, therefore, dominated by the emission from the Ce1 center. For LSO [1] and YSO, two types of excitation spectra and decay time constants were also shown, which also suggests the existence of two Ce centers in these compounds.

In chapter 3, the origin of two decay time constants in the gamma-ray excited scintillation decay of GSO is discussed. When GSO is excited by gamma rays, the Ce1 and Ce2 centers are either directly excited by the recombination of electrons and holes (causing prompt emission), or indirectly excited by the energy transfer from the Gd^{3+} ions (causing delayed emission). The recombination process of electrons and holes at a Ce^{3+} site is rather fast (< 1 ns), but the energy transfer from Gd to Ce is slow and lengthens the time over which emission decay of Ce^{3+} occurs. Thus, the initial build-up and the slow component in the gamma-ray excited decay were attributed to the energy transfer from the ^6I_J and ^6P_J states of Gd^{3+} to Ce^{3+}, respectively. The overall scintillation processes in GSO

are shown in fig. 3.16.

In chapter 4, the energy migration through the Gd sublattice is discussed. The energy of excited Gd^{3+} migrates through the Gd sublattice before one of the Gd^{3+} ions transfers its energy to a nearby Ce^{3+} ion. The dilution of the Gd by Y or Lu increases the average Gd-Gd distance and lengthens the migration time through the Gd sublattice. In addition, the macroscopic energy transfer rate from Gd^{3+} to Ce^{3+} depends on the product of Ce and Gd concentrations.

These results show how the two Ce centers emit photons and how energy is transferred from Gd to these two Ce centers. However, what is still not well understood is how the energy of electron-hole pairs or excitons is transferred to the Gd and to the two Ce centers. That is, the transfer process, which determines the transfer efficiency β (see section 1.2.2), is not known for GSO or for YSO or LSO. We now discuss this problem, by comparing the scintillation processes between GSO, YSO and LSO.

As discussed in section 1.2.2, the scintillation efficiency η (light output) is expressed by

$$\eta = \beta SQ \qquad (5.1)$$

where β, S and Q are conversion efficiency, transfer efficiency and quantum efficiency, respectively. The method for determining these three partial efficiencies for LSO, GSO and YSO can now be described. First estimate the quantum efficiency Q. Then we calculate the total scintillation efficiency η ($\eta = \beta SQ = 2.3\ E_g L \times 10^{-6}$), knowing the band gap E_g (~ 6 eV) and the light output L (light yield in photons / MeV) from the literature [2,3]. Then we find β, as described in section 1.2.2, and calculate the transfer efficiency S. Note that the transfer efficiency S is a derived quantity and that currently there is no theory that can be used to calculate S.

Recently, we have further investigated the decay time of each center in the three scintillator crystals as a function of temperature (11 K to 300 K) using the National Synchrotron Light Source at Brookhaven National Laboratory (see section 3.2). The

Table 5.1 Lifetimes of Ce1 and Ce2 centers at 11 K and 300 K

	11 K	300 K
GSO	27 ns (Ce1), 43 ns (Ce2)	22 ns (Ce1), 5 ns (Ce2)
LSO	32 ns (Ce1), 47 ns (Ce2)	32 ns (Ce1), 47 ns (Ce2)
YSO	32 ns (Ce1), 47 ns (Ce2)	32 ns (Ce1), 47 ns (Ce2)

results are summarized in table 5.1.

The quantum efficiency Q of the two Ce centers at 300 K, which is described as (lifetime at 300 K) / (lifetime at 11 K), can be easily calculated using table 5.1, assuming the quantum efficiency of each center at 11 K is unity. The results are shown in table 5.2. The lifetimes of the Ce1 and Ce2 centers in LSO and YSO at room temperature are nearly the same as those at 11 K, indicating the quantum efficiencies of the two Ce centers in LSO and YSO at room temperature are close to unity. The scintillation efficiencies η estimated with the values from the literature [2,3] are also in table 5.2.

The evaluation of β for LSO is as follows: the longitudinal optical (LO) phonon energy $\hbar\omega_{LO} = 0.130\,\text{eV}$ was taken from the literature [2,4] and the static dielectric constant ε_s was measured in our laboratory as ~7.85. With the values of E_g (~6 eV) and ε_∞ (= n^2 = 3.31) previously known, the loss parameter K was determined to be ~2.22.

Table 5.2 Parameters characterizing the scintillation process at room temperature

	β	S	Q	η
GSO	low (~0.35)	low (~0.64)	Ce1 ~ 0.9 Ce2 ~ 0.1	0.13
LSO	low (~0.35)	high (~1.0)	Ce1 ~ 1.0 Ce2 ~ 1.0	0.38
YSO	low (~0.35)	low (~0.37)	Ce1 ~ 1.0 Ce2 ~ 1.0	0.13

Using fig. 1 (the conversion efficiency β vs. the energy loss ratio K) of Lempicki's paper [2], a conversion efficiency of ~0.35 is obtained. Substituting this value of β, and η (~0.38) and Q (~1) into eq. (1.3), we obtain a transfer efficiency S of ~ 1.0 for LSO. The superior scintillation efficiency of LSO, therefore, can be ascribed to its high transfer efficiency.

Next we estimate the β for GSO. Although GSO has a different crystal structure than LSO, GSO also has $(SiO_4)^{4-}$ tetrahedra and the weight of Gd is close to that of Lu. We thus expect that GSO has similar values of $\hbar\omega_{LO}$ and ε_s to those of LSO and the same ~0.35 is used for β in GSO. To evaluate the overall quantum efficiency Q of GSO at room temperature, we have to know the ratio of Ce1 and Ce2 emissions in the gamma-ray excited emission spectrum. As shown in fig. 5.1, the gamma-ray excited emission curve of 0.5 mol% GSO can be decomposed into Ce1 and Ce2 emission spectra. It was estimated from fig. 5.1, by integrating the area under each emission curve, that 60% of the emitted photons originate from Ce1 and the remaining 40% originate from Ce2. By substituting these values into eq. (1.3), we obtain:

$$0.35 \times S \times (0.6 \times 0.9 + 0.4 \times 0.1) = 0.13$$

$$S \sim 0.64 \text{ for GSO.}$$

For YSO, we again use the same value of the conversion efficiency as that of LSO. The reason for using same value is because Y has about half the weight of Lu and thus the LO phonon frequency of YSO can be a little higher than that of LSO. However, a small difference in LO phonon frequency does not significantly affect the conversion efficiency β. The expected small difference of dielectric constant ε_s between LSO and YSO also has a negligible effect on the conversion efficiency. Substituting 0.35 for β in eq. (1.3) yields a transfer efficiency of ~0.37 for YSO.

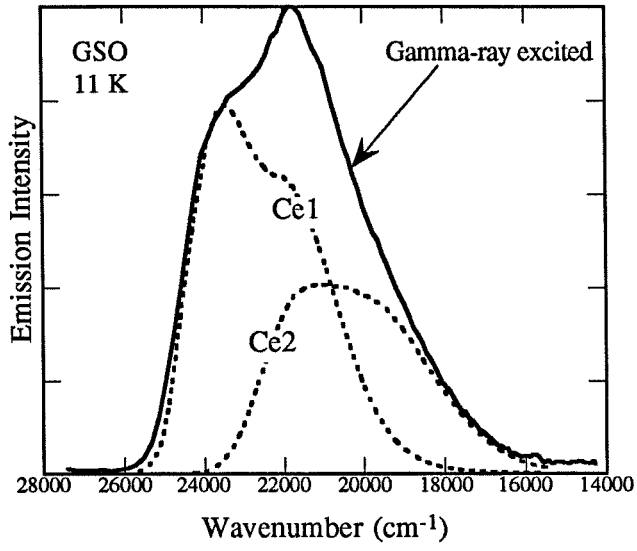

Fig. 5.1 The gamma-ray excited emission with Ce1 and Ce2 emissions at 11 K.

Let us now compare the above results for the transfer efficiency S with the experimental data. Fig. 5.2 (a)~(c) show the gamma-ray excited decay curves of the Ce1 center from LSO, GSO and YSO. The Ce1 emission was chosen since its emission is more intense than the Ce2 emission at room temperature. The Ce1 emission was separated from Ce2 emission by using a S40-400 bandpass filter. This filter is transparent at ~ 400 nm (near the Ce1 emission peak) and eliminates Ce2 emission.

The Ce1 decay in LSO (fig. 5.2 (a)) is a single exponential (~34 ns), indicating fast energy transfer from electron-hole pairs or excitons to the Ce1 center. Although the fast transfer rate does not necessarily guarantee high transfer efficiency, as is observed for some poor quality LSO samples [5], for which the fast and direct excitation process is highly inefficient due to the possible high concentration of non-radiative recombination centers, the fast transfer rate reduces the probability that the energy of the electron-hole pair gets lost before it reaches the activation center. Thus the observation of a fast transfer rate for Ce1 in LSO is consistent with our calculation of a transfer efficiency of ~1.0 for LSO.

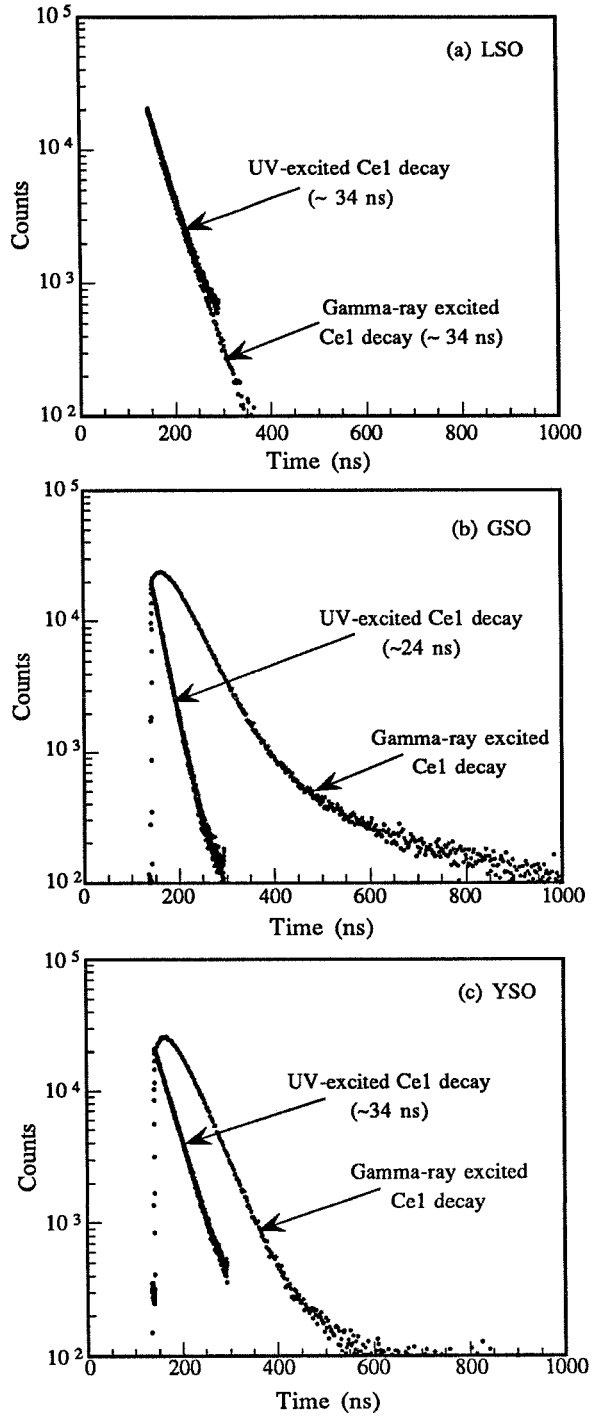

Fig. 5.2 UV- and gamma-ray excited Ce1 decays of (a) LSO, (b) GSO and (c) YSO.

The Ce1 in GSO (fig. 5.2 (b)), as discussed in chapter 3 (see fig. 3.16), is excited either directly by prompt recombination of electrons and holes, or indirectly by energy transfer from Gd. We consider that the transfer efficiency from an electron-hole pair to Ce is highly efficient since the ratio of the populations of initially excited Ce^{3+} to that of Gd^{3+} (^6I_J state), $N_A^{1*}(0) / N_D^{I*}(0)$, is very high (see fig. 3.14), suggesting a much more efficient energy transfer to Ce^{3+} centers than to Gd^{3+} centers. In addition, when energy is initially absorbed by Gd, there is high probability that one of the Gd ions transfers its energy to quenching centers such as Gd traps during the migration process through the Gd sublattice. This migration through the Gd sublattice is slow compared with the time scale for prompt recombination of electrons and holes (< 1 ns), which increases the probability of energy being lost during the migration. In fact, the trap emission was observed at low temperatures (< 60 K) in GSO (fig. 4.5). This trap emission is thermalized above 60 K and its energy is lost to the lattice. We thus attribute the low transfer efficiency of GSO to the energy transfer from unperturbed Gd to perturbed Gd (Gd traps) during the migration process.

The Ce1 decay in YSO (fig. 5.2 (c)) shows a build-up, although there do not exist any obvious slow excitation centers in YSO such as the Gd in GSO. This build-up in YSO indicates a slow energy transfer from electron-hole pairs or excitons to the Ce1 center. The presence of slow energy transfer is also observed in cerium-doped yttrium orthophosphates YPO_4:Ce crystal [6]. Since such a slow transfer has been observed neither in LSO nor in $LuPO_4$:Ce, these slow transfers in Y compounds might be due to the presence of Y in those materials. We ascribe the low transfer efficiency of YSO to the slow transfer rate, which increases the probability that the energy is trapped or dissipated in the lattice without reaching the activation center.

5.2 Future work

In the previous section the conversion efficiencies β for three compounds were estimated as ~0.35. If this estimation of β is correct, the maximum possible scintillation efficiency becomes at most 0.35 when $S = Q = 1$. Thus this value of β is a significant limitation on the possibility of improving the properties of these three crystal scintillators. For instance, the scintillation efficiency of LSO calculated from the light output is already ~0.38, which indicates that the current maximum value of light output for LSO is already close to its theoretical limit; thus, higher light output from LSO is unlikely.

As Visser et al. [5] reported, the light output of LSO samples varies within this theoretical limit ($\eta < 0.38$) from variations in crystal growth conditions such as atmosphere, annealing temperature, etc. This variation of light output reflects the difficulty of controlling the transfer processes in LSO. Visser et al. [5] reported that the Ce centers in these poor LSO samples still have a high quantum efficiency of ~1. Thus the low light outputs of these LSO samples are due to low transfer efficiency induced by the crystal growth conditions.

For GSO and YSO, the derived transfer efficiencies are still below unity and, theoretically, they can be improved. However, the poor understanding of the transfer processes makes it difficult to propose ways to improve the transfer efficiencies.

Future study of the cerium-doped rare earth oxyorthosilicates should, thus, be directed toward clarifying the energy transfer mechanism from the electron-hole pairs or excitons to the activation center, and toward improving the crystal quality. Once the material is chosen, the conversion efficiency is determined by the four material constants ($\hbar\omega_{LO}$, E_g, ε_∞, ε_s) and it is unlikely that they are influenced by the crystal quality. Also, once energy gets to the Ce centers, most of the excitation energy is emitted as photons unless there are strong nonradiative processes or quenching centers near the Ce. On the other hand, the transfer efficiency is very sensitive to crystal conditions, such as the impurity concentration, the lattice defects, the activator concentration, etc., and their effects

are still unknown. As Lempicki et al. [2] stated in general for scintillators, and is also true for cerium-doped rare earth oxyorthosilicates, improvements in scintillator performance will result from a unifying theory that can describe the transfer efficiency.

References

[1] H. Suzuki, T.A. Tombrello, C.L. Melcher and J.S. Schweitzer, IEEE Trans. Nuc. Sci. NS-40 (4) (1993) 380.

[2] A. Lempicki, A.J. Wojtowicz and E. Berman, Nucl. Instr. and Meth. A333 (1993) 304.

[3] H. Suzuki, T.A. Tombrello, C.L. Melcher and J.S. Schweitzer, Nucl. Instr. and Meth. A320 (1992) 263.

[4] K. Nakamoto, Infrared Spectra of Inorganic and Coordination Compounds (John Wiley and Sons, 1963).

[5] R. Visser, C. L. Melcher, J. S. Schweitzer, H. Suzuki and T. A. Tombrello, submitted to IEEE Trans. Nuc. Sci. (1994).

[6] A. Lempicki, E. Berman, A. J. Wojtowicz, M. Balcerzyk and L. A. Boatner, IEEE Trans. Nuc. Sci. 40 (1993) 384.